Effects of Louver Length and Vortex Generators to Augment Tube Wall Heat Transfer in Louvered Fin Heat Exchangers

Paul A. Sanders

Thesis submitted to the faculty of the Virginia Polytechnic Institute and State University in partial fulfillment of the requirements for the degree of

Master of Science
in
Mechanical Engineering

Dr. Karen A Thole, Chair
Dr. Brian Vick
Dr. Scott Huxtable

September 14, 2005
Blacksburg, Virginia

Keywords: Louvered Fin, Compact Heat Exchanger, Tube Wall, Vortex Generator, Delta Winglet

Effects of Louver Length and Vortex Generators to Augment Tube Wall Heat Transfer in Louvered Fin Heat Exchangers

Paul A. Sanders

(Abstract)

There are several different types of compact heat exchangers used in applications where small size and weight are required. One particular type of compact heat exchanger, the louvered fin heat exchanger, has been used heavily in the automotive and air conditioning industries. Over the last several decades, the majority of the work towards improving louvered fin exchanger efficiency has focused on designing more efficient fins by optimizing fin parameters like louver angle, fin pitch, louver pitch, and louver length. At this point in time, many improvements to standard louver geometry have been made, so other surfaces and methods of enhancing exchanger performance need to be studied if any significant future efficiency gains are to be expected.

This thesis presents a detailed experimental study that has two major foci relative to the performance of the louvered fin compact heat exchanger. The first is to determine the effect of louver length on pressure drop and tube wall heat transfer, which is the primary heat transfer surface in the heat exchanger. The second is to augment tube wall heat transfer with the use of delta winglets placed on the fins near the tube wall. These studies were completed on a 20X scale model of a louvered fin exchanger with a fin pitch to louver pitch ratio of 0.76 and a louver angle of 27°, over a Reynolds number range based on louver pitch of $230 < Re_{Lp} < 1016$. The three louver lengths evaluated were 100%, 82%, and 70% of the fin height and delta winglet experiments were performed for louver length to fin pitch ratios of 100% and 70%. Heat transfer results for the louver length tests show that decreasing louver length leads to increases in tube wall heat transfer of 0% to 50% depending on Reynolds number. Also, delta winglets placed on the fins near the tube wall have been shown to produce average tube wall heat transfer augmentations of up to 52%.

Acknowledgements

First of all, I'd like to thank my parents for giving me a reasonably sized brain and providing me with the means to succeed in every facet of life. Your love and constant support has been unbelievable and has helped me make it through this. I would like to thank my brother, Lee, for making the trek to Virginia with me. I know it was a difficult decision but only good things have and will continue to happen because you came. I am sorry that my busy schedule kept us from hanging out often.

I want to thank Dr. Karen Thole for giving me the opportunity to work in the VTExCCL lab. You are the toughest and most demanding boss I have ever had but your guidance has been invaluable to my learning experience. I would also like to thank all of my lab mates and everyone in the extended friends network for all of the good times. It was a difficult decision to leave my friends and family behind in sunny Florida to come to the frozen tundra of Virginia Tech. However, you all made the transition very easy and have given me so many lasting memories. I will miss all of you.

Finally, I want to thank Stephanie and Chandler. The Bingo, you are my favorite dog ever and I will miss the midnight make out. You learn some manners and keep your mother happy. Steph, it is impossible to sum up the amount of time we have spent together and the memories we have shared. I believe being apart will be very difficult for both of us. Just remember, start here and move forward. We'll figure it all out eventually.

Table of Contents

Nomenclature

A_{ff}	Minimum cross sectional free flow area
A_{heater}	Area of strip heater
A_{in}	Cross sectional area of test section inlet
AOA	Winglet angle of attack
AR	Delta winglet aspect ratio, AR = 4(b/2)/c
b	Half of winglet height
c	Winglet chord
DFW	Distance of delta winglet from wall
D_H	Hydraulic diameter, $D_H = \frac{4 \cdot A_{ff}}{P_{wetted}} = \frac{4(F_p - t)F_h}{2(F_p - t) + 2F_h}$
f	Fanning friction factor
F	View factor
f_0	Baseline friction factor
f_{aug}	Friction factor augmentation, $f_{aug} = f/f_0 - 1$
F_d	Fin depth, distance from leading edge of entrance louver to trailing edge of turnover louver
F_h	Fin Height
F_p	Fin pitch
I_{heater}	Current through strip heater
k	Thermal conductivity
K_c	Loss coefficient for sudden contraction of flow entering louvered array
K_e	Loss coefficient for sudden expansion of flow leaving louvered array
L_l	Louver length
L_p	Louver Pitch
n_{louver}	Number of louver rows at inlet of test section
Nu_0	Baseline Nusselt number
Nu_{aug}	Nusselt augmentation, $Nu_{aug} = \overline{Nu/Nu_0 - 1}$
Nu	Nusselt number
P_{wetted}	Wetted perimeter, $P_{wetted} = 2(F_p\text{-}t) + 2F_h$

Q	Volumetric flow rate through test section
$q''_{conduction}$	Heat flux lost by conduction through instrumented wall
q''_{heater}	Applied heat flux at heated wall
$q''_{radiation}$	Heat flux lost by radiation from the heated wall
R	Resistance of strip heater
Re_{Lp}	Reynolds number based on louver pitch, $Re_{Lp} = U_{ff}L_p/\nu$
R_{heater}	Resistance of strip heater
R_p	Resistance of precision resistor
t	Louver thickness
T_{film}	Film temperature, $T_{film} = \frac{\frac{T_{wall}(X=0)+T_{inlet}}{2} + \frac{T_{wall}(X=1)+T_{inlet}}{2}}{2}$
T_{guard}	Temperature measured on guard heater plate
T_{inlet}	Temperature measured at test section inlet
T_{wall}	Temperature measured on heated wall
U_{ff}	Maximum free flow velocity
VG-F	Forwards facing delta winglet
VG-B	Backwards facing delta winglet
V_{heater}	Voltage drop across Kapton/Inconel heater
V_p	Voltage drop across precision resistor
w	Louver width
x	Horizontal coordinate through test facility
X	Non-dimensional fin depth

Greek

θ	Louver angle
η	Efficiency index, $\eta = Nu_{aug}/f_{aug}$
ΔP	Pressure drop through louvered array
ε	Surface emissivity
ρ_{air}	Density of air
ν	Kinematic viscosity
σ	Stefan-Boltzman constant

List of Figures

List of Tables

Chapter 1 – Introduction

Louvered fins provide advantages over continuous fin designs because each louver initiates new boundary layer growth, producing higher heat transfer and reducing exchanger size. Figure 1.1 illustrates a typical louvered fin heat exchanger geometry comprised of louvered fins and tubes. Because nearly 85% of the total thermal resistance in a typical louvered fin heat exchanger is due to air side performance, most work aimed at increasing exchanger efficiency has been geared towards designing better louvered fins. Although the fins account for around 70% to 90% of the total exchanger surface area, they are still a secondary surface for removing heat from the tube wall. The tube wall is the primary surface where greater temperature differences between itself and the surrounding fluid provide more of a potential for heat transfer. Understanding the mechanisms that govern tube wall heat transfer could provide information to help maximize the performance of the tube wall heat transfer. Ultimately, further augmentation of the tube wall heat transfer is desired as a means to improve overall exchanger heat transfer.

1.1 Literature Review

There were two main objectives of this study, the first of which was to determine the effect of louver length (three louver lengths were tested) on tube wall heat transfer and louvered array pressure drop. The second was to find a manufacturable means of incorporating delta winglets on the louvered fin surfaces and to quantify the associated tube wall heat transfer augmentation and pressure drop penalty for two different louver lengths. Due to the complete lack of published studies showing the mixed effects of louver length and vortex generators in louvered fin heat exchangers, a literature review for general louvered fin exchangers and general vortex generator studies will be given.

Much of the research related to louvered fin heat exchangers has been geared towards overall heat exchanger performance, while the majority of the remaining work, mostly done on scaled-up models of heat exchangers or with computational methods, has focused on the flow field and heat transfer for the louver portion of the fin. There are very few studies to date that have given any detailed information of the heat transfer and flow field near the tube wall surface. The research performed on actual-sized louvered fin heat exchangers has been related to overall

heat transfer and pressure drop performance. Kays and London (1984) gave a compilation of such data for a large number of available heat exchangers at the time. Other studies of actual-sized heat exchangers, like the one performed by Achaicha and Cowell (1988), showed performance data for heat exchangers for a wide range of influential parameters such as fin pitch, louver pitch, tube pitch, and louver angle. Although information like this is very valuable, it does not provide any details of the performance determining heat transfer and flow field mechanisms within the exchanger.

Studies performed with scaled-up heat exchangers provided more of this detailed information, however, the majority of these studies have focused on the two-dimensional flow region over the louvers, ignoring effects of the tube surface. For example, Webb and Trauger (1991) performed flow visualization studies that showed the relationship of flow alignment with louvers for different louver angles, louver pitches, and fin pitches. This is also true of many of the first CFD studies where three-dimensional computations were not possible due to computing power constraints. Because louvers make up the majority of the exchanger surface area, studies focused on two-dimensional effects are certainly understandable, however, more recent studies have shown that the three-dimensional flow near the tube wall does impact the performance of the exchanger.

Atkinson et al. (1998) ran two-dimensional and three-dimensional simulations for overall heat transfer and friction factor and then compared them to experimental results of Achaicha and Cowell. They reported that the ability to match computational heat transfer results to experimental heat exchanger data was much better for the three-dimensional models. They also reported that two-dimensional and three-dimensional simulations matched actual exchanger data well for friction factor, but the three-dimensional model provided better results for small tube pitches. Cui and Tafti (2002) performed computational studies on a more realistic three-dimensional fin geometry. This geometry was comprised of a louver, a transition region, and a flat landing leading to the tube wall, which are features created in the stamping process of an actual louvered fin (Figure 1.2). They showed strong three-dimensional flow field effects in the transition region caused by high energy vortex jets. These vortices were also shown to have a positive effect on tube wall heat transfer. Tafti and Cui (2003) extended their 2002 study to four different louver lengths. This was a computational study detailing the heat transfer performance on the louver surface and tube wall and giving friction factors for three of these geometries.

Results indicated that increasing louver length caused a decrease in tube wall heat transfer and an increase in friction factor. However, both of the studies from Tafti and Cui considered only a single periodic louver, ignoring the effects of the entrance, turnover, and exit louvers.

Ebeling and Thole (2004) gave experimental and computational results for straight louvers with no transition to flat landing. These results showed that compared to a flat plate, the tube wall provides higher heat transfer performance due to repeated interruptions on the tube wall boundary layer by the leading edges of the louvers. This study also showed that entrance, turnover, and exit louvers provide a substantial benefit to tube wall heat transfer as the flow turns lead to significant thermal boundary layer thinning. This study provided good information for the straight louver case, but gave no comparative louver lengths and also no friction factor data.

Although no studies have been done with vortex generators incorporated on the fins of a louvered fin heat exchanger, several have been done with them on flat plates, in channels, and in other types of heat exchangers. These types of studies give an idea of what improvements might be possible when used in a louvered fin heat exchanger. Gentry and Jacobi (2002) performed studies with delta wings on a flat plate and in a developing channel flow, both of which were done with laminar flow and with other considerations that were aimed towards providing useful information for heat exchanger application. For both flow situations, mass transfer, pressure drop, and vortex strength were measured. The developing channel experiments in this study showed the influence of the vortices on the surface that the wing was applied to as well as the surface above the wing, which had not been done until then. The flat plate results indicate that vortex strength and convection benefits increased with increasing Reynolds number (based on winglet chord), winglet aspect ratio, and angle of attack. Maximum spatially-averaged enhancements in the vortex affected area were between 35% and 80% for $Re_c = 300$ and 1300 respectively. The vortex strength and heat transfer enhancements in the developing channel flow also increased with increasing Reynolds number (based on hydraulic diameter), winglet aspect ratio, and angle of attack. Vortices were shown to have a significant effect on both surfaces, leading to heat transfer augmentations averaged through the entire channel of 20% and 50% at $Re_{dh} = 400$ and 2000 respectively. Friction factor in both the flat plate and channel flow experiments was shown to increase with increasing Re, winglet aspect ratio, and angle of attack. As mentioned earlier, these studies were done with delta wings which create two longitudinal vortices that interact with each other in the streamwise direction. Although our studies were

done with delta winglets which only produce one streamwise vortex, the general idea of augmentation through the use of vortices still applies.

Several studies have also been completed with delta winglets placed in finned oval tube heat exchangers, of which a few will be highlighted. These types of exchangers lend themselves to enhancement with vortex generation due to the large plate areas from which winglets can be stamped. Chen et al. (1998) performed a computational study where three different configurations of inline punched delta winglets were placed on either side of the tube (Figure 1.3). This study showed that the longitudinal vortex from the upstream winglet merges with the vortex from the downstream winglets to form a larger, stronger vortex that provides higher heat transfer than a single winglet. When a third winglet was added in line, the same trends occurred. These studies also showed that each successive winglet increases the pressure drop though the exchanger. A similar computational study by Tiwari et al. (2003) had configurations with one, two, three, and four inline pairs of non-punched delta winglets in a flat plate oval tube exchanger (Figure 1.4). Their results also showed an increase in heat transfer with increasing number of inline winglets. They also showed results for winglets that were staggered and alternating in direction, which produced higher heat transfer augmentations than the in-line winglets in the same direction. Although these and other similar studies in tube plate heat exchangers have winglets applied to the fin surface in the near tube region, it seems that no research has been done where winglets have been placed near enough to the tube wall to try and augment tube wall heat transfer.

Joardar and Jacobi (2005) seem to be the only researchers who have combined delta wings and louvered fin heat exchangers. In this study, nearly 1500 delta wings were glued to the tubes at the leading edge of the fins in an actual louvered fin heat exchanger (Figure 1.5). The exchanger was tested in dry and wet conditions and overall heat transfer and friction factor measurements were made. Heat transfer augmentations of 21% and 23% were shown for dry and wet conditions, respectively, with an associated pressure drop penalty around 6%. Although this method showed a vast improvement over baseline conditions, there is some issue about the manufacturability of adding strips of winglets to the front of a heat exchanger.

1.2 Necessity and Objectives of Current Study

Although the studies listed above have certainly added to the general knowledge of louvered fin heat exchangers and vortex generators, there are still several gaps in this knowledge that need to be filled. To this point, there has been no comparison of louver lengths as related to friction factor and tube wall heat transfer for a louvered array with entrance, turnover, and exit louvers. These effects need to be determined. It has been shown in several past studies that the use of longitudinal vortices on flat plates, in channels, and in heat exchangers is beneficial due to positive heat transfer gains with a relatively minor pressure drop penalty. The majority of work in delta winglet applications has been in flat plate fin heat exchangers because of the large amount of space from which to stamp the winglets. Although these studies have shown gains on the fin surface, none have been aimed at increasing tube wall heat transfer. The single study with longitudinal vortices in louvered fin heat exchangers did not incorporate winglets into the exchanger itself, but applied wings to the outside of the exchanger. Due to the manufacturing constraints of this setup, it makes sense to attempt to use winglets in a manner so that they may be punched from a surface in a standard manufacturing process. The work presented in this thesis is aimed at addressing these two major issues, and is therefore well warranted.

This study experimentally explores the effect of louver length and the incorporation of delta winglets on tube wall heat transfer and louvered array pressure drop. Heat transfer and pressure drop experiments were performed on a 20X scale version of a louvered fin exchanger. Three different louver lengths were studied (L_l/F_h = 100%, 82%, and 70%) and several delta winglet parameters were studied to give a wide range of results for determining important trends. A diagram comparing the different louver lengths tested in this study as well as definitions of geometrical features can be seen in Figure 1.6. All experiments were performed for a louvered array geometry with a fin pitch to louver pitch ratio of $F_p/L_p = 0.76$ at a louver angle of $\theta = 27°$ and over a Reynolds number range based on L_p of $230 < Re < 1016$ (Figure 1.7). This document presents a detailed record of this study from the experimental setup to the heat transfer and friction factor results obtained from experiments. It also provides full description of these results, conclusions made from them, and possible directions for future studies.

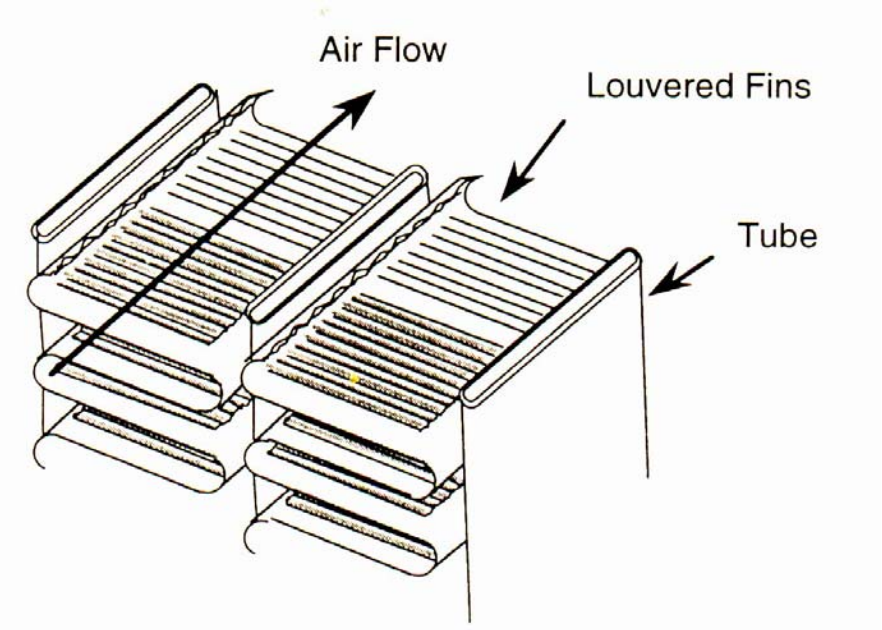

Figure 1.1 Diagram of realistic louvered fin heat exchanger.

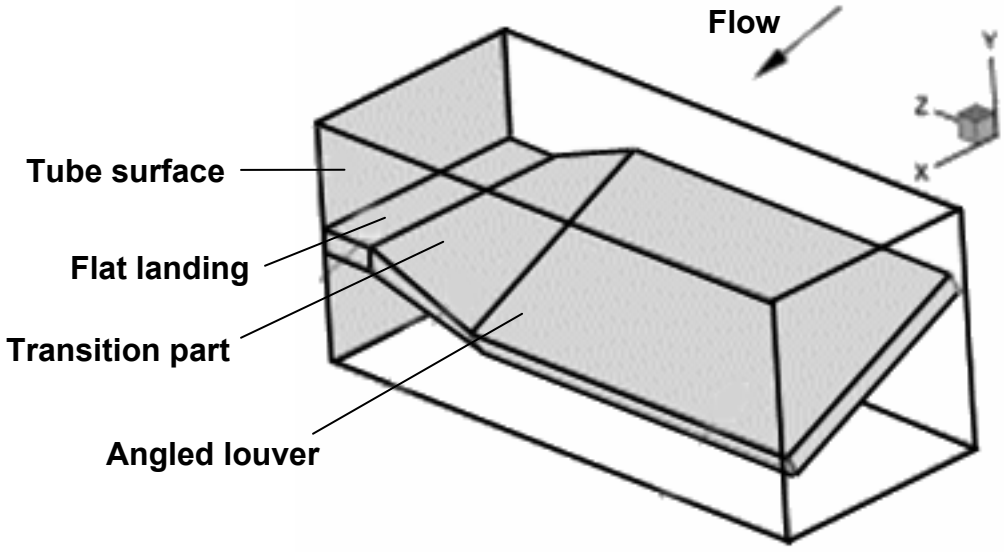

Figure 1.2 Realistic three-dimensional geometry used in computational studies by Tafti and Cui (2003).

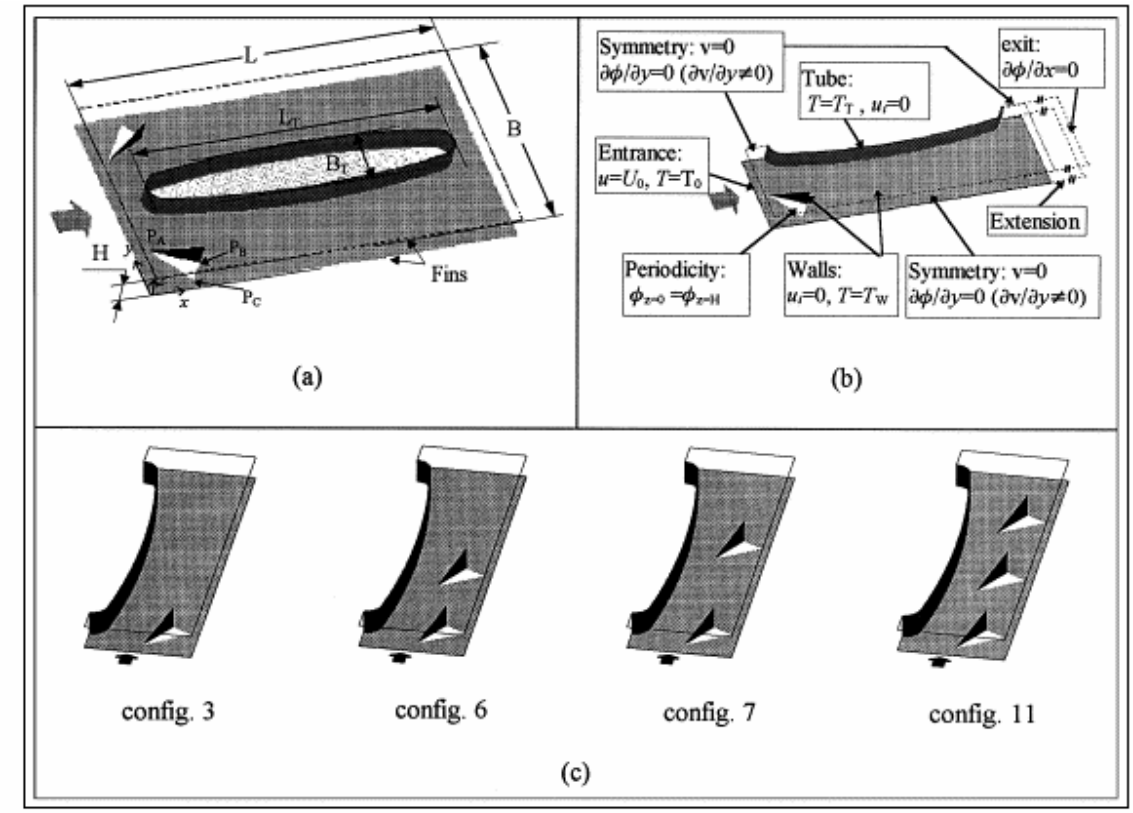

Figure 1.3 Diagram of delta winglet configurations used in the computational studies of Chen et al. (1998).

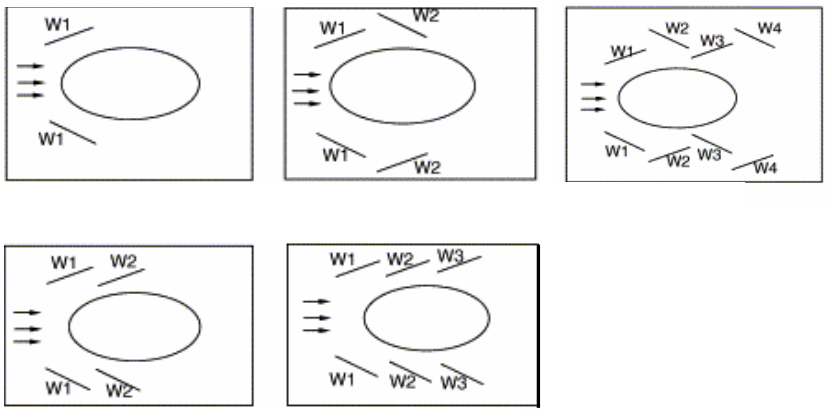

Figure 1.4 Diagram of delta winglet configurations used in the computational studies of Tiwari et al. (2003).

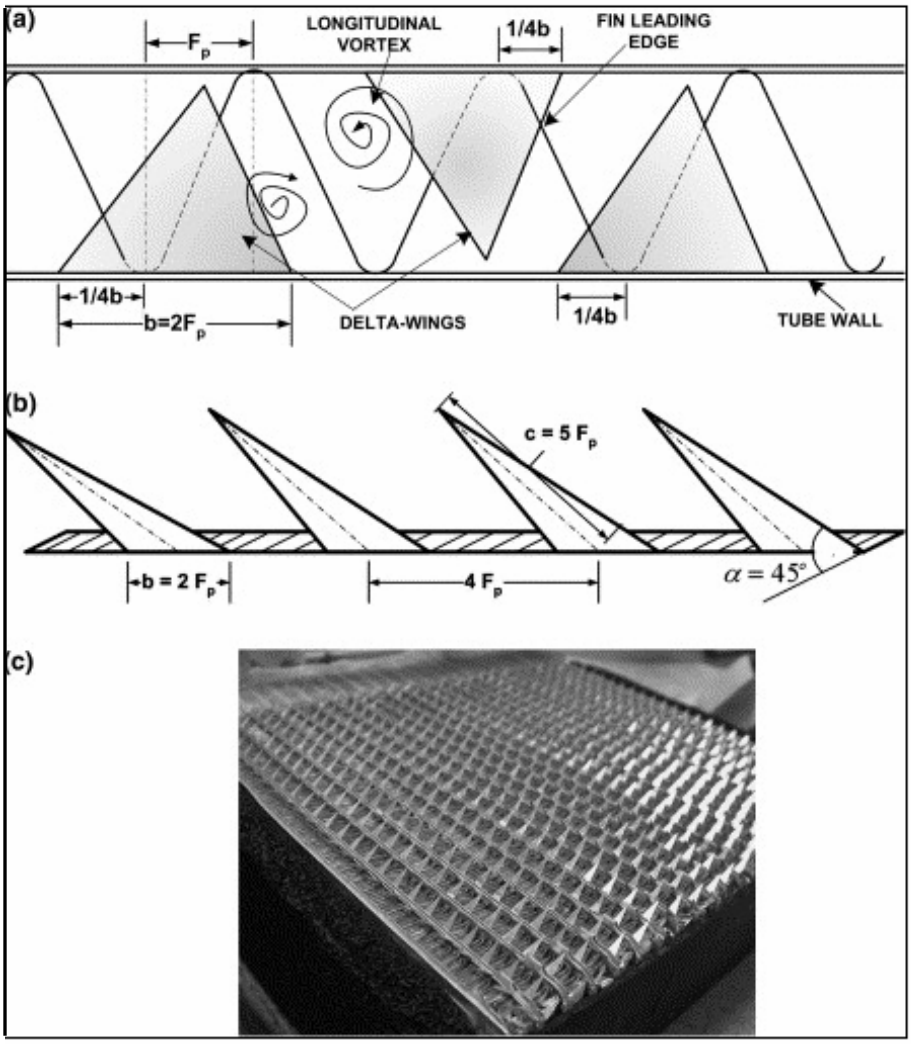

Figure 1.5 Diagrams and picture of delta wing configuration studied by Joardar and Jacobi (2005).

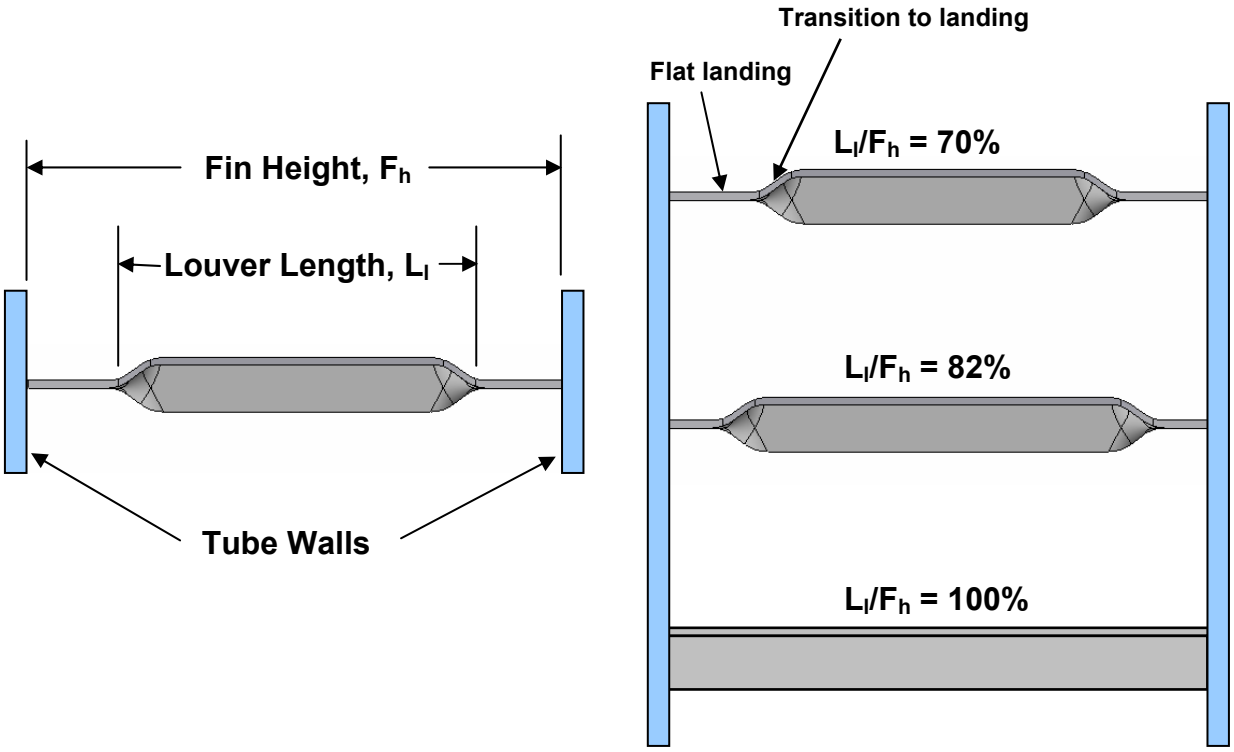

Figure 1.6 Comparison of different louver lengths and definitions of geometries.

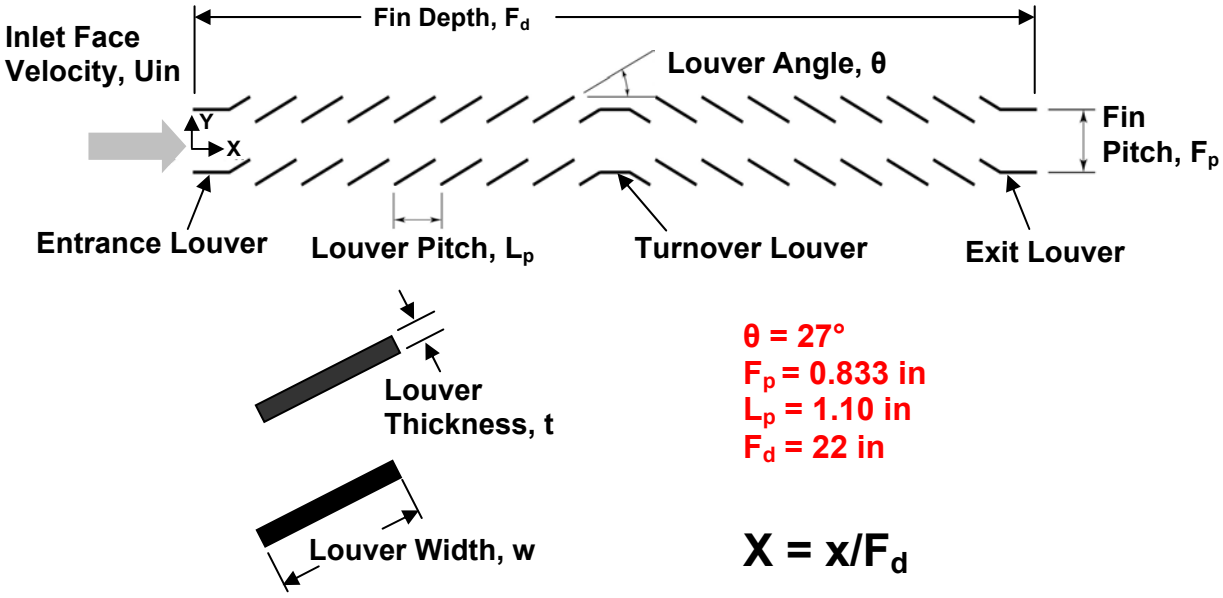

Figure 1.7 Louvered array geometry and definitions used in this study.

Chapter 2 - Experimental Facility and Instrumentation

As stated in the previous chapter, this study had two major foci:
1) to find how louver length affects tube wall heat transfer and overall array pressure drop
2) to study the effect of delta winglets of different aspect ratios, angles of attack, and distances from the tube wall. All tests were carried out in a 20X scale version of a louvered fin exchanger. The test section used for the $L_l/F_h = 100\%$ studies is the same as the one used in the studies of Ebeling and Thole (2004). However, there have been some modifications for the $L_l/F_h = 70\%$ and $L_l/F_h = 82\%$ geometries that will be described in this section.

The first section of this chapter provides details of the fin array geometry and the three louver lengths that were tested. The second section describes the major parts of the experimental facility including the inlet nozzle, test section, laminar flow element, and motor-controlled blower. The third section discusses the winglet parameters and flow conditions used in experimentation. Section four gives information on the instrumentation used to collect data including thermocouples and pressure transducers. The fifth section describes the data acquisition system as well as the methodology used in data collection. Section six describes data reduction techniques used to convert the raw temperature and pressure drop data into Nusselt numbers, friction factors, and efficiency indexes. Section seven deals with the uncertainty estimates related to the experimental methods. Finally, the last section discusses the benchmarking of the test sections.

2.1 Louver Length and Fin Array Geometry

Figure 2.1 shows a representative geometry used in this study as well as the nomenclature that will be used throughout this document. There are many different geometries of louvered fin exchangers that correspond to different applications. All of the experiments in this study were done on a high density (small L_p) louvered fin array that is typically used in a large truck radiator application. Specifically, the geometry used for all testing was $\theta = 27^\circ$, $F_p/L_p = 0.76$, $w = L_p$, $t = 0.079L_p$. This array geometry was comprised of an entrance louver, seven louvers, a turnover louver, seven additional louvers, and finally an exit louver. The entrance, turnover, and exit

louvers are each twice the width of the other louvers. These special louvers turn the flow to the desired louver angle to ensure that it follows the louvers and provides good heat transfer.

The first goal of this study was to determine the effects of different louver lengths on the tube wall heat transfer as well as the pressure drops associated with the different lengths. Figure 2.2 shows the three different louver lengths studied as well as the nomenclature that will be used throughout this document. In a realistic louvered fin heat exchanger, the fin is a flat piece of metal from which the louvers are stamped and bent to the desired louver angle. This process produces the louver, the transition to the flat landing, and the flat landing that connects to the tube wall. These characteristics can be seen in Figure 2.2 for the L_l/F_h = 70%, and L_l/F_h = 82% geometries. It is important to mention that the fins in this study connect perpendicularly to the tube. In an actual louvered fin exchanger the fins are cut into long strips that wind back and forth between the tube walls, creating a slight curvature of the landing (Figure 2.3). The L_l/F_h = 100% geometry is an ideal case where the fin height is the same as the louver length. Since L_l/F_h = 100% is the maximum louver length that could ever be achieved, it is used as a comparator to the more realistic geometries. It is important because over the years companies have been trying to increase efficiency by increasing the louver length. The second portion of this research is to determine how delta winglets applied to the flat landing affect heat transfer on the tube. Due to space restrictions, the louver length needs to be shortened so the winglet can be applied to the flat landing. It is important to know if this shortening can have an adverse effect on tube wall heat transfer or pressure drop.

2.2 Experimental Facility

The test facility used in this study was an open loop wind tunnel that consisted of an inlet nozzle, a test section, a laminar flow element, and a motor-controlled blower (Figure 2.4). All of the major components in the test facility were the same used in the studies of Lyman et al. (2002), Stephan and Thole (2004), and Ebeling and Thole (2004), with the exception of the test section. The test section used for the L_l/F_h = 100% louver length and winglet tests was the same used by Ebeling and Thole (2004) in their tube wall heat transfer studies, but was changed for the L_l/F_h = 70% and L_l/F_h = 82% tests. Those modifications will be discussed later in this section.

The inlet contraction was designed by Lyman (2000) using Fluent 5.0, a commercially available CFD program. The contraction was designed to provide a uniform inlet flow to the test section so that an infinite stack of louvers could be modeled as accurately as possible. The nozzle had a 16:1 area reduction decreasing from an inlet area of 6.57 ft^2 (0.61 m^2) to an exit area, or test section inlet area (A_{in}), of 0.41 ft^2 (0.038m^2). There was a 2.01 in (51 mm) thick piece of aluminum honeycomb and a window screen at the inlet of the nozzle for flow uniformity.

Flow through the tunnel was measured by a Meriam 50MC2-2 laminar flow element (LFE). The LFE was capable of measuring a maximum volumetric flow rate of 2.79 m^3/min with a corresponding pressure drop of 203 mm H_20. By measuring the pressure drop across the LFE and using a pressure drop to flow rate correlation given by the manufacturer, the volumetric flow rate (Q) through the tunnel could be determined. The volumetric flow rate was used in the Reynolds number calculation,

$$Re_{L_p} = \frac{L_p Q / A_{ff}}{\nu} \tag{2.1}$$

A_{ff} was defined as

$$A_{ff} = A_{in} - t \cdot F_h \cdot n_{louver} \tag{2.2}$$

Volumetric flow rates were set for desired Reynolds numbers. For this study, the desired Reynolds numbers were Re_{Lp} = 230, 615, and 1016, as chosen by the project sponsor (Modine) to match a range of important driving speeds at which a radiator would perform. The pressure drop across the LFE was measured with a Setra model 264, 0 to 5 in H_2O pressure transducer which had an accuracy of 0.25 % full scale value (FSV). A full description of the measurement devices and techniques will be given later in this chapter.

Air was pulled through the test rig with a Dayton 3N1786 1.5 hp, 3-phase motor powering a Dayton 4C108 centrifugal fan. The fan speed was controlled with a 60 Hz Dayton 3HX72 AC inverter. The smallest increment of the inverter was 0.01 Hz which produced flow changes that were within the uncertainty of the pressure transducer mentioned earlier.

The test section was comprised of the louvered fin array, a constant heat flux heater, a conduction guard heater, top and bottom walls, and the thermocouples and pressure taps used to

make measurements. As stated earlier, the $L_l/F_h = 100\%$, $L_l/F_h = 82\%$, and $L_l/F_h = 70\%$ test sections had some dissimilarities so each test section arrangement will be discussed separately.

Full Louver Length Test Section

The test section used for the $L_l/F_h = 100\%$ testing was built and used by Ebeling and Thole (2004) in their $L_l/F_h = 100\%$ tube wall heat transfer studies. An exploded detail view of the test section can be seen in Figure 2.5. The channel for the louvered fin array was bound on top and bottom by two walls and the sides were bound by the milled lexan wall and the instrumented heated wall. The louvers can be seen extending between the two walls. On the back side of the heated wall is the guard heater assembly which reduces conductive losses.

The heated wall was a constant heat flux boundary condition that modeled the tube wall in a real louvered fin exchanger. It was made by placing 20 equally sized strip heaters side by side and applying them with double-sided tape to a 0.375 in (9.53 mm) sheet of Lexan. The heater was painted black ($\varepsilon = 0.98$) for infrared camera pictures that were done in previous studies. The entire heater spanned from the beginning of the entrance louver to the end of the exit louver and from the bottom wall to the top wall. Each strip was cut from 0.002 in (0.0508 mm) thick grade 316 stainless steel foil with average electrical resistance of 74 μΩ-cm. The strips were wired together in series to so that equal current could be supplied to each. On the top and bottom of each strip, 0.06 in (1.58 mm) thick copper bus bars were soldered to ensure a uniform current distribution throughout the foil. Each foil was measured to a resistance of $R = 0.14\ \Omega \pm 1\%$. Current through the strip heater circuit was measured by a precision resistor of $R_p = 1\ \Omega \pm 0.1\%$ that was connected in series with the heater. This current, along with the heater resistance and surface area were used to calculate the heater power flux. For each of the Reynolds numbers tested, a different power flux was required. The goal was to adjust the heater so that when the air moved through the test section, there was a 10 ˚C to 12 ˚C difference between the temperature measured at the test section inlet and at the first heated wall thermocouple. This temperature difference was chosen to reduce property variation effects in tube wall Nusselt number calculations. In order to adjust the heater power flux, an Invensys Lambda model GEN100-15, 1500W power supply was wired in series with the heater circuit and the precision resistor.

The louvers in the test section were made from 0.094 in (2.38 mm) thick balsa wood to minimize conduction losses from the heated walls. With the low thermal conductivity of balsa wood, they could be modeled as adiabatic fins. The louvers were also painted silver ($\varepsilon = 0.3$) to minimize radiation losses from the wall to the louver surfaces. The fins were attached to the heated wall by using small Lexan brackets that were adhered with double sided tape to the wall in the array geometry. The other end of the louver was held in place by a milled wall, made by the Virginia Tech machine shop, with slots matching the array geometry. To avoid air leaks through the slots, a sheet of adhesive backed rubber was placed along the entire milled wall. The test section had 12 louver rows based on studies by Lyman (2000) and Springer and Thole (1998) that showed 12 rows were required to model an infinite stack of louvers.

The louver rows were bounded by the top and bottom walls. The walls were made using wooden pieces shaped to match the geometry of the array that served to produce louver directed flow in the channel. The walls for each of the three louver lengths were geometrically dissimilar. For the $L_l/F_h = 100\%$ louver length, both walls spanned the entire width of the test section. Walls for the $L_l/F_h = 70\%$ and $L_l/F_h = 82\%$ louver lengths will be discussed in their respective sections.

Temperature measurements were made with type E thermocouples placed behind the strip heaters and pressure drop measurements were made from pressure taps on the milled wall. Details of instrumentation will be given in section 2.4.

To minimize the conduction losses through the back side of the instrumented wall, a 0.81 in (20.57 mm) thick sheet of foam of thermal conductivity, k = 0.033 W/mK, was placed directly behind it. (see Figure 2.6). On the outside of the insulation was the conduction guard heater assembly which was comprised of a 0.125 in (3.18 mm) thick aluminum sheet with thermocouples bonded on one side and patch heaters on the other side (see Figure 2.7). The thermocouples were in the same configuration as the instrumented wall thermocouples so conduction losses could be quantified with a simple one-dimensional conduction calculation. There were two patch heaters that were used to actively minimize conduction losses by matching the temperatures on the aluminum plate thermocouples to the heated wall thermocouples as closely as possible. Using the patch heaters, typically only 0.5% to 4.0% of the applied heat flux at the heated wall was lost by conduction depending on Reynolds number and streamwise location. Each patch heater was powered by a HP model 6024A, 200 W, power supply so they

could be adjusted separately. Like the strip heaters, the conduction guard heater power flux was set based on the Reynolds number of the test. On the back side of this assembly was another piece of 2 in (50.8 mm) thick foam to further reduce conduction losses.

Short Louver Length Test Sections

The L_l/F_h = 70% and L_l/F_h = 82% test sections were redesigned and built to accommodate the new fin lengths as well as to make the test section more accessible and easier to modify later. An exploded view of the test section used for the realistic fin testing can be seen in Figure 2.8. The conduction guard heater assembly is not shown in the diagram but is in the same location as seen for the L_l/F_h = 100% test section. In Figure 2.8, noticeable changes can be seen to the milled wall, top wall, and bottom wall, as well as the fins themselves. These changes will be discussed in upcoming sections.

The tube wall heater used in the L_l/F_h = 100% was replaced by a custom Kapton and Inconel constant heat flux heater made by Electrofilm Manufacturing Co. (see Figure 2.9). The heater was made by sandwiching a winding strip of Inconel between layers of Kapton. Approximately 15.67 ft (4.78 m) of 0.22 in wide Inconel was used at 0.19 Ω/ft unit resistance, giving an overall heater resistance of 2.94 Ω. On one side of the heater, a very thin copper surface was added by deposition to help spread the heat between the gaps in the Inconel. The heater was shaped to fit the channel geometry established in the L_l/F_h = 100% test section and was made with an area large enough for later testing on array geometries with larger fin pitches. The heater had a maximum heat flux of 310 W/m^2 which was high enough to produce the needed flux for the highest Reynolds number tested (Re = 1016). Since it was established by Ebeling (2003) that infrared pictures could not be taken of the tube wall, the new heater was not painted black. The shiny copper surface had a much lower emissivity (ε = 0.10) than black paint so radiation losses from the tube wall were greatly reduced. The heater was adhered to the instrumented Lexan wall with 3M tape 401B double sided paper tape of thickness 0.003 in (0.08 mm).

Due to the increased geometrical complexity of the realistic fins, they had to be specially made by a molding process at Milwaukee School of Engineering. The mold for the fins was made at Prototype Techniques, based in Milwaukee, using stereolithography. Dimensioned

drawings for the mold were sent directly from Modine to the manufacturer, and were a 20X scale replica of actual Modine fins. The fins, seen in Figure 2.10, came in pieces that were half of the test section length. Each piece formed the entrance louver, seven normal louvers, and half of the turnover louver (or half of the turnover, seven normal louvers, and the exit louver, if turned 180˚). One forward facing fin and one backward facing fin completed a full fin row. The fins were not made to be put directly in the test section, but were made universally to go in the forwards or backwards orientation. To be centered in the test section, one side was kept long to slide into the milled wall while the other side had to be cut due to the protrusion of the bracket. Once the cut was made, the louvers were centered in the test section. The fins were spray painted shiny silver (Premium Décor PDS-94 Chrome) to reduce radiation loss from the wall. Even though the plastic fins had a higher thermal conductivity than the balsa wood louvers, the conduction loss to the fins was still considered negligible compared to radiation and conduction losses through the instrumented wall.

Once again, the louvers were held in place by the milled wall and brackets. The L_l/F_h = 70% and L_l/F_h = 82% brackets and milled wall were made to fit the flat landing which did not exist on the L_l/F_h = 100% louvers. Brackets were placed in rows of fin pitch spacing that stretched the length of the heater (Figure 2.11). The slots on the milled wall started at the test section inlet and ended at the rear of the heater. By milling the wall to the entrance of the test section, fin insertion and removal became very easy, which was especially important for delta winglet testing (Figure 2.12).

The top and bottom walls were redesigned relative to the L_l/F_h = 100% walls due to the different fin geometry. The flow through the realistic fin array had two distinct regions:

1) Louver directed flow that would turn at the entrance, turnover, and exit louvers
2) Channel flow on the flat landings that would continue straight through the test section without turning

It was important to allow each of these flow regions to take a periodic course as they would in a real heat exchanger. To facilitate this, the bottom wall was made to angle only over the louver length while the sides remained flat and straight (Figure 2.13). When the L_l/F_h = 82% louver length fins were used, two extra pieces were attached to the outside of the 70% wall to provide the necessary extra width. Figure 2.14 shows the side piece additions and their orientation with respect to the bottom wall. Since the angled portion of the bottom wall no longer extended to the

tube wall, the custom heater shape did not match. The heater was moved down to avoid a large unheated portion on the wall. The top wall was shaped the same as it was in the $L_l/F_h = 100\%$ test section, however, the flat landings of the fins placed within the angled portions of the top flow wall were blocked to allow only louver directed flow (Figure 2.15). This was done because there was no inlet air to these fins to produce a flat landing flow. All of the air in this area of the test section would be forced up by the louvers and the bottom flow forcer. The flat landings were blocked off using 1 in (25.4 mm) thick foam custom cut to fit a particular louver length and fin. Both walls were made less than the channel width to allow room for adhesive-backed 0.19 in (0.48 mm) thick rubber on either side that prevented air leaks from the channel (see Figure 2.11).

The instrumented wall was remade with a different setup than the $L_l/F_h = 100\%$ wall. The wall was created with 0.5 in (12.7 mm) thick Lexan instead of the 0.375 in (9.53 mm) thick Lexan used in the $L_l/F_h = 100\%$ test section. The conduction guard heaters were the same used in the $L_l/F_h = 100\%$ test section and were applied to the aluminum plate in the same manner. Thermocouple and pressure tap placement will be discussed in section 2.4.

2.3 Winglets setup

The second goal of this study was to find a way to augment the heat transfer on the tube wall while quantifying the augmentation in heat transfer and pressure drop. Based on results shown in the literature, delta winglets were chosen for this study as a promising method for tube wall augmentation with a relatively minor increase in pressure drop. Delta winglets, not to be confused with delta wings, are triangular shaped pieces that are either applied to or stamped and bent from a surface (Figure 2.16). The winglet enhances heat transfer by producing a single longitudinal vortex that thins the thermal boundary layer on the surface of application and mixes the bulk fluid in a given flow region. The delta winglet normally has two different parameters that can be altered to influence heat transfer and pressure drop performance. These two parameters are aspect ratio (AR) and angle of attack (AOA). AR is a means of quantifying the relative lengths of the sides of the triangle and is defined as

$$AR = \frac{4(b/2)}{c} \tag{2.3}$$

The definition is slightly vague in that the same AR can be achieved with two combinations of winglet height and length. In this study, all of the winglets had the same height of 0.29 in (7.5 mm, $0.27L_p$) and the winglet length was changed to vary the AR. For the $L_l/F_h = 100\%$ tests, ARs of 1.5, 2, and 3 were chosen with AR = 1.5 being the largest winglet by the definition in Equation 2.3. Table 2.1 gives dimension of the winglets and Figure 2.17 shows the relative sizes of winglets at the different ARs. Rectangular winglets that were twice the surface area of the AR = 1.5 winglets with the same height were also tried in a few tests for the $L_l/F_h = 100\%$ geometry. For the $L_l/F_h = 70\%$ tests, only the AR = 1.5 delta winglet was used and no winglet tests were completed for the $L_l/F_h = 82\%$ geometry.

The AOA is the angle of the winglet with respect to the incoming air flow (Figure 2.18). The AOAs used for the $L_l/F_h = 100\%$ tests were 20°, 30°, and 40° while only the 40° AOA was used for the $L_l/F_h = 70\%$ tests.

As mentioned earlier, AR and AOA were often the only geometric parameters that were varied in past winglet studies. In this study however, there were four other geometric parameters that were tested: distance from wall (DFW), winglet orientation, winglet direction, and winglet thickness. The DFW parameter describes the distance between the heated wall and the part of the winglet in closest proximity (Figure 2.18). This parameter does not apply in any other study where winglets were placed in the middle of a flat plate, in the middle of a flat plate in a channel, or in the middle of a flat plate in a tube-fin heat exchanger. All of these studies measured the heat transfer enhancement on the surface to which the winglet was applied due to the lack of a second nearby surface. In this study, however, the winglets were placed on the fins while the heat transfer enhancement was measured on the heated wall (Figure 2.18). The DFWs chosen for the $L_l/F_h = 100\%$ tests were $0.15L_p$, $0.22L_p$, and $0.29L_p$ while all of the $L_l/F_h = 70\%$ tests were done at DFW = $0.22L_p$. The $0.15L_p$ distance was chosen as the smallest DFW value because the brackets protruded from the wall by this distance.

Although initially only winglets in the normal orientation (large end of winglet downstream) were to be tested, many tests were done with the winglets placed backwards with respect to the incoming flow (Figure 2.19). These two orientations will be referred to in the rest

of this document as vortex generators forwards (VG-F) and backwards (VG-B). Winglet direction describes whether the downstream portion of the winglet is aimed towards or away from the heated wall. Finally, two different winglet thicknesses were used in the experiments. The majority of the $L_l/F_h = 100\%$ winglet tests were done with 0.003 in (0.08 mm, 0.03t) thick Inconel winglets (Figure 2.20). If winglets were used in a real heat exchanger, they would be stamped and bent out of the fin material, making them the same thickness as the fin. Therefore, some of the $L_l/F_h = 100\%$ tests were done with 0.105 in (1.6 mm, 1.03t) thick balsa wood winglets which were much closer to the fin thickness (Figure 2.20). All of the $L_l/F_h = 70\%$ tests were done with 0.063 in (1.6mm, 0.69t) winglets. Overviews and details of the parameters tested will be given in the results chapters. The Inconel winglets were too thin to attach to the fin, so an extra attachment was included when the winglets were cut out. The winglet was bent 90° to this extra material which was taped to the louvers with 3M Scotch® tape 137, 0.002 in (0.05 mm) thick double-sided tape. To ensure repeatable winglet placement, an apparatus was made that defined winglet placement for all combinations of AOA and DFW (Figure 2.21). When the thick winglets were tested for the $L_l/F_h = 100\%$ geometry, they were first glued to the Inconel winglets.

The setup for the $L_l/F_h = 70\%$ geometry tests was completely different from that of the $L_l/F_h = 100\%$ tests. Strips of paper with lines that defined correct winglet spacing and angle were drawn in AutoCAD (Figure 2.22). These strips were taped to file folder paper for strength and then to the flat landings on the fins. Finally, one more layer of double-sided tape was applied on top of the strips so the winglets could be applied. The winglets were stuck to the tape on edge with no extra material for support. The DFW could be changed by moving the strips closer to or further from the wall. It is also important to mention that all the tests were done with solid fins. No holes were cut out to match the holes that would be left by a real stamping and bending process.

So far, the parameters mentioned have only dealt with the geometry and placement of a single delta winglet. By placing multiple winglets in series, as done in this study, there were additional parameters that dealt with the overall winglet setup. Several different setups were tested, including aiming all winglets toward the wall, alternating the winglet direction of every other winglet, using winglets at every louver position, using winglets at half of the louver positions, putting winglets on the underside of the louvers, and various others. These specific tests will be covered in greater detail in later chapters.

All tests were completed with winglets on both sides of the louvers (heated wall side and milled wall side) and on every fin row for accurate pressure drop measurements. The obvious exception to this was in the top flow forcer section for the realistic fins because the flat landing was blocked off.

2.4 Instrumentation

The thermocouple arrangement for the $L_l/F_h = 100\%$ was the same used by Ebeling and Thole (2004) (see Figure 2.23). It consisted of 20 center channel thermocouples, 10 top periodic thermocouples, and 10 bottom periodic thermocouples, all centered with respect to F_p and L_p. All thermocouples were type E and were made with a thermocouple welder to reduce bead impurities. Temperature measurements for convection calculations were only collected from the center channel thermocouples while the periodic thermocouples were used to test Nusselt periodicity in the pitch. The condition for periodicity was the Nusselt number calculated for the top, center, and bottom thermocouples at a given streamwise location could not be more than 5% different than the average of the three. Ebeling and Thole (2004) found that the channel was periodic with the exception of the entrance and turnover louvers where strong gradients dominate. Holes for the thermocouples were drilled into the back side of the instrumented Lexan wall and were filled with Omega Bond 400 before the thermocouples were put in place (Figure 2.24). Omega Bond is a high thermal conductivity paste that was used to ensure good thermal contact between the heater and the thermocouple bead. As mentioned earlier, another set of thermocouples of identical setup were bonded to the guard heater aluminum plate to quantify conduction losses through the back side of the instrumented Lexan wall. These thermocouples can also be seen in Figure 2.24.

The changes in geometry related to the $L_l/F_h = 70\%$ and $L_l/F_h = 82\%$ test section required that the thermocouple arrangement be changed to obtain periodic conditions around the center channel thermocouples. The periodicity requirements and results for the $L_l/F_h = 70\%$ and $L_l/F_h = 82\%$ test section will be discussed in section 2.8, however, the thermocouple arrangements that produced periodic results can be seen in Figure 2.25. The thermocouples were applied to the back side of the heater and the aluminum guard heater plate in the same manner as they were in the $L_l/F_h = 100\%$ test section.

All of the thermocouples in this study were wired to an Omega thermocouple panel. Omega plugs were inserted into the panel and run to the DAQ chassis with shielded thermocouple wire to avoid interference from nearby electromagnetic noise sources.

Pressure drop measurements through the louvered array were made from a pressure tap $0.73L_p$ upstream of the entrance louver and one $0.73L_p$ downstream of the exit louver (see Figure 2.26). The pressure taps were made from hollow copper tubing and were sealed flush to the milled wall with silicone. A Setra model 264, 0 to 0.1 in H_2O pressure transducer with 0.25% FSV accuracy was used to measure the pressure drop through the louvered array. This was the smallest range of any commercially available pressure transducer, however, pressure drop measurements were so small that there were problems with taking accurate measurements. Typical pressure drop values for Re=1016, 615, and 230 were on the order of 0.004 in H_2O, 0.002 in H_2O, and 0.0006 in H_2O. Details of the errors associated with the pressure drop through the louvered array will be discussed in section 2.7.

2.5 Data Acquisition Hardware and Data Collection Techniques

The data acquisition hardware used was a SCXI-1000 chassis into which three SCXI-1102 modules and one SCXI-1100 module were inserted. The SCXI-1102 modules were coupled with SCXI-1303 terminal blocks which were made for thermocouple readings and provided cold junction temperature compensation for more accurate measurements. An SCXI-1300 was inserted into the SCXI-1100 module for pressure transducer, tube wall heater, and conduction guard heater voltage measurements. The chassis was connected to a 16 bit PCI-MIO-16XE-50 DAQ card. Codes were written in LabView 7.0 to acquire temperature and pressure drop measurements. One code was written to obtain thermocouple readings, the LFE pressure drop, and the voltages from the tube wall and conduction guard heaters. A separate code was written to collect pressure drop measurements through the channel.

Once the tunnel was at steady state, 200 temperature measurements were taken and averaged at each of the center channel thermocouple locations. Steady state was found by taking temperature measurements at one, two, three, four, and five hours and comparing the average Nusselt numbers at a given hour with the previous hour, as given in the following equation:

$$Nu_{\%difference} = \frac{Nu - Nu_{previoushour}}{Nu_{previoushour}} \tag{2.4}$$

The results of these hourly tests for $L_l/F_h = 70\%$ and $L_l/F_h = 82\%$ can be seen in Table 2.2. Steady state was chosen as four hours because of the small percent change in average Nusselt number from four to five hours. Although times to achieve steady state for the $L_l/F_h = 100\%$ tests are not shown, all $L_l/F_h = 100\%$ data was taken after four hours as well. Much care was taken to obtain data at the four hour mark and results were very repeatable. Once all temperatures, heater voltages, and the LFE pressure drop were collected, they were written to a file for later use in calculating the test Reynolds number and Nusselt numbers.

Although Reynolds number had no direct bearing on the calculation of Nusselt numbers, as will be seen in the next section, it still had a large impact on the tube wall heat transfer. Therefore, Reynolds numbers for heat transfer tests were typically matched to the goal Reynolds number to within Re = ± 2. If the Reynolds number was much higher or lower than these bounds, the test was rerun.

To obtain pressure drop measurements through the louvered array and the LFE, 1500 and 500 samples, respectively, were taken and averaged. Typically, six 1500 sample measurements were made and averaged together to obtain the louvered array pressure drop at each Reynolds number. Pressure transducers were re-zeroed everyday because room temperature, which typically changed daily depending on other lab activities, affected the zero point. All of the pressure drop measurements were completed with the heaters turned off to avoid other complications with air temperature. Reynolds numbers for the pressure drop measurements were always matched to within Re = ±0.5 of the target Reynolds number before data was collected.

2.6 Data Reduction

The previous section described the methods used to collect the temperature and pressure drop measurements. This section will detail the steps taken to convert this raw data into Nusselt

numbers and friction factors, as well as how heat transfer and friction factor augmentations were defined.

The heat transfer data was broken into two different parts: localized Nusselt numbers at each of the thermocouple locations and an averaged Nusselt augmentation percentage for the winglet tests. To isolate the convective heat transfer coefficient at a given location, the losses due to conduction through the instrumented wall and radiation from the heater had to be accounted for. Therefore, the Nusselt number at each discrete location was defined as

$$Nu(X) = \frac{q''_{heater} - q''_{conduction}(X) - q''_{radiation}(X)}{T_{wall}(X) - T_{inlet}} \frac{L_p}{k_{air}} \tag{2.5}$$

where,

$$q''_{heater} = \frac{I_{heater} V_{heater}}{A_{heater}} \tag{2.6}$$

$$q''_{conduction}(X) = \frac{T_{wall}(X) - T_{guard}(X)}{L_{lexan}/k_{lexan} + L_{foam}/k_{foam}} \tag{2.7}$$

$$q''_{radiation}(X) = \frac{\sigma(T_1(X)^4 - T_2^4)}{\frac{1-\varepsilon_1}{\varepsilon_1} + \frac{1}{F_{12}} + \frac{1-\varepsilon_2}{\varepsilon_2}} + 2\left[\frac{\sigma(T_1(X)^4 - T_3^4)}{\frac{1-\varepsilon_1}{\varepsilon_1} + \frac{1}{F_{13}} + \frac{1-\varepsilon_3}{\varepsilon_3}}\right] \tag{2.8}$$

The thermal conductivity and viscosity of air was interpolated using the film temperature, T_{film}, defined as:

$$T_{film} = \frac{\frac{T_{wall}(X=0) + T_{inlet}}{2} + \frac{T_{wall}(X=1) + T_{inlet}}{2}}{2} \tag{2.9}$$

Equation 2.9 is based on a flat plate boundary layer formulation which applies because the boundary layers from the heated wall and the milled wall do not meet to form a channel flow.

Equation 2.8 is a radiation network equation applied to the test section setup. In equation 2.8, subscript 1 refers to the heated wall, subscript 2 refers to the milled wall, and subscript 3 refers to the fin surface. For this calculation, T_2 and T_3 were assumed equal to the inlet temperature. The view factors F_{12} and F_{13} were found using the view factor equations in Modest (2003) as well as the law of reciprocity. F_{12} and F_{31} were defined as

$$F_{12} = (1+H^2)^{0.5} - H \tag{2.10}$$

$$F_{31} = 0.5\left[1 + H_2 - (1+H_2{}^2)^{0.5}\right] \tag{2.11}$$

Where H_2 is the reciprocal of H. Equation 2.8 was applied at every streamwise thermocouple position to obtain losses at each location.

This method of calculating the radiation losses from the heated wall was chosen over the radiation correction factor used in the studies of Ebeling and Thole (2004) because similar results were obtained for baseline tests but this method could be extended to the winglet studies. The Nusselt numbers for winglet tests vary widely, so using a method where radiation losses can be calculated for each test case was desirable.

For each of the louver lengths and Reynolds numbers, baseline heat transfer measurements were taken at each of the 20 center channel thermocouple locations. In order to calculate the overall average Nusselt augmentation, the augmentation at each of the streamwise locations is first determined:

$$Nu_{aug}(X) = \frac{Nu(X) - Nu_0(X)}{Nu_0(X)} = \frac{Nu(X)}{Nu_0(X)} - 1 \tag{2.12}$$

where Nu_0 refers to baseline Nusselt number. The $Nu_{aug}(X)$ values were then averaged to get the overall average Nusselt augmentation:

$$Nu_{aug} = \overline{Nu_{aug}(X)} \tag{2.13}$$

The vast majority of tests did not include winglets on the entrance louver, so the Nusselt numbers at X=0.025 and 0.075 were usually not used in the averages. By excluding these two points, Nu_{aug} only reflects the average over the winglet affected region. For the few cases where entrance louver winglets were used, these points were used in the average.

The pressure drop measurements through the array were converted to Fanning friction factors with the following equation,

$$f = \frac{D_H}{4F_d}\left(\frac{2\Delta P}{U_{ff}{}^2 \rho_{air}} - K_c - K_e\right) \tag{2.14}$$

where K_c and K_e are loss coefficients of the sudden contraction and expansion associated with the air entering and leaving the finned array. Both coefficients were found to be 0.03 by using a duct area reduction and expansion chart (White 1999). U_{ff} is the maximum air velocity through the test section. F_d is the fin depth and is defined by the distance from leading edge of the entrance louver to the trailing edge of the exit louver. The hydraulic diameter, D_H, is defined as

$$D_H = \frac{4 \cdot A_{ff}}{P_{wetted}} = \frac{4(F_p - t)F_h}{2(F_p - t) + 2F_h} \tag{2.15}$$

Friction factor augmentation was simply defined as

$$f_{aug} = \frac{f - f_0}{f_0} = \frac{f}{f_0} - 1 \tag{2.16}$$

where f_0 was the baseline friction factor.

2.7 Uncertainty Estimates

The uncertainties of experimental Nusselt numbers, Reynolds numbers, and friction factors were calculated using the method developed by Kline and McClintock (1953) which is

based on the chain rule of differentiation. Consider some quantity y that is a function of several variables

$$y = f(x_1, x_2, x_3, ..., x_n)$$

The error associated with y is given as

$$dy = \left[\left(\frac{\partial y}{\partial x_1} dx_1 \right)^2 + \left(\frac{\partial y}{\partial x_2} dx_2 \right)^2 + ... + \left(\frac{\partial y}{\partial x_n} dx_n \right)^2 \right]^{1/2} \tag{2.17}$$

where each of the dx terms is a combination of bias and precision uncertainties. The most basic forms of the Nusselt number, Reynolds number, and friction factor equation were used so that the errors associated with the directly measured quantities could be found. For example, the Nusselt number equation used was,

$$Nu = \frac{\dfrac{V_p \cdot V_{heater}}{R_p \cdot A_{heater}} - \left[\dfrac{\sigma \cdot \left(T_{wall}^{\,4} - T_{inlet}^{\,4} \right)}{\dfrac{1-\varepsilon_1}{\varepsilon_1} + \dfrac{1}{F_{14}} + \dfrac{1-\varepsilon_4}{\varepsilon_4}} + 2 \cdot \dfrac{\sigma \cdot \left(T_{wall}^{\,4} - T_{inlet}^{\,4} \right)}{\dfrac{1-\varepsilon_1}{\varepsilon_1} + \dfrac{1}{F_{13}} + \dfrac{1-\varepsilon_3}{\varepsilon_3}} \right] - \dfrac{T_{wall} - T_{guard}}{\dfrac{L_{lexan}}{k_{lexan}} + \dfrac{L_{foam}}{k_{foam}}}}{T_{wall} - T_{inlet}} \cdot \frac{L_p}{k_{air}} \tag{2.18}$$

The thermal conductivities were the only quantities that were not accounted for in the error analysis because this information was not available.

Basic forms of the friction factor, friction factor augmentation, Reynolds number, average Nusselt augmentation, and efficiency index equations were also found. Table 2.3 gives uncertainties in these values, winglet tests with high heat transfer augmentation, and winglet tests with low augmentation at Re = 230 and 1016 for L_l/F_h = 70%. The Nusselt number uncertainties are given at three discrete locations (X = 0.025, 0.475, and 0.975) to give the range of possible errors. Reynolds number and friction factor are not dependent on streamwise position, so there is only one value given for each of these quantities.

2.8 Benchmarking the Test Sections

The test facility used in this study was the same used by Lyman (2000) with the exception of the changes to louver length, so benchmarking related to inlet flow uniformity and number of louvers necessary to assume an infinite stack of louvers was not repeated. The benchmarking done for heat transfer measurements involved confirming periodicity in the pitch for the L_l/F_h = 70% and L_l/F_h = 82% test section and comparing L_l/F_h = 100% baseline results to those shown by Ebeling and Thole (2004). Friction factor results were compared to actual heat exchanger data sent by Modine as well as CFD results reported by Tafti and Cui (2003). No pressure drop measurements were made by past students on this project for a direct comparison.

Before the winglet testing began, baseline heat transfer results for L_l/F_h = 100% were compared to Ebeling and Thole's (2004) to make sure the test section and the students were behaving consistently. Comparisons of the baseline results for all three Reynolds numbers can be seen in Figure 2.27. Ebeling and Thole's (2004) results have been reanalyzed to account for the new radiation loss calculation method. The absolute relative percent differences between my results and Ebeling and Thole's (2004) corrected results were 4.56%, 5.58%, and 2.95% for Re = 1016, 615, and 230 respectively. Variations in the data may be due to the difference in data collection time. Ebeling took data three hours after each test was started while data in this study was collected after four hours. In general, results taken at 3 hours are higher than those at four hours, especially upstream of the turnover louver.

Flow periodicity was tested for the L_l/F_h = 70% and L_l/F_h = 82% test section like Ebeling and Thole (2004) had done for the L_l/F_h = 100% test section. Thermocouples were placed one F_p above and below the center channel thermocouples at the locations shown in Figure 2.25. The condition set for periodicity was that the Nusselt number calculated at the top, center, and bottom thermocouples at each streamwise location must be less than 5% different than the average of all three Nusselt numbers at the same streamwise location. Periodicity results for the L_l/F_h = 70% setup for Re=1016, 615, and 230 can be seen in Figures 2.28 through 2.30 respectively. The Nusselt numbers as well as the percent differences in the Nusselt numbers at each thermocouple location compared to the average Nusselt number at all three thermocouple locations are given. Figures 2.28 through 2.30 show that there was less than 4% variation in Nusselt number at all of the periodicity points, which was below the 5% condition for periodicity. After running these tests, it was assumed that the test section setup accurately modeled an infinite stack of louvers.

Friction factor results can be seen compared to Modine data for the same louvered array geometry in Figure 2.31. The data taken for the L_l/F_h = 100% geometry over predict while the L_l/F_h = 70% and L_l/F_h = 82% under predict Modine's results. It is believed that the L_l/F_h = 70% and L_l/F_h = 82% friction factors are lower than the Modine data because our test section does not model the tubes that exist in a real exchanger. Tafti and Cui's (2003) studies relating friction factor to louver length showed an increase in friction factor with increasing L_l/F_h. Although certain test parameters do not match Tafti and Cui's (2003) well enough for a direct comparison, the trends of the results are the same, explaining why the L_l/F_h = 100% results are much higher than the realistic louver results.

Repeatability of heat transfer and friction factor measurements was proven often during the course of testing. Heat transfer tests were very repeatable, while friction factor tests were only repeatable at Re = 1016 and Re = 615, due to the large associated uncertainty with Re = 230 tests. Examples of heat transfer and friction factor repeatability for L_l/F_h = 82% baseline tests at all three Reynolds numbers can be seen in Figures 2.32 and 2.33. The names of the lines in the plots are given as "Date_Re_L_l/F_h". The heat transfer tests shown in Figure 2.32 were run nearly four months apart, showing very good repeatability. The absolute relative percent differences in the average Nusselt numbers for these two tests is 1.2%, 0.2%, and 2.0% for Re = 1016, 615, and 230 respectively.

The friction factor results for L_l/F_h = 82% shown in Figure 2.33 also show good repeatability at Re = 1016, but get worse with decreasing Reynolds number. The absolute relative percent differences in the friction factors for the two tests shown are 0.02%, 8.5%, and 60.4% for Re = 1016, 615, and 230 respectively. For a given Reynolds number, the error bars of the two points overlap, meaning that differences in results fall within experimental uncertainty.

Table 2.1 Height and Lengths Used to Determine AR

AR	b/2		c	
1.5	$0.268L_p$	7.5 mm	$0.716L_p$	20 mm
2	$0.268L_p$	7.5 mm	$0.537L_p$	15 mm
3	$0.268L_p$	7.5 mm	$0.358L_p$	10 mm

Table 2.2 Percent Differences in Average Nusselt Number by Hour

L_l/F_h = 82%

	% Difference in Average Nusselt Number from Previous Hour			
Re	2 hours	3 hours	4 hours	5 hours
230	-21.74%	-8.02%	-3.71%	-1.47%
1016	-20.69%	-6.28%	-2.64%	-0.51%

L_l/F_h = 70%

	% Difference in Average Nusselt Number from Previous Hour			
Re	2 hours	3 hours	4 hours	5 hours
230	-22.34%	-9.55%	-3.76%	-0.43%
1016	-19.10%	-5.69%	-2.56%	-0.78%

Table 2.3 Representative Uncertainty Estimates for Calculated Values

		Baseline Uncertainties					
		Re = 230			Re = 1016		
X		Value	Uncertainty	Uncertainty [%]	Value	Uncertainty	Uncertainty [%]
0.025	Nu_0	10.48	0.67	6.38	16.77	0.77	4.57
0.475		4.83	0.21	4.27	6.58	0.17	2.60
0.975		5.93	0.26	4.44	8.21	0.23	2.83
	f_0	0.19	0.10	51.40	0.06	0.01	8.20

		Representative Winglet Uncertainties for Low Augmentation					
		Re = 230			Re = 1016		
X		Value	Uncertainty	Uncertainty [%]	Value	Uncertainty	Uncertainty [%]
0.025	Nu	10.701	0.685	6.401	16.509	0.728	4.409
0.475		5.057	0.22	4.341	7.537	0.203	2.697
0.975		4.846	0.203	4.186	7.881	0.216	2.737
	Avg. Nu_{aug}	-0.033	0.06	-183.243	0.072	0.041	57.196
	f	0.152	0.093	61.433	0.075	0.005	6.8
	f_{aug}	-0.187	0.652	-349.089	0.212	0.129	60.823
	η	0.175	0.688	394.26	0.339	0.283	83.492

		Representative Winglet Uncertainties for High Augmentation					
		Re = 230			Re = 1016		
X		Value	Uncertainty	Uncertainty [%]	Value	Uncertainty	Uncertainty [%]
0.025	Nu	10.18	0.622	6.109	16.51	0.73	4.41
0.475		5.04	0.215	4.263	7.54	0.20	2.70
0.975		5.549	0.239	4.301	7.88	0.22	2.74
	Avg. Nu_{aug}	0.013	0.062	476.136	0.07	0.04	57.20
	f	0.195	0.096	49.203	0.07	0.01	7.20
	f_{aug}	0.041	0.74	1821.926	0.14	0.13	87.42
	η	0.321	6.036	1883.115	0.50	0.53	104.47

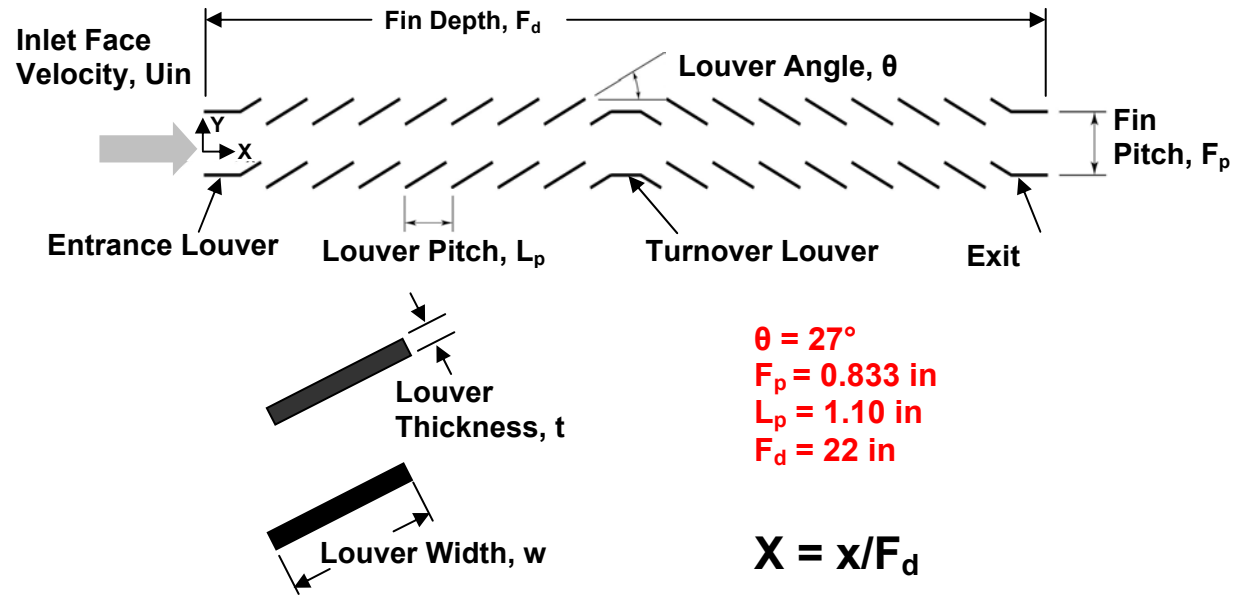

Figure 2.1 Louvered array geometry and definitions used in this study.

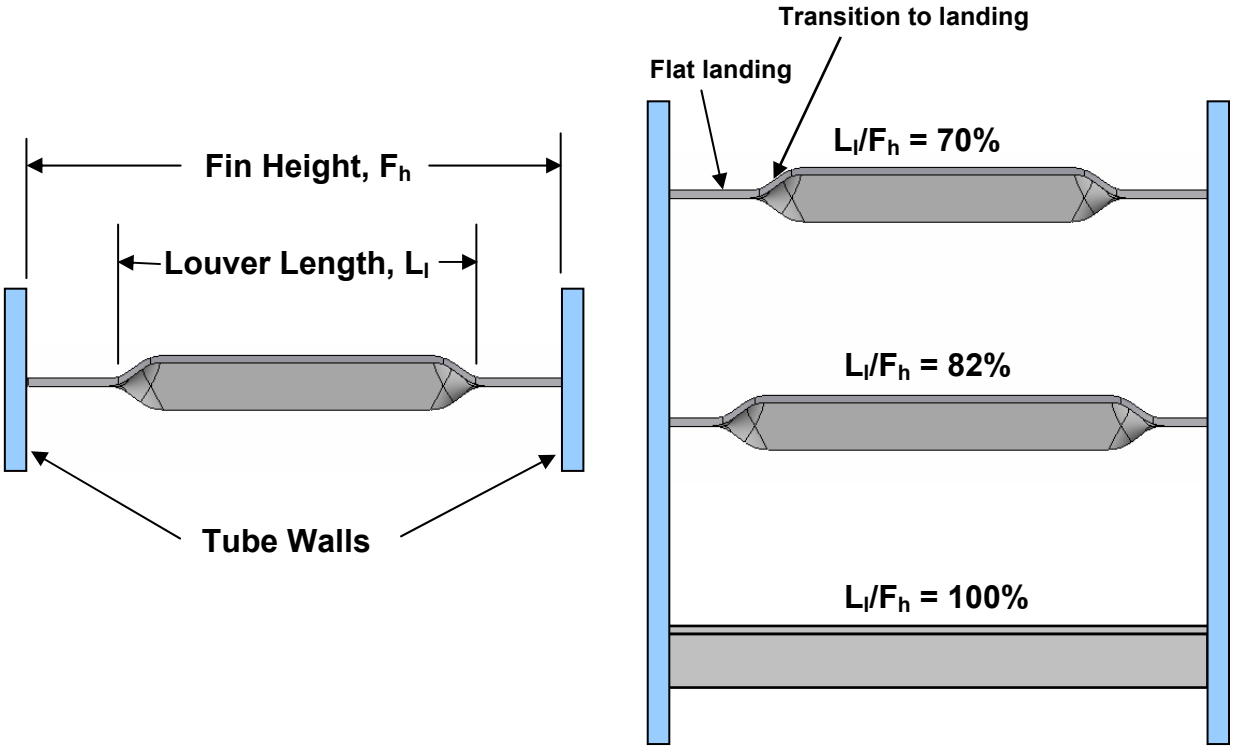

Figure 2.2 Comparison of different louver lengths and definitions of geometries.

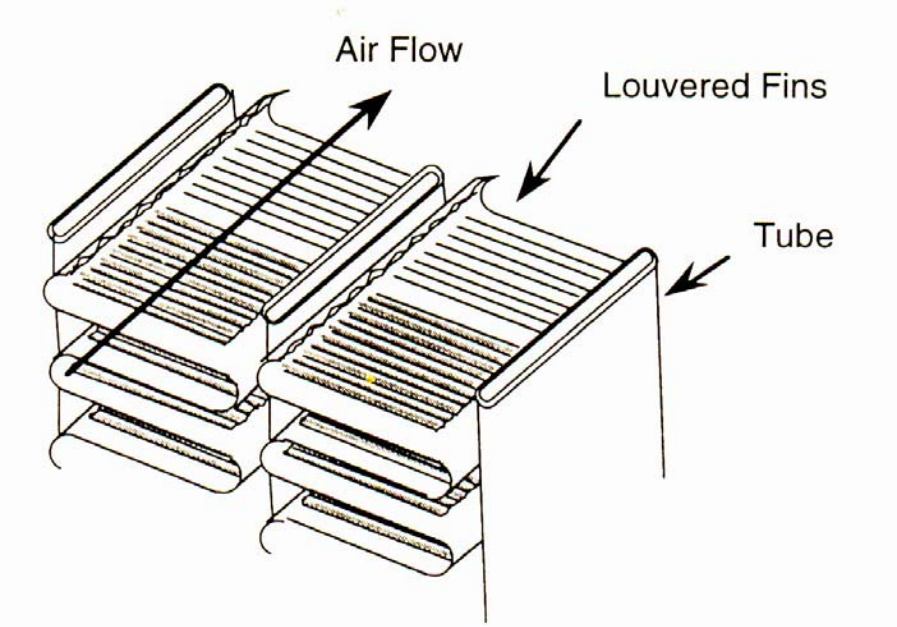

Figure 2.3 Diagram of realistic louvered fin heat exchanger.

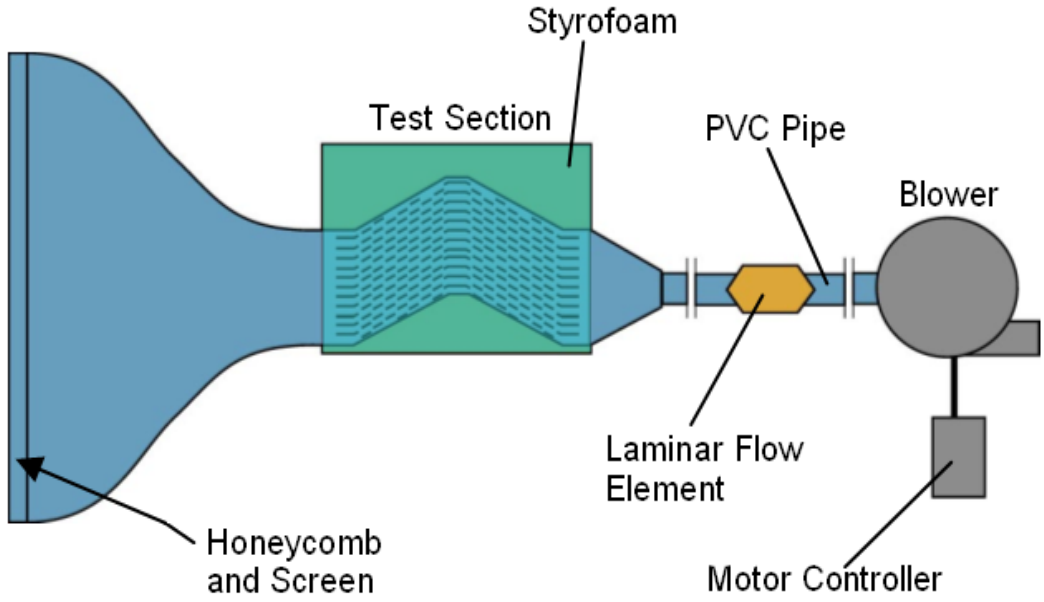

Figure 2.4 Test facility components.

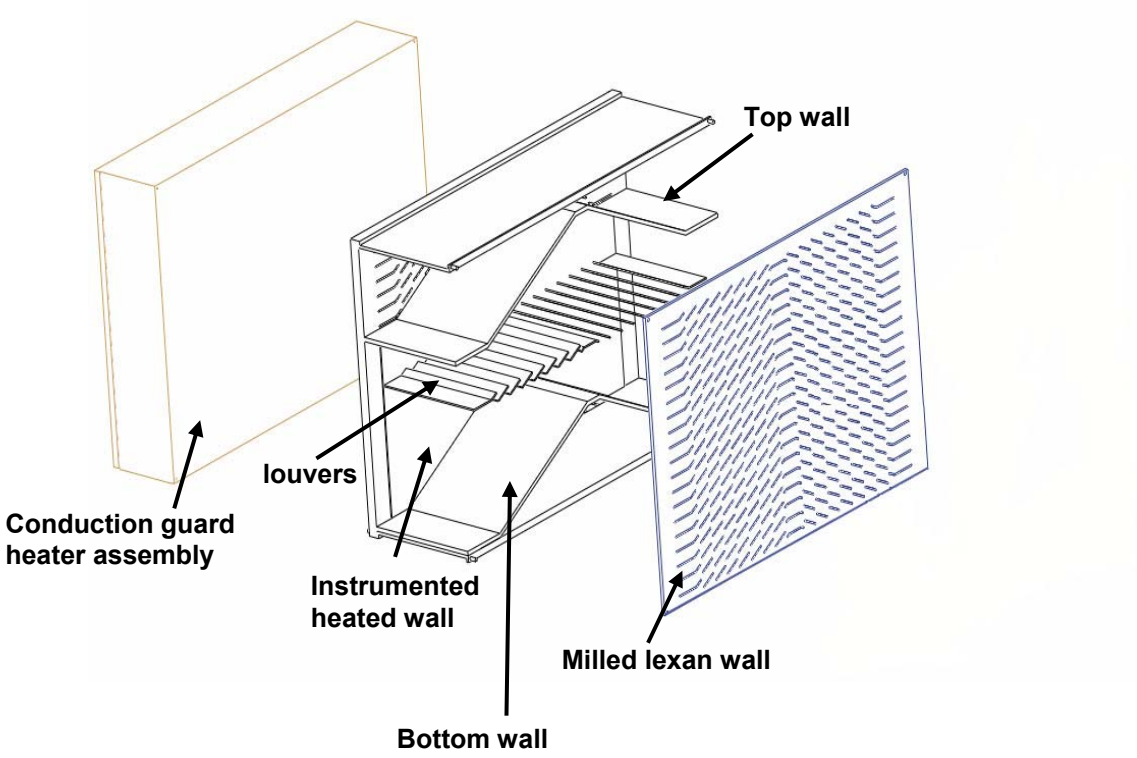

Figure 2.5 Exploded view of the L_l/F_h = 100% test section (Ebeling and Thole, 2004).

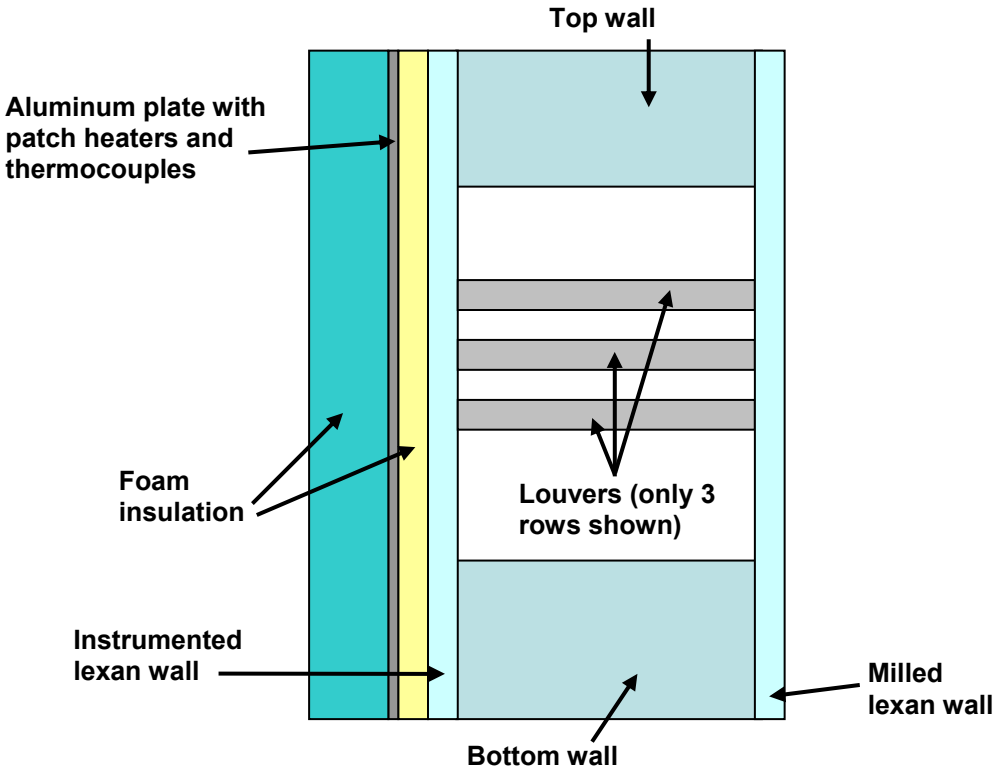

Figure 2.6 Conduction guard heater assembly components.

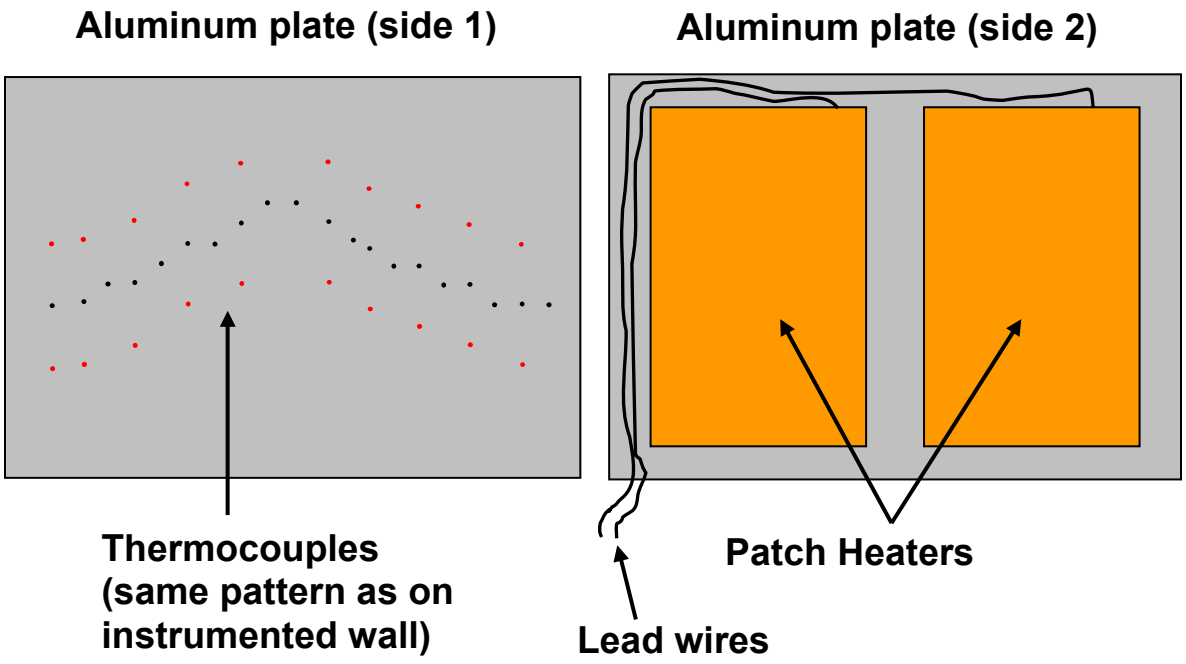

Figure 2.7 Conduction guard heater and guard heater thermocouples.

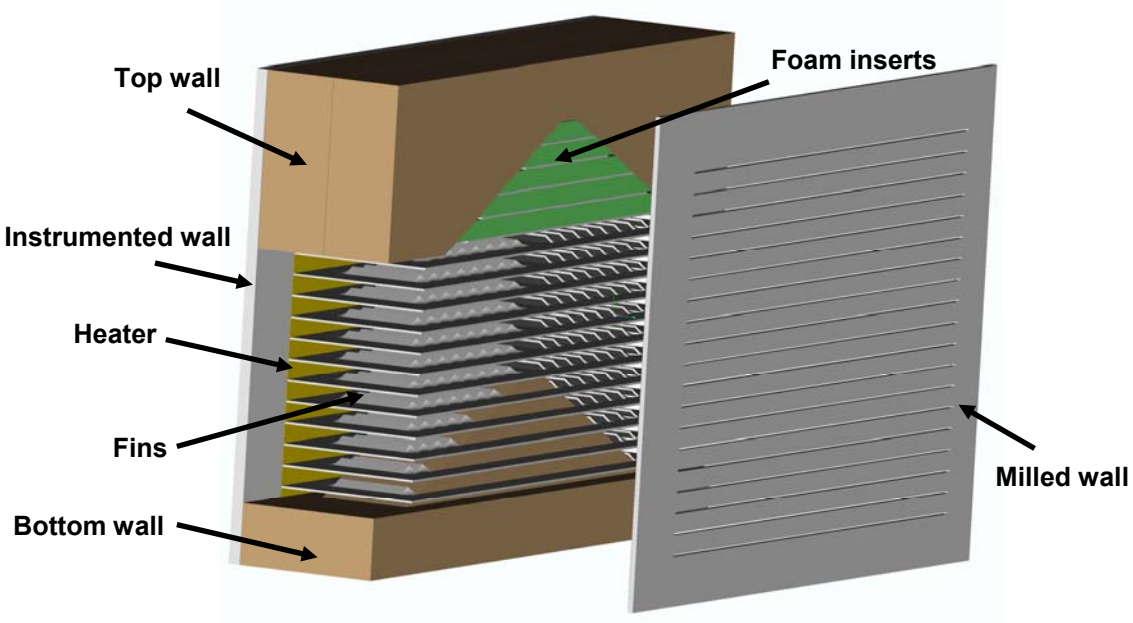

Figure 2.8 Exploded view of the L_l/F_h = 70% and L_l/F_h = 82% test section.

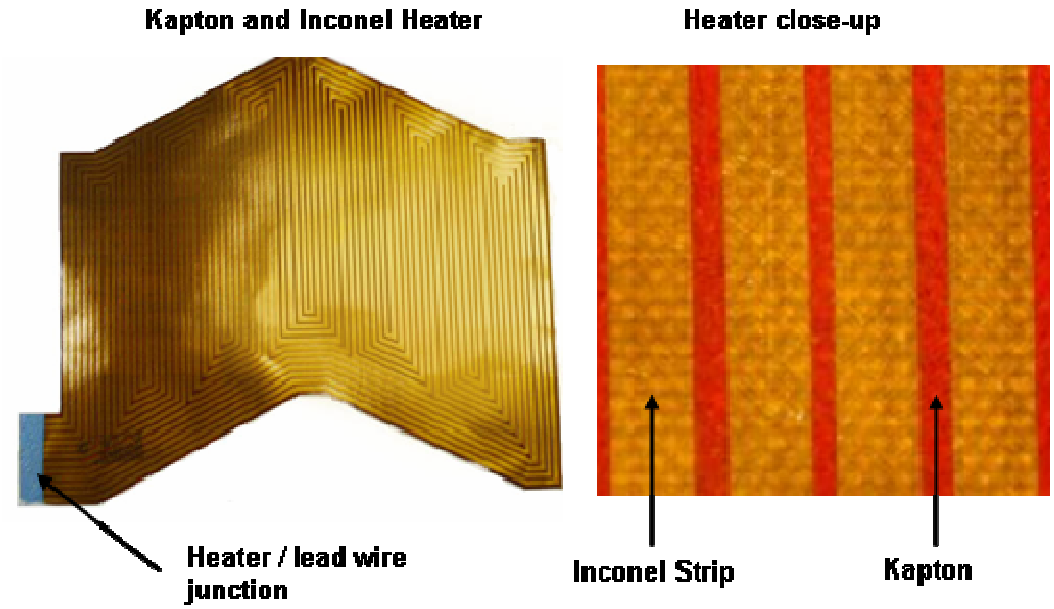

Figure 2.9 Custom Inconel/Kapton constant heat flux heater.

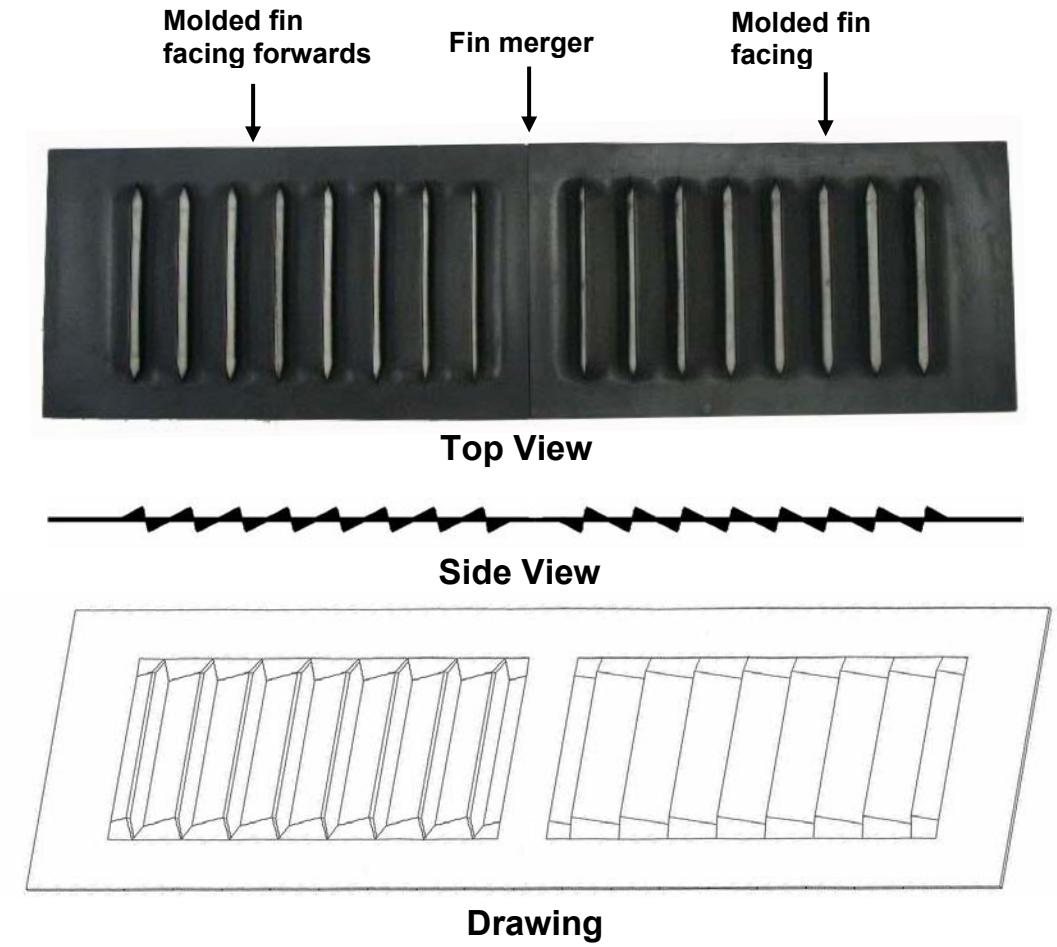

Figure 2.10 Top view, side view, and drawing of realistic molded fin.

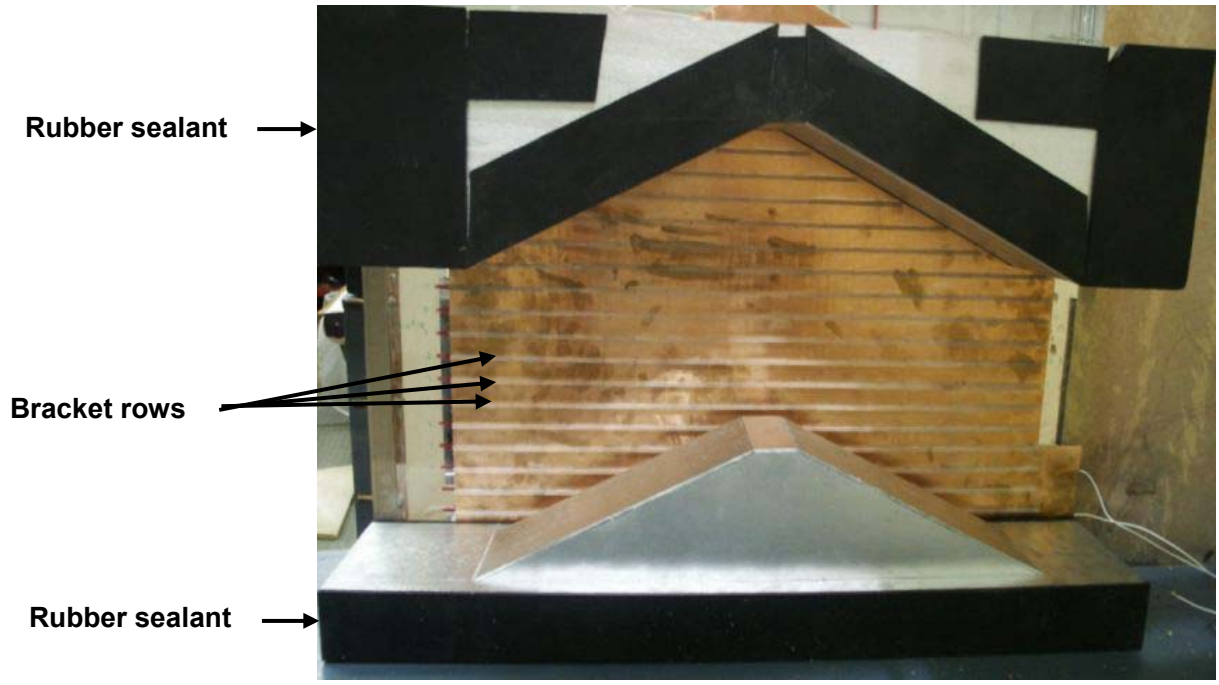

Figure 2.11 L_l/F_h = 70% and L_l/F_h = 82% test section side view showing fin brackets and rubber seals.

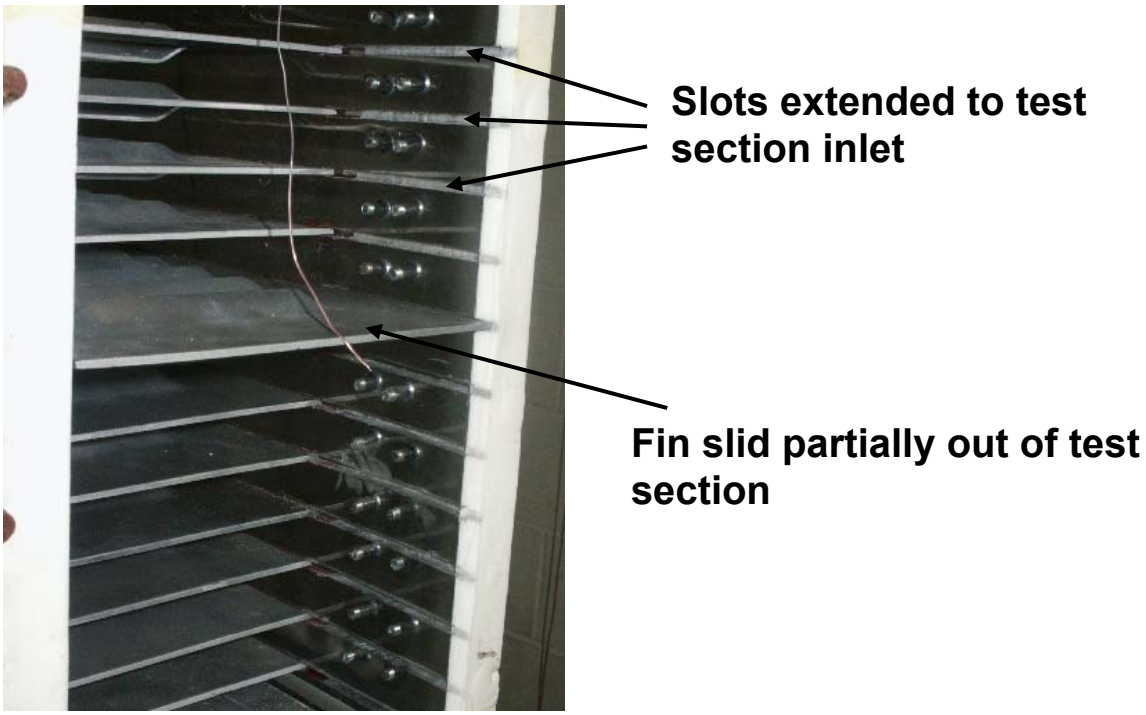

Figure 2.12 View of test section inlet showing slots for easy fin removal.

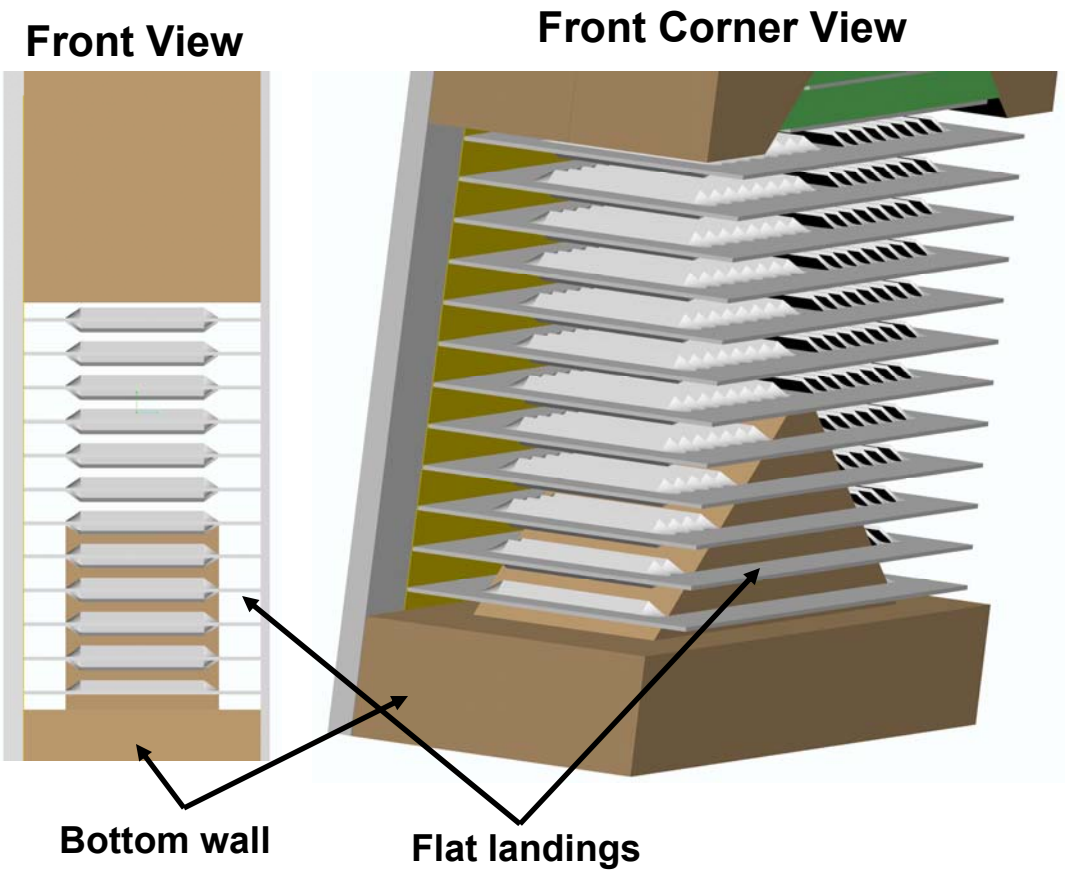

Figure 2.13 Diagrams showing geometric features of the bottom wall and surrounding fins.

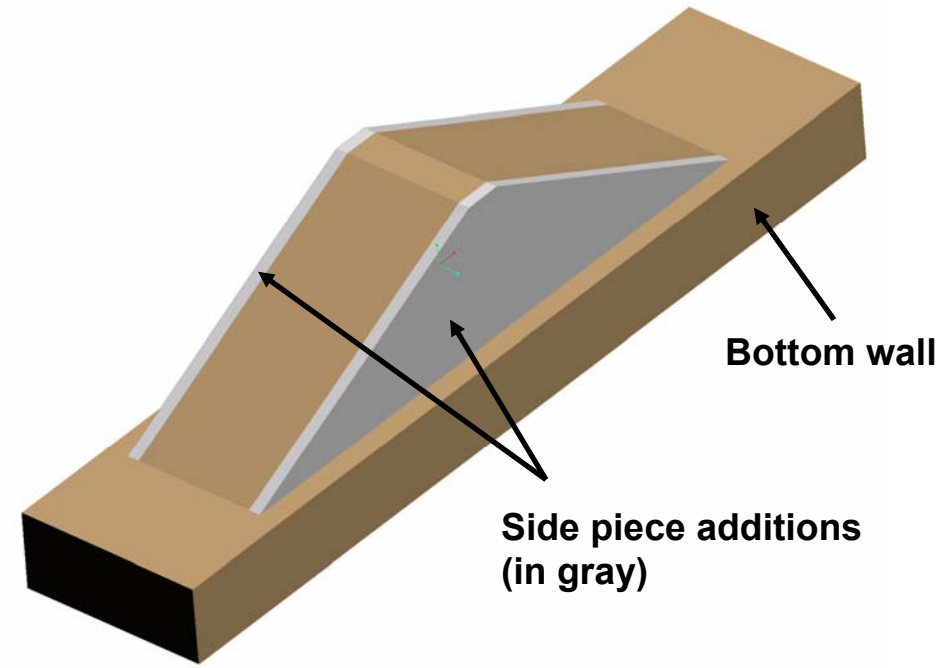

Figure 2.14 Diagram of bottom wall side piece additions for converting from L_l/F_h = 70% to L_l/F_h = 82% louver lengths.

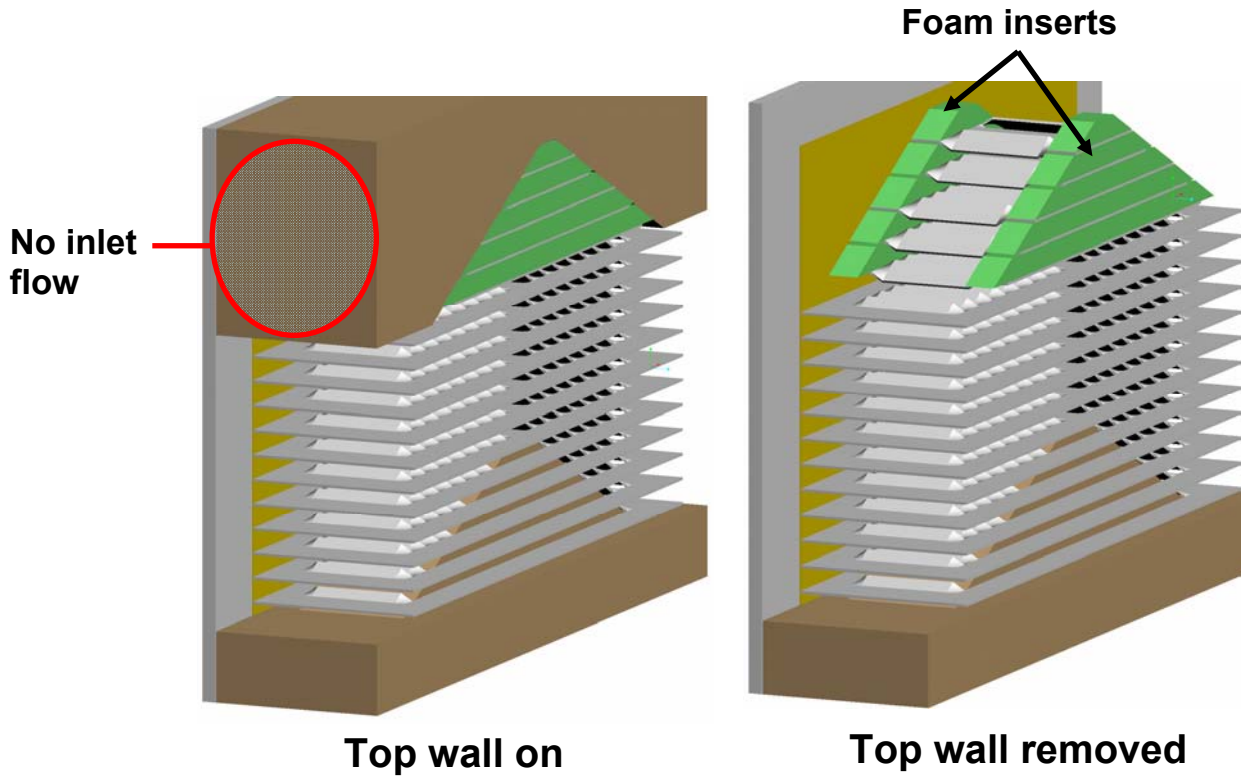

Figure 2.15 Diagram showing blocked off channel flow in top wall area.

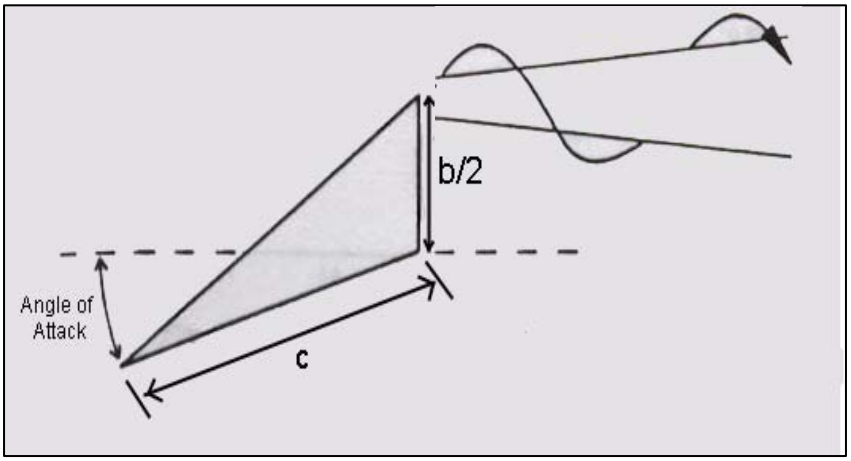

Figure 2.16 Diagram of delta winglet vortex generator (Eibeck and Eaton 1987).

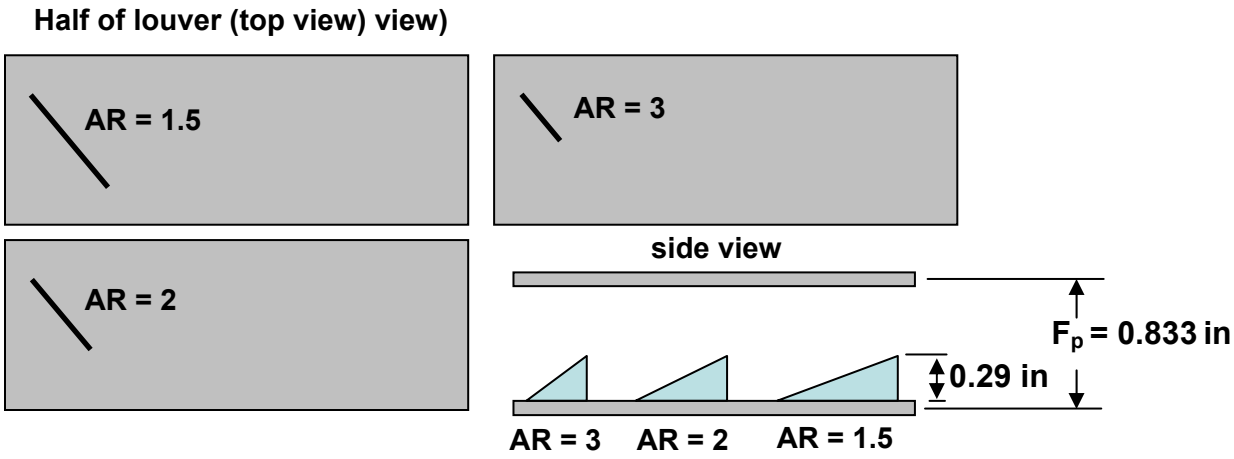

Figure 2.17 Diagram showing relative sizes of the three ARs on top of a louver and relative to F_p.

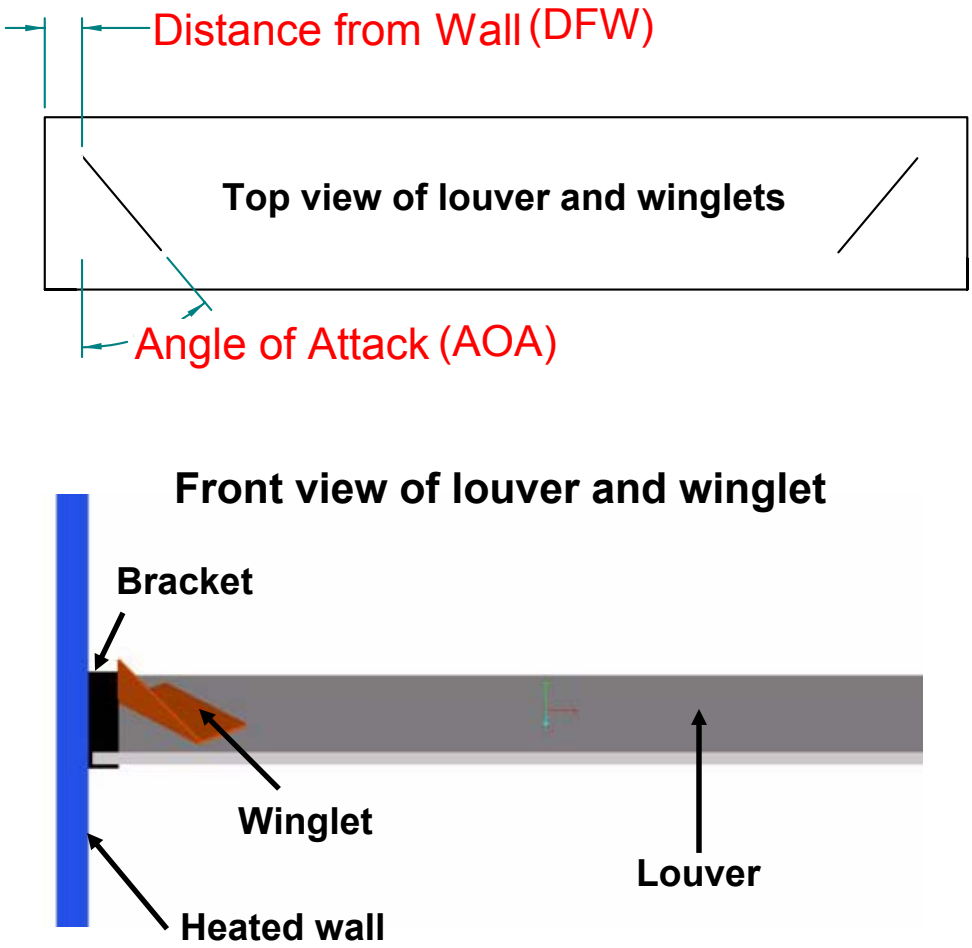

Figure 2.18 Definition of distance from wall and diagram showing L_l/F_h = 100% delta winglet setup.

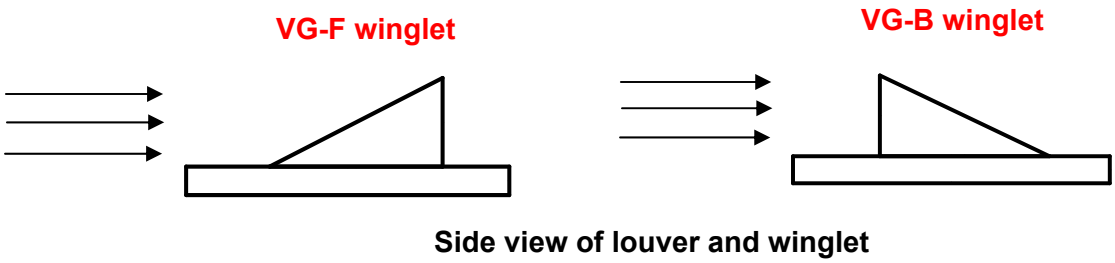

Figure 2.19 Comparison of forward and backwards delta winglet.

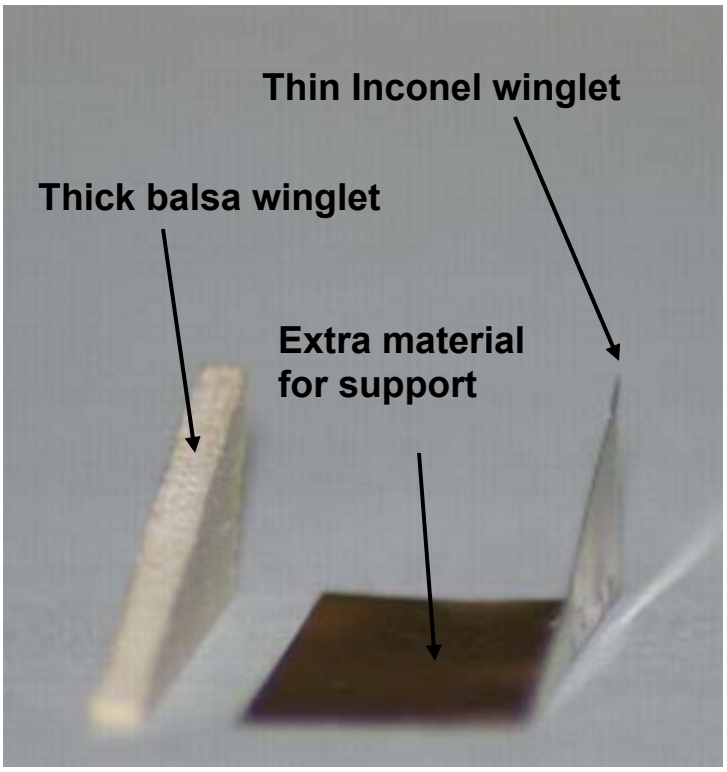

Figure 2.20 Comparison of thick balsa wood winglet and thin Inconel winglet at AR = 1.5.

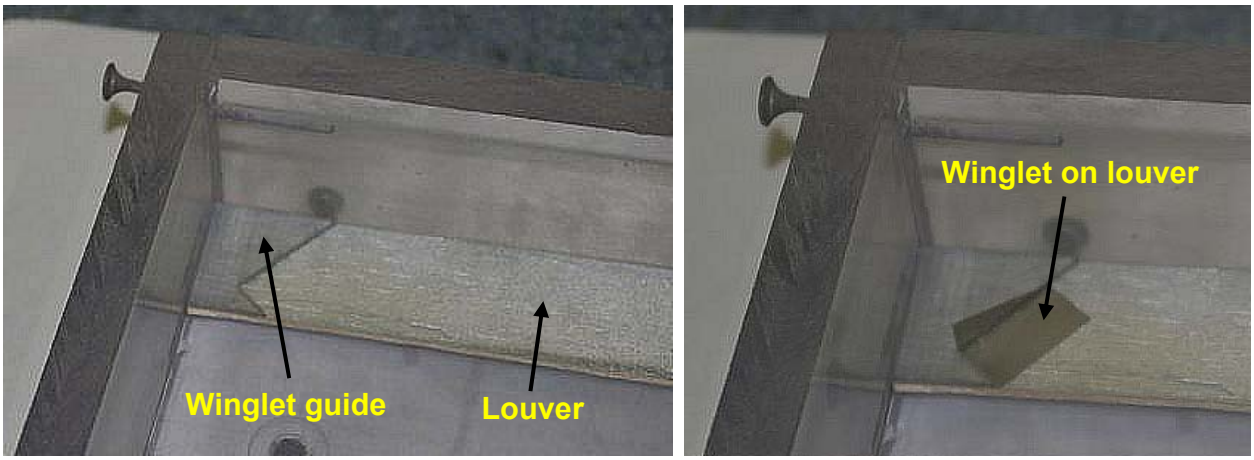

Figure 2.21 Apparatus used to apply Inconel winglets to L_l/F_h = 100% louvers.

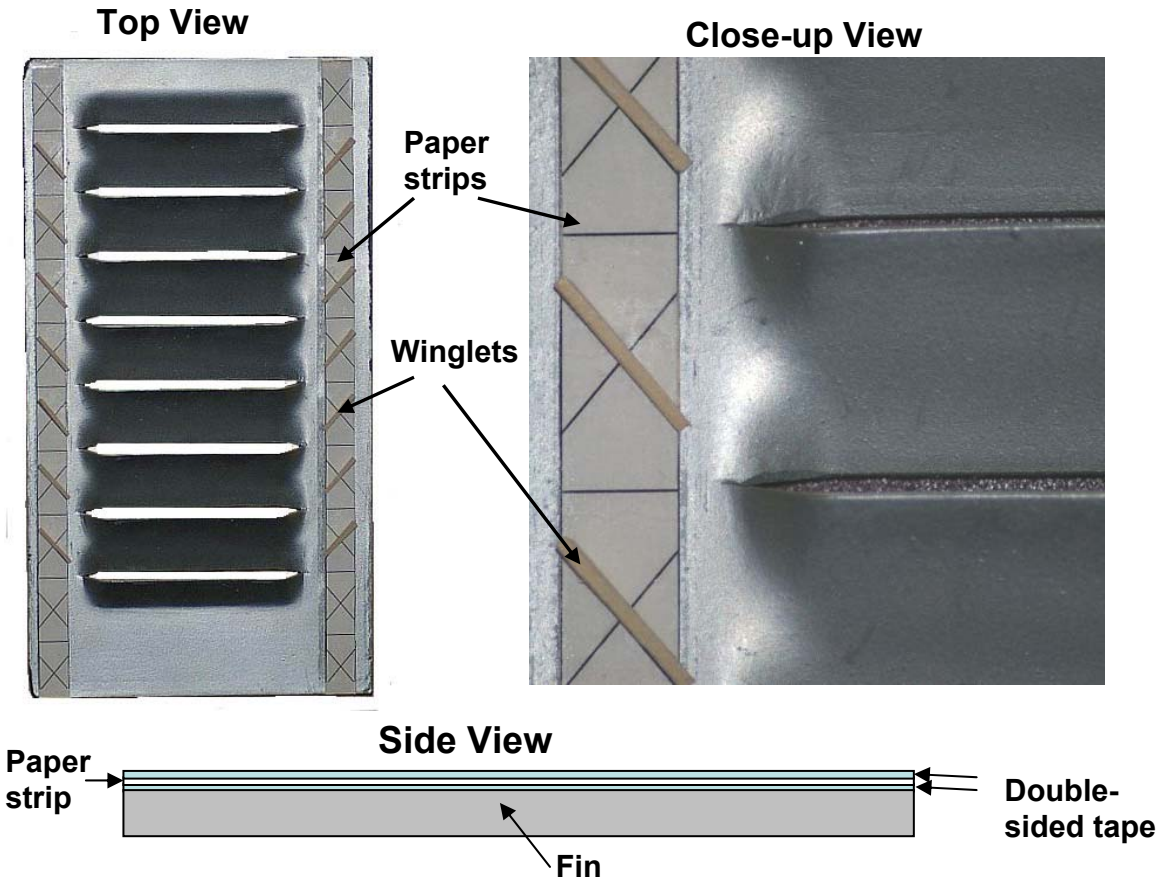

Figure 2.22 Paper strips used to define winglet placement for L_l/F_h = 70% fins.

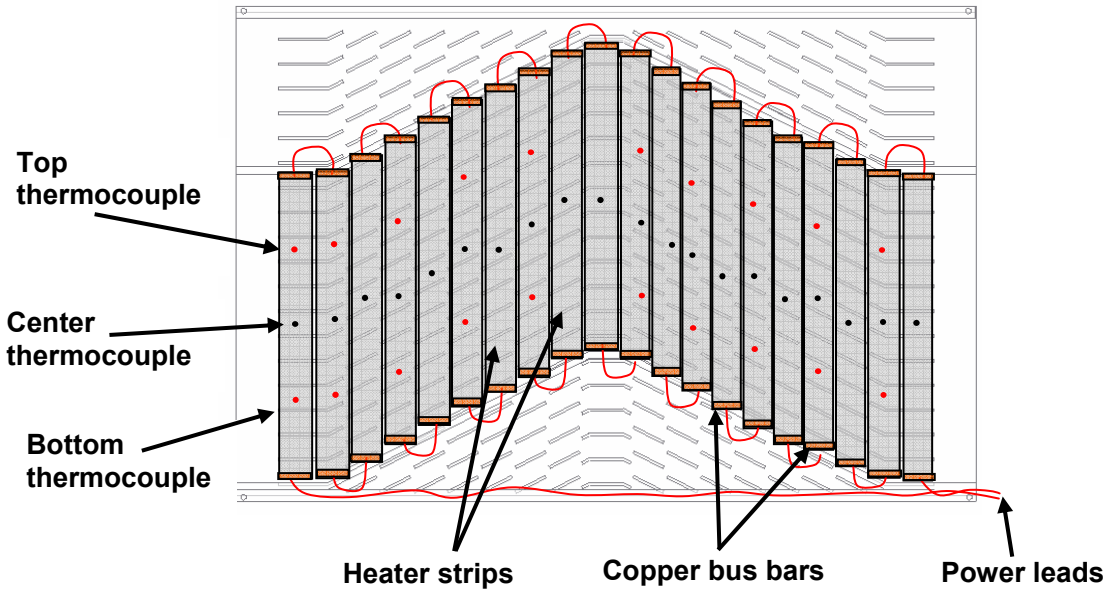

Figure 2.23 Thermocouple and strip heater setup for the L_l/F_h = 100% test section (Ebeling and Thole, 2004).

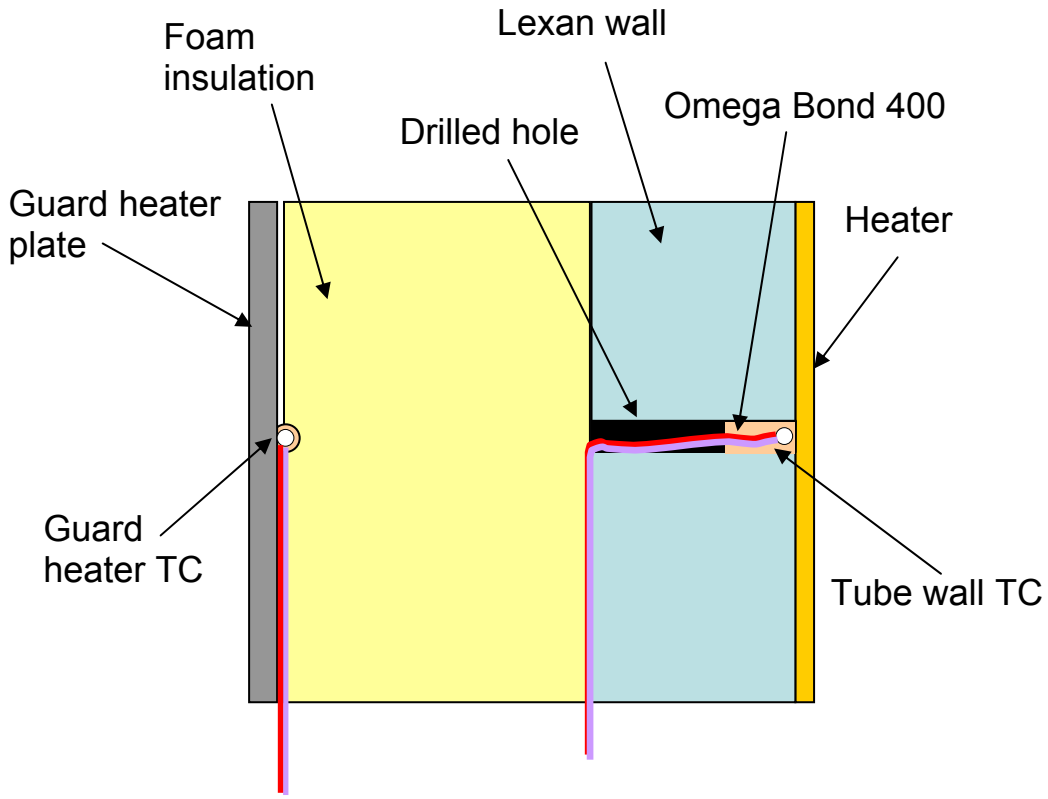

Figure 2.24 Diagram showing thermocouple placement in instrumented wall and on conduction guard heater plate.

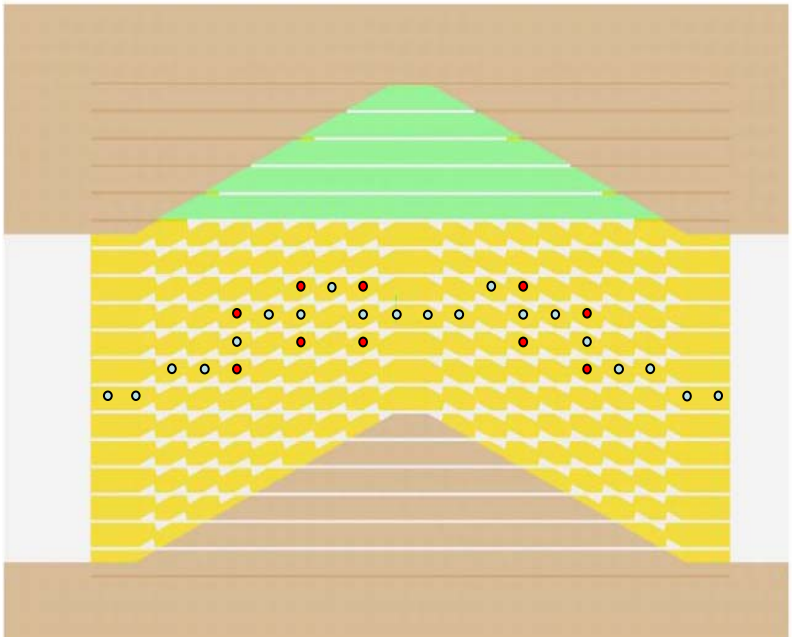

Figure 2.25 Thermocouple setup for the L_l/F_h = 70% and L_l/F_h = 82% test section.

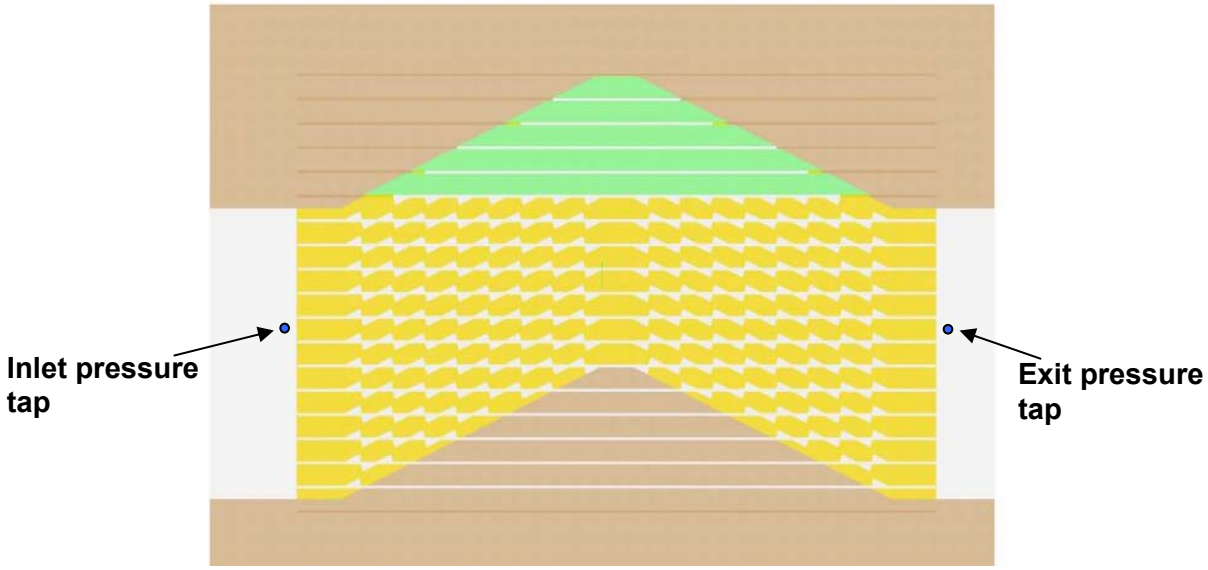

Figure 2.26 Side view of test section showing pressure tap placement.

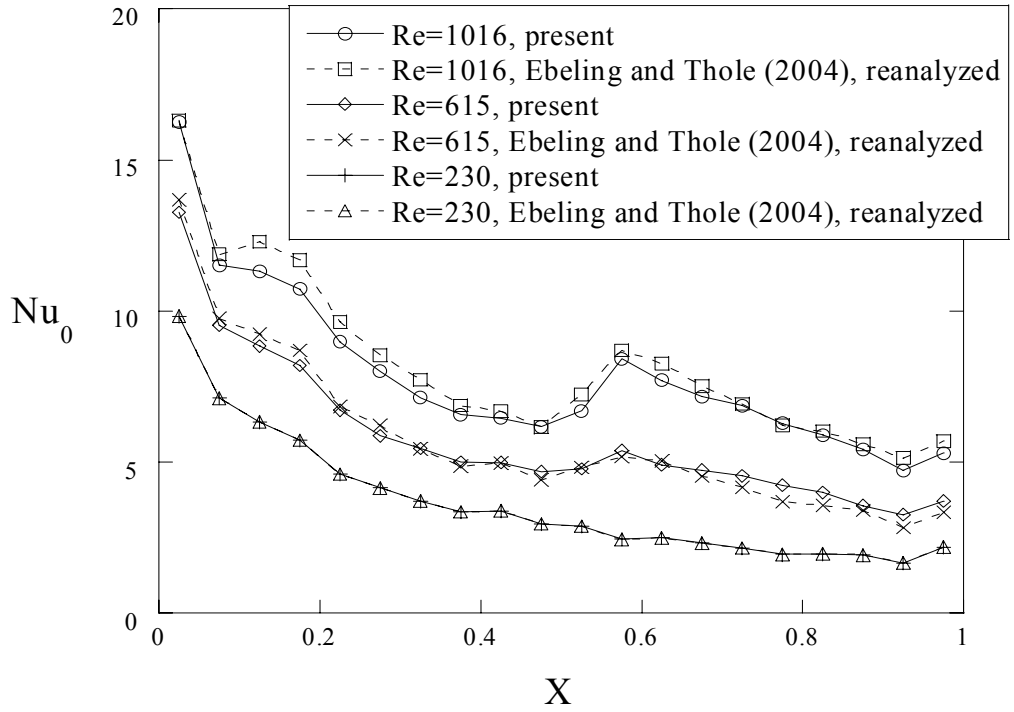

Figure 2.27 Comparison of present to Ebeling and Thole's (2004) L_l/F_h = 100% baseline heat transfer results at Re = 1016, 615, 230.

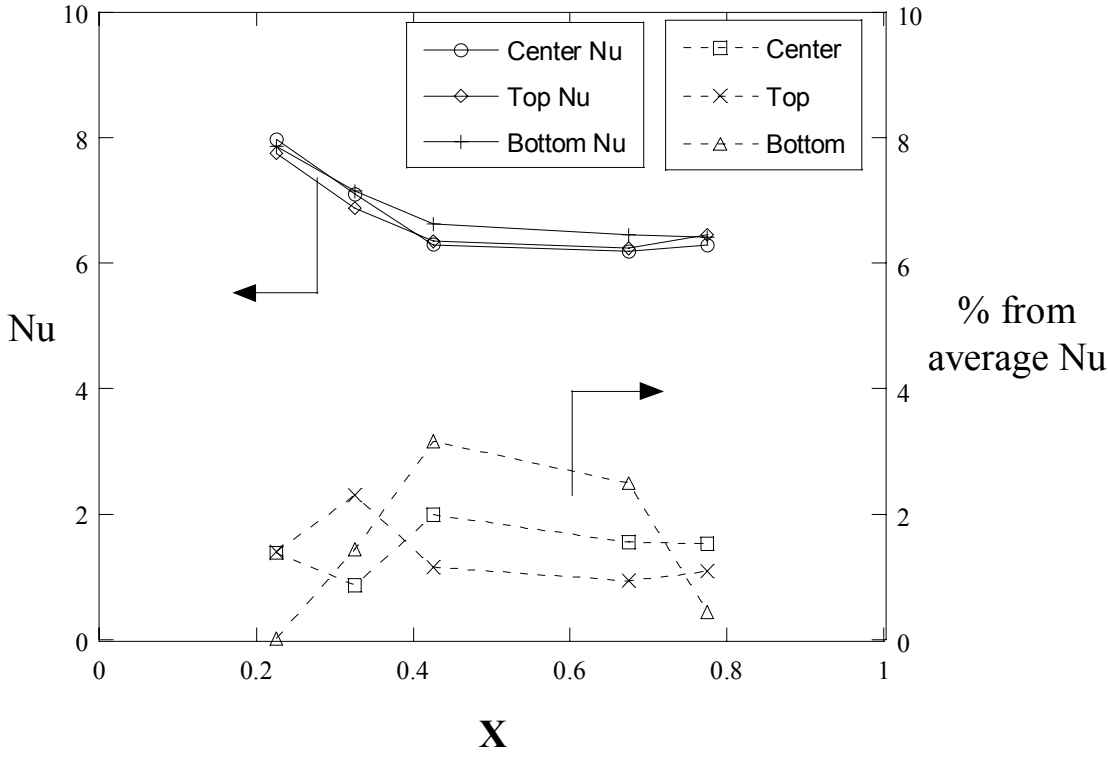

Figure 2.28 Nusselt periodicity for L_l/F_h = 70% at Re = 1016.

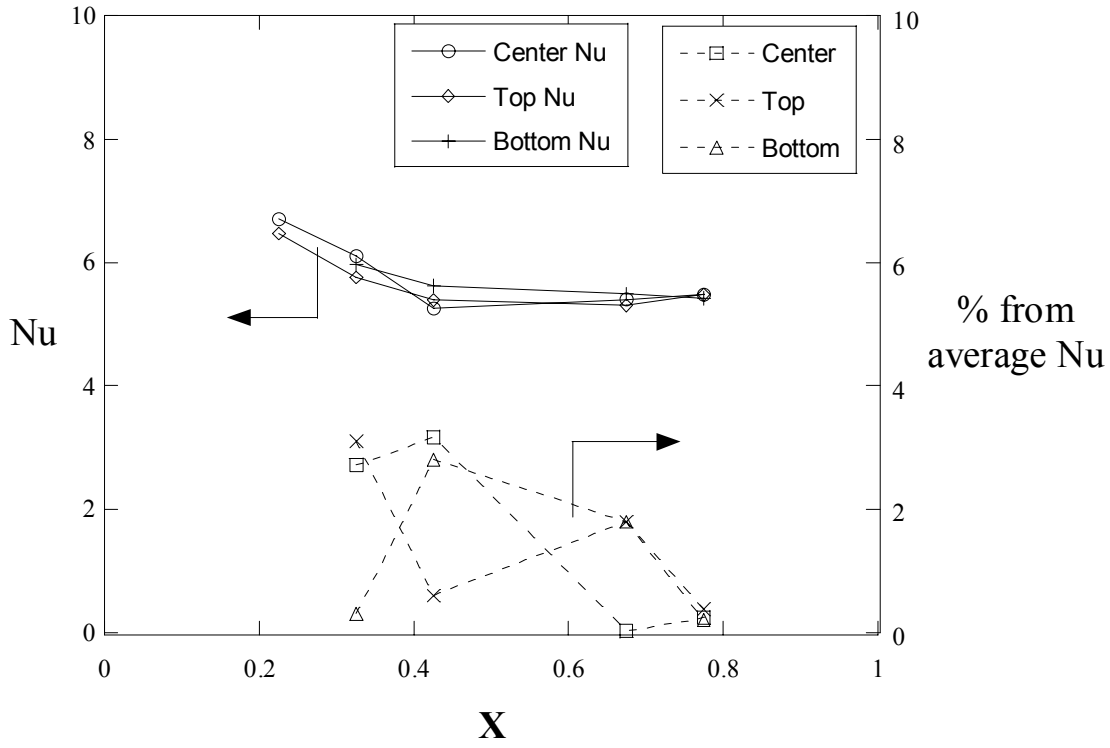

Figure 2.29 Nusselt periodicity for L_l/F_h = 70% at Re = 615.

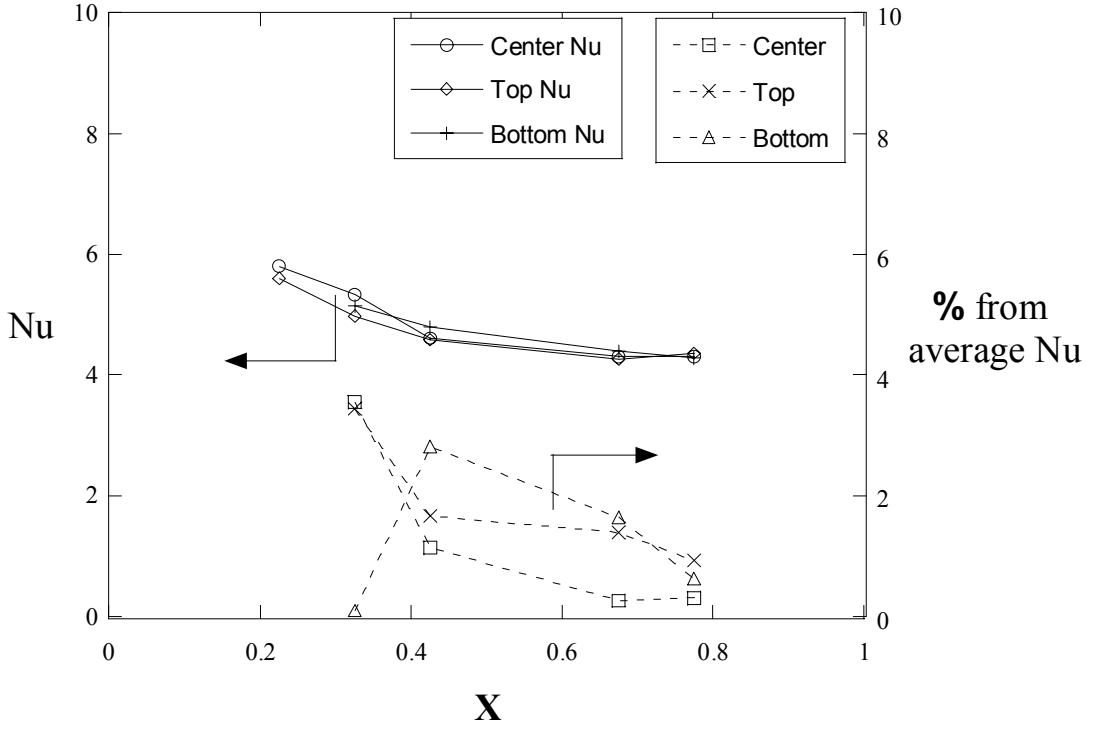

Figure 2.30 Nusselt periodicity for L_l/F_h = 70% at Re = 230.

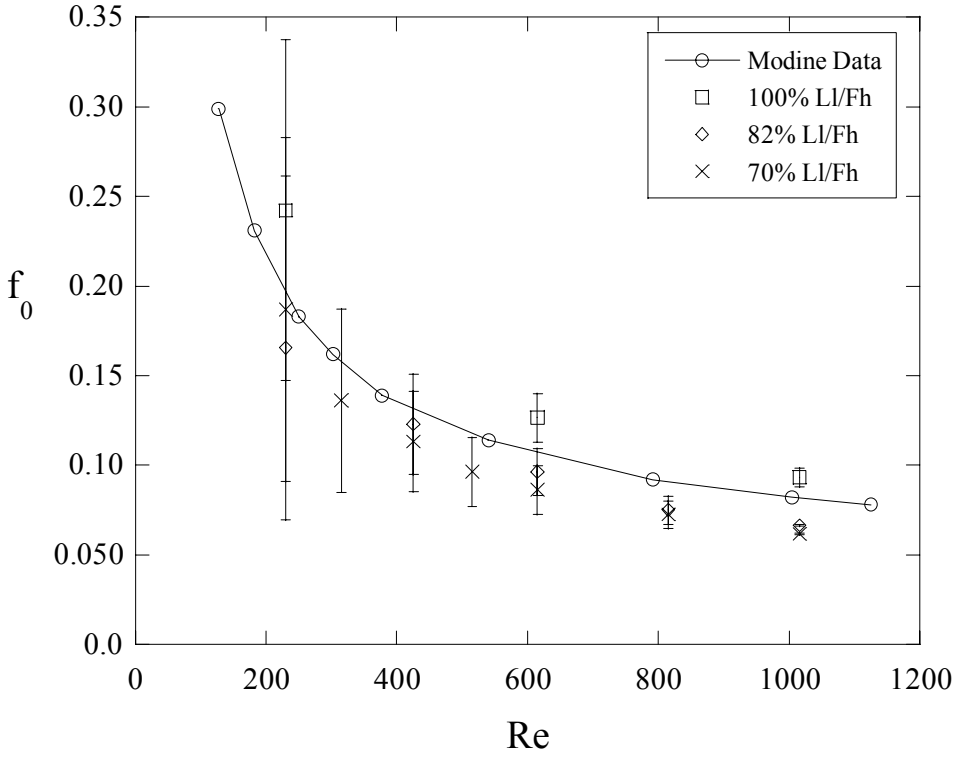

Figure 2.31 Comparison of friction factor results from this study to Modine heat exchanger data.

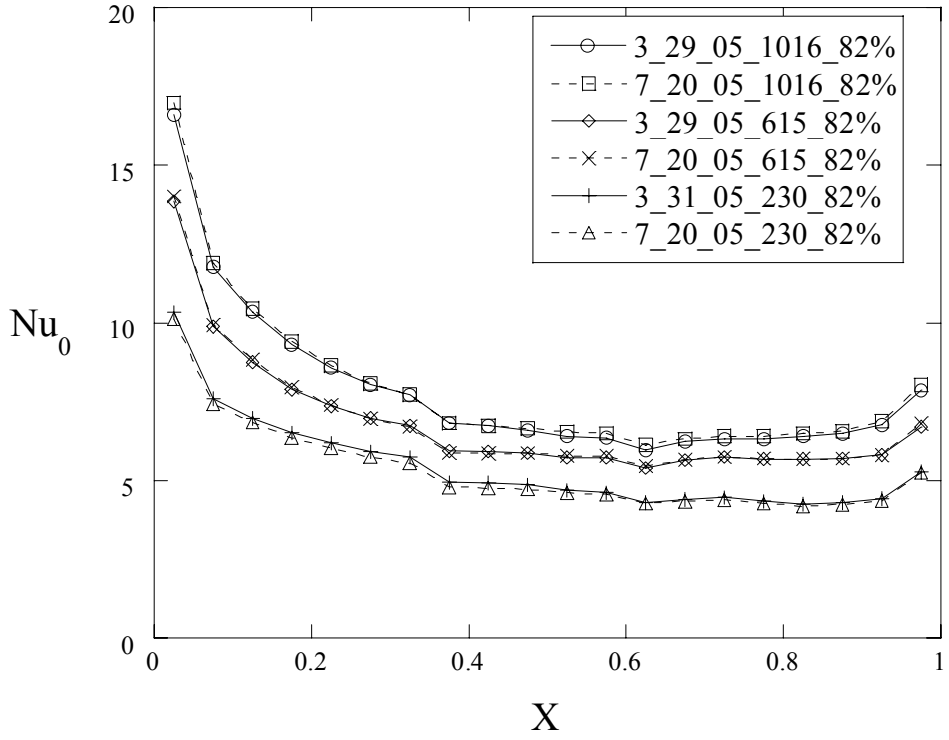

Figure 2.32 Repeatability of heat transfer results for L_l/F_h = 82%, Re = 1016, 615, 230.

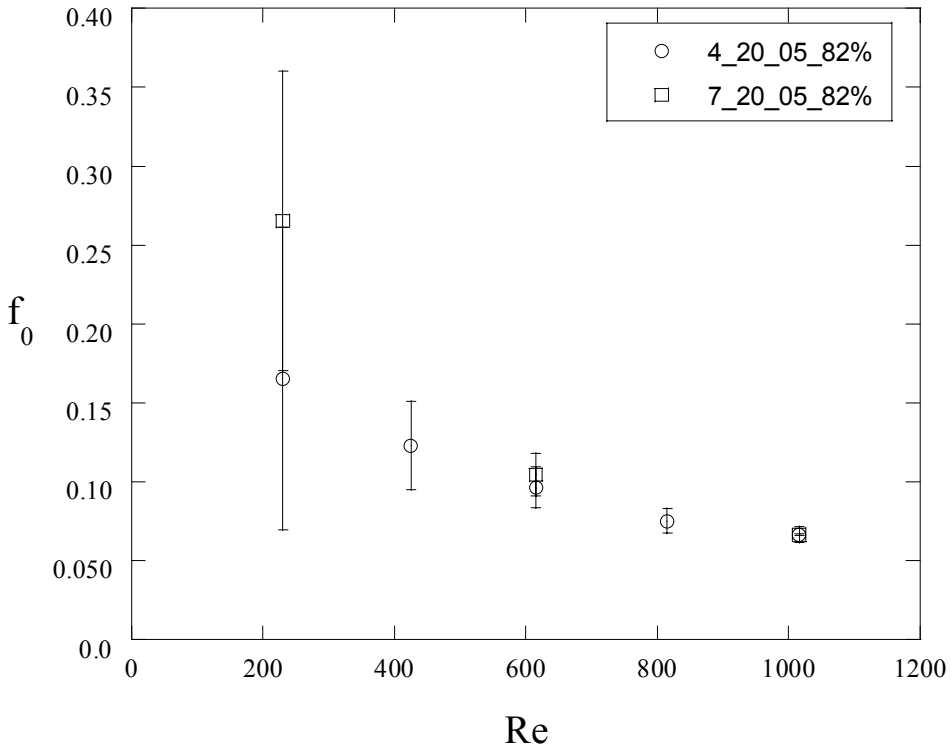

Figure 2.33 Repeatability of friction factor results for L_l/F_h = 82% at various Reynolds numbers.

Chapter 3 – Comparison of Baseline Heat Transfer and Friction Factor

The first focus of this study was to find how changes in louver length affected heat transfer on the tube wall and the friction factor of the louvered array. Experimental heat transfer measurements were made at 20 streamwise locations with the use of thermocouples imbedded in the heated wall. These measurements were made at Re = 230, 615, and 1016 for L_l/F_h = 100% baseline tests. For L_l/F_h = 70% and 82%, tests were run at Re = 1001, 606, and 227 which were only 1.4% below the Reynolds numbers for L_l/F_h = 100%, so accurate comparisons can still be made between louver lengths. Nusselt numbers based on L_p were used to compare the tube wall heat transfer for all Re and louver lengths. Pressure drop measurements were made from pressure taps placed upstream of the entrance louver and downstream of the exit louver, as was mentioned in Chapter 2. The pressure drops measured were converted to Fanning friction factors for comparison purposes. The definitions for Reynolds number, streamwise Nusselt number, and Fanning friction factor related to this study were also given in Chapter 2.

Ebeling and Thole (2004) reported experimental and computational tube wall heat transfer results for the L_l/F_h = 100%. Since changes were made to the calculation of the radiation losses from the tube wall and the L_l/F_h = 100% baseline tests were rerun in this study, only the results from this study will be shown for comparison to the short louver lengths.

3.1 Tube Wall Heat Transfer Coefficients

Figures 3.1 through 3.3 show experimental Nusselt numbers with respect to non-dimensional fin depth (X) for the three louver lengths and Reynolds numbers. The Nusselt numbers shown were calculated only with the center channel thermocouples mentioned in Chapter 2 as the thermocouples located above and below the center channel thermocouples were used solely to determine periodicity. Figure 3.1 shows the heat transfer results for the L_l/F_h = 100% baseline tests at all three Reynolds numbers along with a diagram of a single full louver row for reference. In the entrance region (X = 0.025) the Nusselt numbers are high for all Reynolds numbers because of the small temperature difference between the inlet air and the temperature at the X = 0.025 thermocouple. At X = 0.075, the flow reacts to the angled portion of the turnover louver and causes an increase in heat transfer. From X = 0.075 to X = 0.225, the

flow is transitioning between duct directed flow to louver directed flow. Flow from X = 0.225 to 0.475 is totally louver directed. The results in this louver directed region look similar to the results one might see for flow over a flat plate, because louver directed flow is essentially flat plate flow with interruptions in the boundary layer from the leading edges of the louvers. The Nusselt numbers start to rise from X = 0.475 and spike at X = 0.575. This spike is caused by the 54˚ turn the flow makes as it goes past the turnover louver. Following the spike, the Nusselt numbers decrease once again until the flow reaches the exit louver. At the exit louver, the flow makes its final turn, and the tube wall heat transfer increases again. These increases in heat transfer at the entrance, turnover, and exit louvers occur because the redirections thin the thermal boundary layer. As the Reynolds number decreases, the response of the flow to these turns diminishes. At Re = 230, there is no increase in heat transfer at the turnover louver, showing that the momentum of the fluid is too low to be strongly redirected.

Figures 3.2 and 3.3 show the tube wall heat transfer results for the L_l/F_h = 82% and 70% louver lengths respectively. Both figures have nearly identical trends and values so only Figure 3.2 will be discussed. Looking at Figure 3.2, the trends are much different than those for the L_l/F_h = 100% louver length. The first noticeable trend is that there are no spikes in the Nusselt numbers at the entrance and turnover louver. The flow is less sensitive to the redirection at these points because the louvers are farther away from the wall. The Nusselt numbers from X = 0.075 to 0.325 resemble the results for the louver directed flow region shown in Figure 3.1. There is a sudden change in the slope of the results from X = 0.325 to 0.375 and then the Nusselt numbers stay fairly constant until X = 0.925 with the exception of the slight dip at 0.625. At X = 0.925, the Nusselt number starts to rise again. However, due to the lack of response at the turnover louver which has twice the redirection angle of the exit louver, we believe that the increase in Nusselt number is caused by conduction losses out the end of the instrumented wall. A thermocouple was placed downstream of the heated portion of the wall in an attempt to make a conduction loss correction, but the loss was two-dimensional in nature and could not be accounted for with a one-dimensional calculation. These conduction losses did not occur in the L_l/F_h = 100% tests because the instrumented Lexan wall used in those tests only extended to the end of the heater.

With the exception of the sudden decreases in Nusselt number at X = 0.375 and the small dip at X = 0.625, the results look similar to results for a channel flow which inherently reaches a

steady value for the heat transfer coefficient after becoming thermally fully developed. However, as the lines for the different Reynolds numbers show augmented constant values, it seems as if there is still some component of flat plate flow which is Reynolds dependent. The difference in results for the 100% louver length and those for the shorter louver lengths can be explained by the differences in geometry between the two. Figure 3.4 shows a comparison of the 100% and 82% louver length geometries and how the geometry for the short louver lengths allows for channel flow results in tube wall heat transfer. Notice for L_l/F_h = 82%, it can be seen that the flow region near the tube wall is bounded by the wall and the flat landings of the top and bottom fin surface (outlined in red). The louver directed flow (outlined in blue), moving at 27˚ relative to the flow over the flat landing acts as the fourth boundary. It was seen with smoke visualization that there are two mostly distinct flow regions for the short louver lengths. This is far different than the flow through the 100% louvers which is all louver directed. With this being said, the flow over the flat landings of the 82% louver length seem to be coming to some thermally fully developed state at X = 0.375 at each of the Reynolds numbers.

No explanation can be given for why the Nusselt numbers drop at X = 0.375 and 0.625. These points coincide with two louver positions upstream and two louver positions downstream of the turnover louver, so possibly the turnover louver is having some extended influence over the flow. As will be shown in Chapter 5, the Nusselt numbers for the 70% louver length winglet tests also show amplified Nusselt number reductions at these same points.

Comparisons of the tube wall Nusselt numbers for the 100%, 82%, and 70% louver lengths are given for all Re in Figures 3.5 through 3.7 so the effect of changing louver length can be seen directly. Also shown in these plots are results for thermally fully developed channel flow for a constant heat flux condition on one wall (Kakaç et al. 1987) and results for a flow over a flat plate with a constant heat flux condition (Incropera and DeWitt 2002). Figure 3.5 shows this comparison for Re = 1016/1001. Notice that all the results are the same at X = 0.025 and 0.075. Following the turnover louver, the 100% louver length results show an increase while the results for the short louver lengths continue downward. The 100% results then drop below the short louver length results from X = 0.325 to 0.475 but go well above them near the turnover louver. Finally they drop below the short louver length results at X = 0.775 and continue downward while the short louver length results remain fairly steady. Another point to mention is that the results for the 70% and 82% louver lengths are nearly identical. Finally, notice how the

experimental results do not match either the fully developed channel flow or the flat plate flow. Ebeling and Thole (2004) showed that 100% louver length tube wall performance is higher than that of a flat plate because of boundary layer thinning from the leading edge of each louver. Because the realistic louver lengths do not match either flow type, we believe this is further evidence that some complex combination of channel and flat plate flow is occurring near the tube wall. Looking at Figures 3.6 and 3.7, as the Reynolds number is reduced, the short louver length results become increasingly higher than those for the 100% louver length. At the lower Reynolds numbers, the short louver length results match each other very well, just as they did for Re = 1016.

Given in Figure 3.8 are the average Nusselt numbers of the baseline tests for each louver length and Re as well as results for the fully developed channel flow and flat plate flow mentioned above. Figure 3.8 shows a linear relationship between Re and average Nusselt number for each louver length, but the slope for the $L_l/F_h = 100\%$ is lower than that of the short louver lengths. Results at Re = 1016 are the same for all louver lengths, however, the short louver lengths show much higher average heat transfer at the lower two Reynolds numbers. All louver lengths achieved higher tube wall Nusselt numbers than the developed channel flow and flat plate flow. As expected from the results seen in the Nusselt plots, the tube wall heat transfer for the short louver lengths was essentially the same over the Reynolds number range. Although the $L_l/F_h = 100\%$ baselines showed large spikes due to boundary layer thinning at the entrance turnover, and exit louvers, the constant heat transfer caused by the channel flow with the short louver lengths produced higher heat transfer over the Re range.

Tafti and Cui (2003) also showed that tube wall heat transfer was higher for their short louver length case than their 100% louver case, however, they reported that the results for each louver length had the same slope over the Reynolds number range. We believe that the reason why we showed a slope change while they did not lies in the fact that they only modeled a single periodic louver for simulation, losing the effect of the spikes in the 100% louver data at the entrance, turnover, and exit louvers. Since the magnitude of these spikes increases with Re, the slope is expected to be higher than that of the short louver length results where no effects are amplified by increasing Re.

One trend we cannot match with Tafti and Cui (2003) is why the 70% and 82% louver lengths showed nearly identical heat transfer results. Their intermediate louver length was such

that the fin had no flat landing and therefore no channel flow. Although no tests were run to determine why our results matched for the short louver lengths, our hypothesis is that results would differ if the louver length decreased significantly and/or the test section was fully heated. Consider the extreme case where louver length is zero and there are only plates aligned with the flow. Since there is no longer a fourth bounding surface, (that was created by the louver directed flow) channel flow would not be possible. It is also possible that if the fins were heated, different temperature profiles on the fins caused by the different louver lengths would yield dissimilar boundary conditions for the 70% and 82% channel flows. Different boundary conditions could easily increase or decrease the length required to become fully developed and therefore the overall heat transfer on the tube wall.

3.2 Friction Factor Measurements

Figure 3.9 shows friction factor results at several Reynolds numbers for all three fin lengths compared to friction factor data for an actual heat exchanger with $L_l/F_h = 82\%$. Results are also shown for fully developed channel flow and flat plate flow. Extra Reynolds numbers were run for the friction factor tests that were not run for the heat transfer tests so that better trends could be seen. Looking at Figure 3.9, friction factor increases with increasing louver length. This trend is consistent with the friction factor results shown by Tafti and Cui (2003) in their studies of different louver lengths. They were able to report drag due to both shear and pressure forces on the fins as a function of fin height. They showed that the $L_l/F_h = 100\%$ louvers have a much higher drag near the tube wall than the short louver lengths, making the overall friction factor higher for the 100% louver case. In a direct comparison of our $L_l/F_h = 82\%$ case to Modine's, the trends match well but our friction factors are lower than Modine's for all Re. When compared to Modine's 82% louver length data, our 82% louver length results were 17.03%, 11.03%, and 19.04% lower at Re = 227, 606, and 1001 respectively. We believe that this discrepancy is due to the fact that our tube wall has zero thickness while Modine's tubes are of finite thickness. This extra tube thickness would cause an increase in friction factor. Once again, friction factor data for fully developed channel flow and flat plate flow do not match those of the different louver lengths.

Through baseline heat transfer and friction factor tests, it was found that the short louver lengths provided better performance than the 100% louver length. Average tube wall Nusselt numbers for L_l/F_h = 82% and L_l/F_h = 70% were equal but both were higher than those for L_l/F_h = 100%. This was attributed to the steady Nusselt number over most of the fin depth. Friction factors were also reduced with the short louver lengths because there is less blockage to the flow over the flat landings than there is for a fully angled louver.

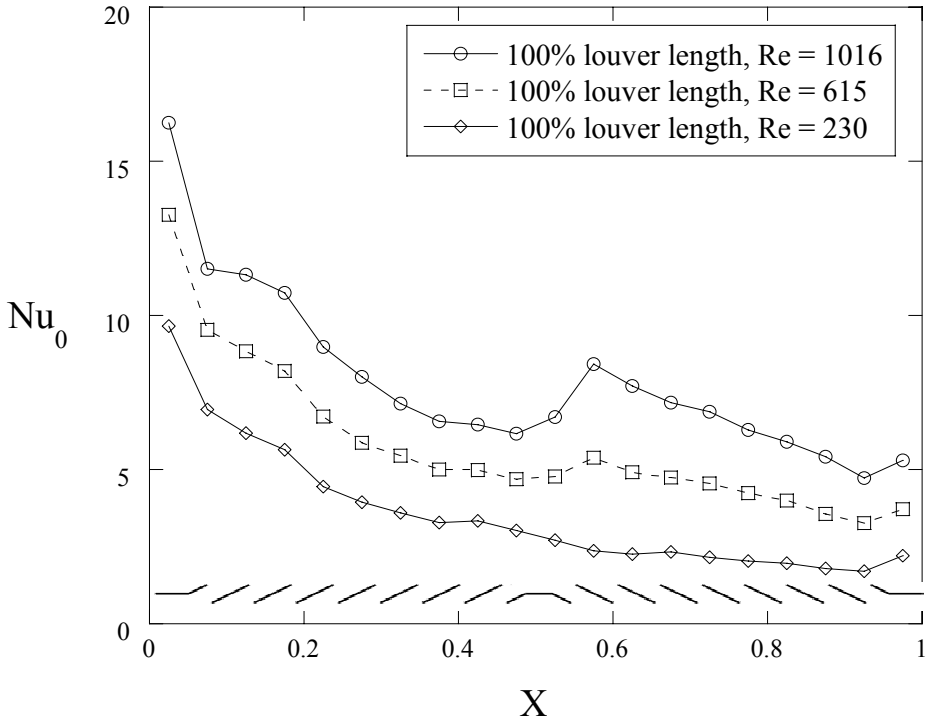

Figure 3.1 Baseline heat transfer measurements along the tube wall for L_l/F_h = 100%.

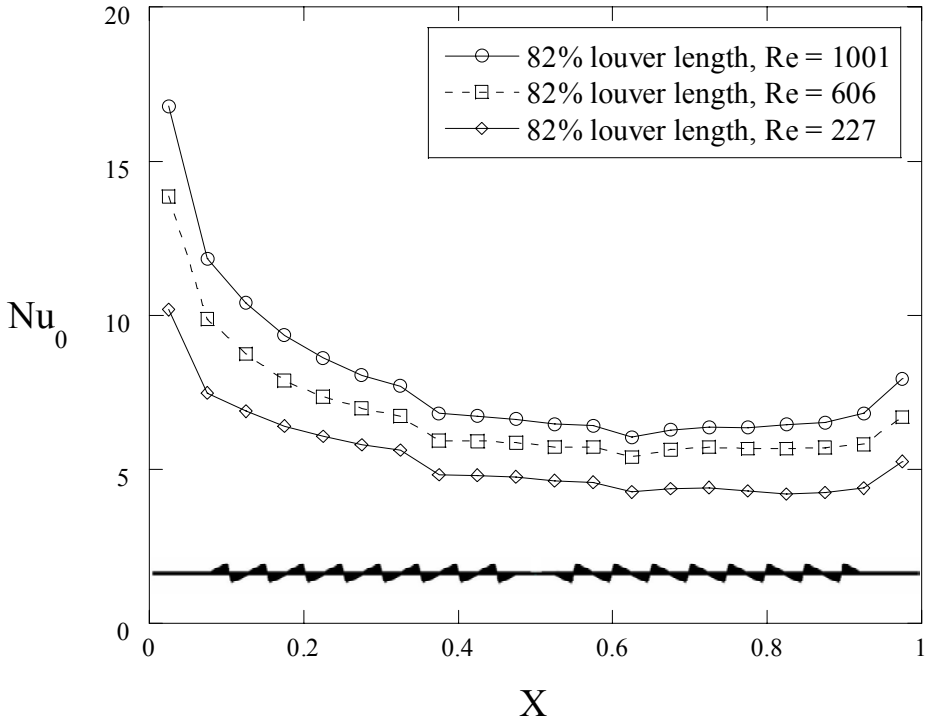

Figure 3.2 Baseline heat transfer measurements along the tube wall for L_l/F_h = 82%.

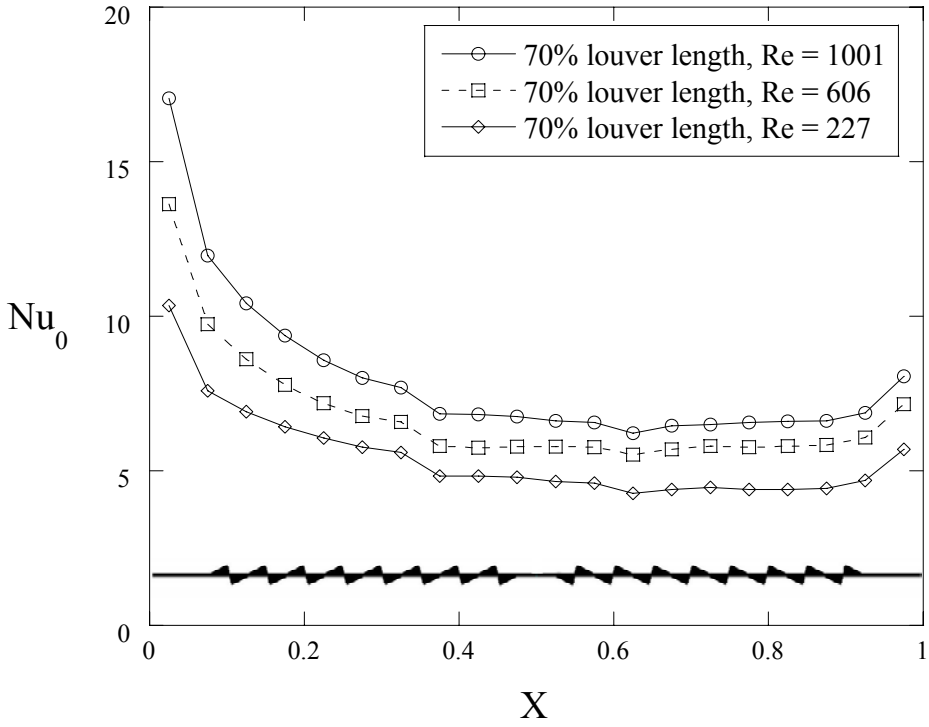

Figure 3.3 Baseline heat transfer measurements along the tube wall for L_l/F_h = 70%.

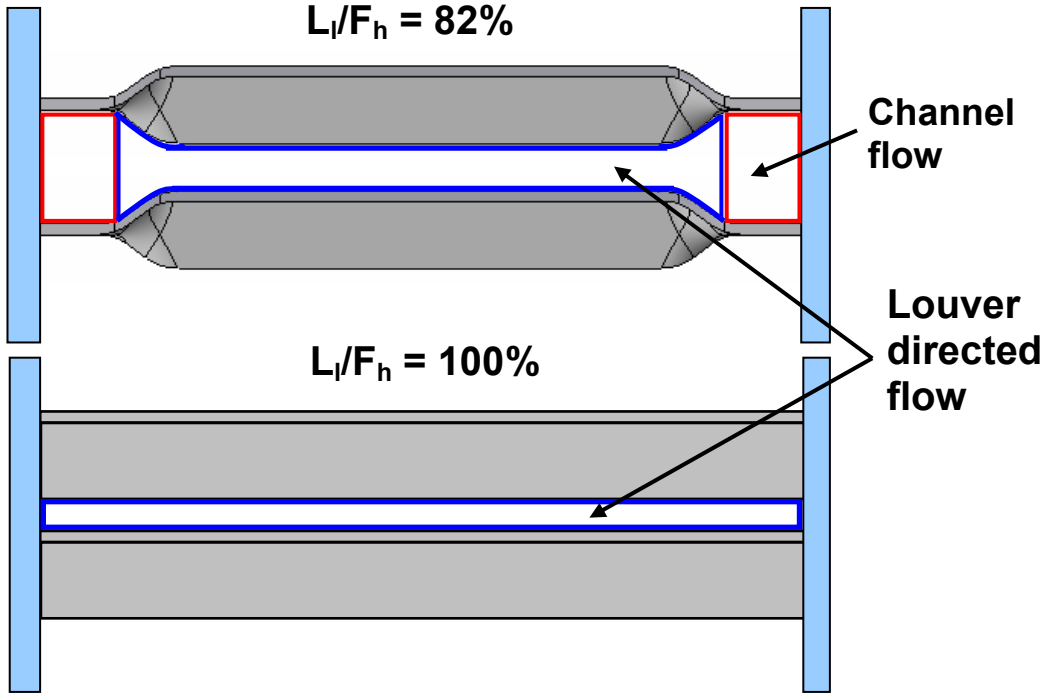

Figure 3.4 Comparison of L_l/F_h = 100% and 82% louver length geometries as related to flow regions.

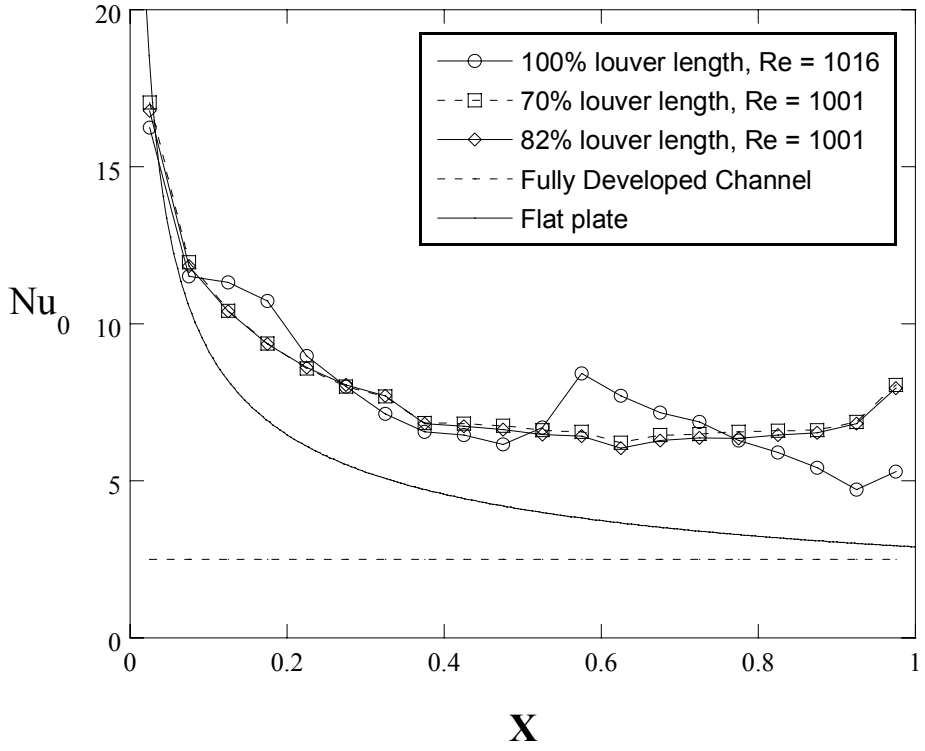

Figure 3.5 Comparison of tube wall Nusselt numbers for all louver lengths at Re = 1016.

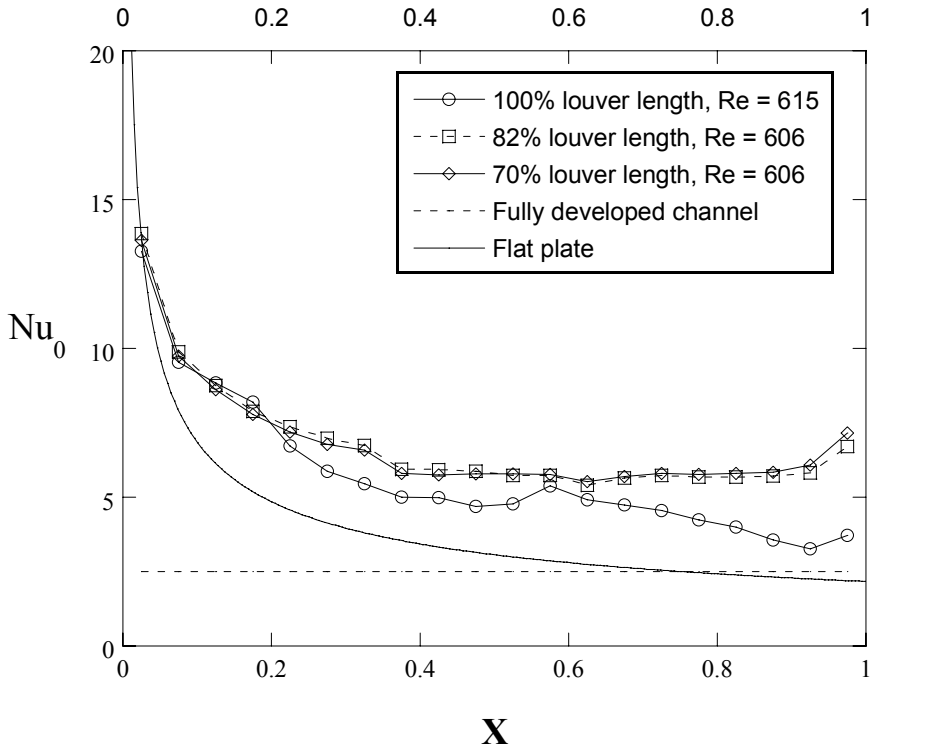

Figure 3.6 Comparison of tube wall Nusselt numbers for all three louver lengths at Re = 615.

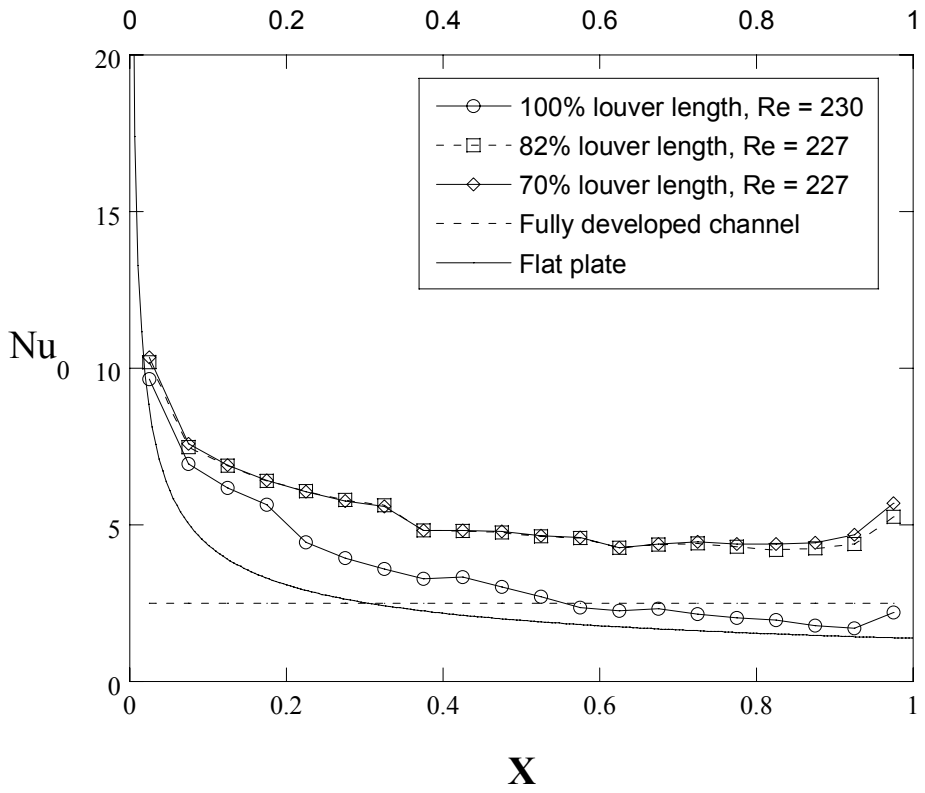

Figure 3.7 Comparison of tube wall Nusselt numbers for all louver lengths at Re = 230.

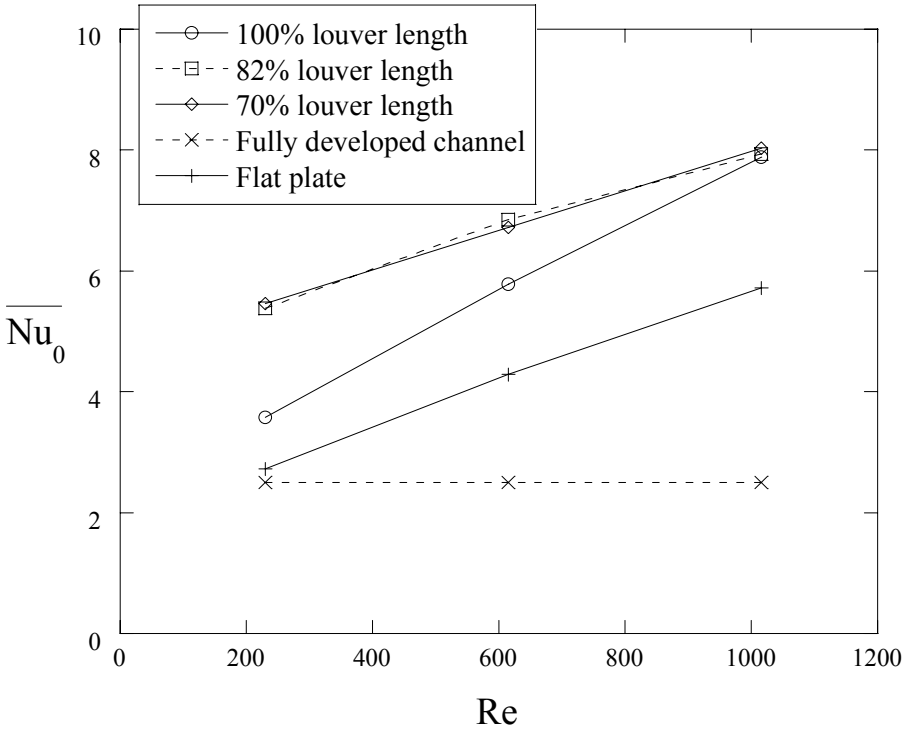

Figure 3.8 Average tube wall Nusselt numbers for all fin lengths and Re.

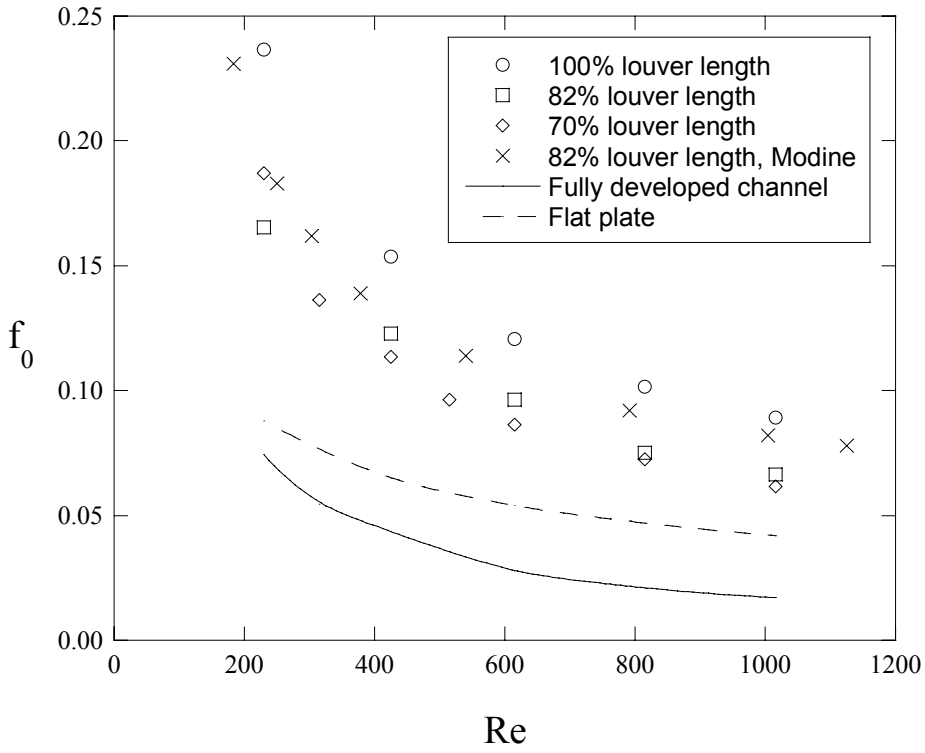

Figure 3.9 Baseline friction factor data for all louver lengths and Re compared to Modine data for actual heat exchanger with 82% louver length.

Chapter 4 – Delta Winglet Studies for L_l/F_h = 100% Louver Length

The first focus of this study was to complete baseline testing to determine the effect of the fins on tube wall heat transfer. The second focus was to design and test a method for augmenting tube wall heat transfer. Although the fins in a heat exchanger account for most of the surface area, the tube wall is the primary heat transfer surface where greater temperature differences provide more potential for convective heat transfer.

Several possible methods for heat transfer augmentation were researched, but not all were practical for incorporation in a louvered fin exchanger. The biggest limitations were the small areas available for application of an augmenting feature and feature manufacturability. Delta winglets were ultimately chosen as the best method for augmentation due to their small size and ability to provide a favorable combination of high heat transfer and low pressure drop. They are also manufacturable using the same stamping technique that cuts and shapes the louvers. Delta winglets work by producing longitudinal vortices that thin the thermal boundary layer of a surface and cause bulk mixing of the fluid downstream of the winglet. It has also been shown in past studies, that placed in series, each successive winglet increases the vortex strength of the upstream winglet and increases surface heat transfer (Chen et al. 1998, Tiwari et al. 2003). This trend lends itself perfectly to the louvered fin exchanger, where a winglet placed on each louver could act as a booster to the winglet on the upstream louver.

In this chapter the results for all of the tests run in the L_l/F_h = 100% winglet studies will be shown and discussed. Heat transfer measurements will be given for all tests. Friction factor measurements were added in the middle of this project, so results will only be shown when available.

4.1 Winglet Testing Overview

As discussed in Chapter 2, there were several winglet parameters that were tested during this segment of the project. Winglet test parameters can be split into three categories: individual winglet parameters, overall winglet setup parameters, and flow parameters. The individual winglet parameters tested were AOA, DFW, AR, shape, orientation, direction, and thickness. The definitions for these parameters were given in section three of Chapter 2. Overall winglet

setup parameters involved how winglet direction and orientation varied through the test section. Examples would be directing all of the winglets towards the tube wall, directing every other winglet away from the tube wall, turning half of the winglets backwards, etc. The specifics of these cases as well as naming conventions and diagrams will be given later in this chapter. The flow parameters were the three Reynolds numbers tested. Testing at the various Reynolds numbers gave comparisons of heat transfer and friction factor augmentations at various driving speeds.

With this many parameters, a full test matrix would have been too large and time consuming. For this reason, a flexible testing scheme was employed so several different avenues could be explored to obtain maximum tube wall heat transfer augmentation. Therefore, the direction of the project as well as the specific parameters being tested may be hard to follow without an overview. All of the tests conducted along with the results of each test can be seen in Table 4.1. In the table, the tests have been divided into main section seen in orange and subsections seen in blue. In most cases, one to three trial repeats were done, but only the average results of the trials are given.

Throughout winglet testing, AOA, DFW, AR, and Re were not changed, however, some were discontinued due to poor performance. Other parameters related to winglet shape, winglet orientation, winglet direction, and overall winglet setup were changed throughout the course of testing based on results that were available at the time. The original testing scheme had winglets on every louver aimed towards the heated wall in the VG-F orientation. Figure 4.1 shows the side, top, and bottom views of this configuration. Winglets were placed on the underside of the louvers downstream of the turnover louver because the air makes contact with the bottom surface in this region. All tests were completed with the winglets in the rear half of the test section on the underside of the louvers. Later testing used an alternating winglet orientation and direction setup. Not including the entrance, turnover, and exit louvers, winglets on the odd louvers had winglets aimed at the wall in the VG-F orientation. The even numbered louvers had winglets aimed away from the wall in the VG-B orientation. Views of this setup can be seen in Figure 4.2. This configuration was changed once more to one with an alternating winglet direction but with all winglets in the VG-B orientation (Figure 4.3).

Different winglet shapes and thicknesses were also used later in testing. Rectangular winglets were added to regular testing, always alternating in direction. Finally, tests with

winglets of louver thickness were run to simulate winglets produced from a stamping process. Only a few thick winglets tests were run, always with alternating direction.

The individual winglet parameters used in experiments can be seen in Table 4.2. All parameter levels, with the exception of DFW, were chosen based on the intermediate levels used in past winglet studies. Since DFW was a new parameter, values were chosen based on geometrical constraints and an educated guess of the expected effect of DFW on tube wall heat transfer. The smallest DFW chosen was the shortest allowable distance due to the size of the louver bracket. Also, we felt that moving the winglet too far from the wall would produce poor heat transfer augmentation, so a relatively small maximum value of DFW = $0.29L_p$ was chosen. The height of the delta winglet (b/2) was kept constant at 0.295 in (7.5 mm, $0.27L_p$) while length (c) was altered to vary the AR. The height was chosen so that the tip of the winglet would be close to half of the fin pitch minus the louver thickness but would not result in a winglet length that was too close to the louver pitch.

Now that an overview of the tests and winglet parameters has been completed, specific details of the test conditions and methods used to reduce the test matrix size will be given.

4.2 Taguchi Trials

To test every combination of the parameters and levels shown in Table 4.2, 81 tests would have had to be run. We felt that a design of experiments was the best approach to obtain useful information on trends while only doing a fraction of the tests. The Taguchi method was chosen as the design of experiments used in this study (Roy 2001).

The Taguchi method was developed by Dr. Genechi Taguchi as a method of improving quality of manufactured products. However, his methods can easily be applied to academic research. The root of his method lies in determining contributions of a single variable to the result of a multi-variable problem by using a predetermined orthogonal test array based on the number of parameters and levels to be tested. In this study, the parameters refer to AOA, DFW, AR, and Re while the levels are the specific values of the parameters (i.e. AOA = 20˚, DFW = $0.15L_p$, etc.). There were four parameters studied and three levels of each parameter. This combination of parameters and levels fit into a Taguchi L-9 array which only required that nine

tests be completed to obtain trend information. The L-9 array used in this study can be seen in Table 4.3.

The results of the Taguchi method are given in parameter level importance plots that give two useful pieces of information. They show the trend of influence over the range of parameter levels and also the sensitivity of the results to the parameters. A statistical analysis is also done that gives an indication of which parameters are the most important to the result and also an idea of what result one might expect from the optimized parameter levels.

Forwards Vortex Generator Testing

Winglet testing began by applying the Taguchi approach to winglets placed on every louver in the VG-F orientation, all aimed towards the wall. Each winglet was aimed towards the wall because it was thought that directing the vortices towards the wall would give the best heat transfer augmentation. Once again, this configuration can be seen in Figure 4.1.

With the Taguchi test matrix set, delta winglet trials began. However, poor initial results stopped the testing within the Taguchi test matrix after only two tests. These two tests, Taguchi test 6 and Taguchi test 1, can be seen in Figures 4.4 and 4.5. In the legend of the streamwise Nusselt plots that will be shown, the percentage of heat transfer augmentations for each test is given. Neither figure shows good positive augmentation with results of 3.76% and -2.58% respectively. Figure 4.4 shows some augmentation from X = 0.125 to X = 0.625, but results after X = 0.625 are less than or equal to the baseline results. In Figure 4.5, the winglet results match the baseline data until X = 0.625 where they are also lower than or equal to the baseline data. As stated earlier, these initial results led to the first stray from the planned test matrix. The next test run consisted of our hypothesized best case parameters. These parameters were the closest DFW ($0.15L_p$), AOA = 40˚, AR = 1.5, and Re = 1016. Seen in Figure 4.6, this configuration only led to an average augmentation of 2.60%. Once again, at X = 0.625, the winglet results fell below the baseline results, meaning that the tube wall temperatures were actually higher in the winglet tests than in the baseline tests. The hot air near the wall was not getting swirled to the center of the channel with the vortices as expected. We decided that circulating the air towards and away from the wall by changing the winglet direction might remedy the hot wall temperatures.

Alternating Winglet Direction and Orientation Testing

Winglet direction and orientation were altered on every other louver in an attempt to create a circulation of the air from the wall to the center channel. Changing the winglet orientation was simply a byproduct of turning the louvers around to change winglet direction. The configuration can be seen in Figure 4.2. In Figure 4.2, notice how the trend of changing direction and orientation does not restart at the turnover louver, but continues through it by starting with a VG-B winglet aimed away from the wall. The same winglet parameters shown in Figure 4.6 were tested with the alternating winglet direction and orientation configuration can be seen in Figure 4.7.

The results in Figure 4.7 show a 25.50% increase in heat transfer augmentation over the baseline. All points show augmentation over the baseline with the exception of the entrance louver (X = 0.025 and X = 0.075) where winglets were not applied. Winglets were also not placed on the turnover and exit louvers, however, wall heat transfer was affected by winglets upstream of these locations. Another noticeable trend in Figure 4.7 is that the Nusselt numbers between X = 0.275 and X = 0.575 shift up and down at every other point. The peaks corresponded to winglets aimed towards the wall while the troughs were in locations where winglets were aimed away from the wall. This trend will be seen in several of the upcoming alternating winglets cases, especially at Re = 1016. It becomes less noticeable with decreasing Re.

The same parameters shown in Figure 4.7 were also tested at Re = 615 and Re = 230 and can be seen in Figures 4.8 and 4.9. Looking at Figure 4.8, Re = 615 showed very similar trends to the Re = 1016 case, yielding an overall average percent augmentation of 22.85%. However, the Re = 230 case seen in Figure 4.9 collapses onto the baseline, yielding only 1.74% augmentation. We believe the lack of response of the flow to the winglets at Re = 230 is due to low fluid momentum and is also the reason why the Re = 230 baseline does not show the Nusselt spikes at the entrance, turnover, and exit louvers.

Although no flow field measurements were made in the louvered array, we believe that the superior cooling with the alternating winglets showed that circulation by general flow redirection and not longitudinal vortices was the most important factor in heat transfer

augmentation. The winglets seemed to be directing the cooler center channel air towards the wall, picking up heat, and forcing the hot air back to the center of the channel.

Due to the increase in heat transfer augmentation achieved by alternating winglet orientation and direction, the Taguchi test matrix was rerun using alternating winglets. Taguchi tests numbers 1 through 9 can be seen in Figures 4.10 through 4.18. Results of these trials will not be discussed because the importance plots based on the Taguchi trials, not the trials themselves, give the useful information.

The Taguchi trial data was analyzed with Qualitek-4 software that came with Roy's (2001) book. With this software, parameter level importance plots were made, ANOVA of the results was computed, relative importance of the parameters was found, and an optimized set of parameter levels was found with an expected optimized augmentation. The only hands-on step was to input the data collected from the Taguchi experiments. There were multiple ways to input the data collected, including average Nusselt number and average Nusselt number augmentation. However, the use of Re as a parameter made average Nusselt augmentation a much better choice. When the results were input using average trial Nusselt numbers, the overriding influential parameter was Re, making up 99% of the parameter significance to Nusselt number. In an actual heat exchanger, Re changes with driving speed and cannot be set to an optimized condition. In order to combine the desire to know how the winglets perform at each Re while still getting an accurate idea of the importance of the winglet parameters to heat transfer, Nusselt augmentations were used. By comparing each Nusselt trial to their respective baseline tests, the influence of Re became based solely on the ability of the winglet parameters to augment heat transfer at each Re, but not Re itself.

The parameter importance plots for DFW, AOA, AR, and Re can be seen in Figures 4.19 through 4.22 respectively. When looking at these figures, it is important to understand what information is being given. Three tests were run at each parameter level. Each point seen in the plots is the average of the average Nu augmentations from the three trials. For example, in Figure 4.19, the value shown at DFW = $0.15L_p$ is an average of the average Nusselt number augmentations collected in Taguchi tests 1, 2, and 3. This double averaging is why the y-axis label has an extra line over the standard definition of average Nusselt augmentation. Also shown in each plot is the average of the average Nusselt augmentations from all of the Taguchi trials, called "Full Taguchi average". Any points below this line are parameter levels that performed

below average in the Taguchi trials, while data points above this line are above average performers.

Looking at Figure 4.19, the first noticeable trend is the flat slope across each of the levels. The flat slope means heat transfer augmentation was not sensitive to changes in DFW over this level range. However, no conclusions can be drawn about how sensitive Nusselt augmentation might be at DFWs outside of this range. The AOA importance plot seen in Figure 4.20 shows a much different trend than the DFW plot. At AOA = 20˚, there was no augmentation benefit, while the points at AOA = 30˚ and 40˚ show an above average benefit to heat transfer augmentation. The plot shows that the 30˚ winglet outperformed the 40˚ winglet. Also, the trends show that tube wall augmentation is a non-linear function of AOA.

In Figure 4.21, there appears to be a linear relationship between AR and heat transfer augmentation. However, if the AR plot was plotted against the actual numbers of 1.5, 2, and 3, instead of labels, there would be a nonlinear trend due to the unequal number spacing. Since the height of the winglets was kept constant, the lengths used to calculate these unequally spaced ARs were themselves equally spaced. Winglet area is also equally spaced since length is changing while the height stays constant. This means that the Nusselt augmentation from AR is actually linearly dependent on either winglet length or winglet surface area. No tests were run with the same winglet area but different length and height in order to see which dependency is true. Also seen in Figure 4.21 is that only an AR of 1.5 gives above average Nusselt augmentation results.

Figure 4.22 shows how Reynolds number levels affected heat transfer augmentation. The trends look similar to the results shown for AOA in Figure 4.20. The Re = 230 tests showed worse heat transfer results than the baseline cases as represented by the negative value. The plot shows that nearly equal augmentations are possible at Re = 615 than at Re = 1016, however, both of the high Re cases yield above average augmentation. Finally, Nusselt augmentation has a non-linear dependency on Re.

The factor importance plots show many important trends even though only nine tests were run. After looking at these plots, it can be said that DFW is not a strong contributor to tube wall heat transfer. Also, AOA = 20˚ and Re = 230 are not good conditions to obtain tube wall augmentation. With these findings, the number of test parameters was reduced so that results could be found for the best augmentation performers. DFW of $0.29L_p$ was discontinued because

all of the DFWs showed nearly equal augmentations. AOA = 20° testing was also stopped due to the lack of augmentation benefit. Finally, ARs of 2 and 3 were dropped from further testing as well because of average augmentation at AR = 2 and below average augmentation at AR = 3. Re = 230 could not be dropped because a radiator must operate in this range. Further testing at Re = 230 focused on maintaining tube wall heat transfer at or near baseline levels.

Figure 4.23 shows a factor significance plot for the parameters tested. Factor significance plots show the relative amount that each parameter contributes to heat transfer augmentation, which is really a measure of the range of augmentation values over the level range. Re had the strongest influence on augmentation (61.1% relative significance) because it showed a wide range over the parameter levels with a negative augmentation value at Re = 230 and above average augmentation values at Re = 615 and Re = 1016. AOA was the second most important factor at 21.8% relative significance, followed by AR at 16.7%. The DFW relative significance barely shows on the chart at 0.4%. The factor significance plot reinforces the earlier statement that DFW is not a significant contributor to wall heat transfer augmentation while all other parameters are.

Based on the Taguchi results, the optimized set of levels for heat transfer augmentation was found to be DFW = $0.22L_p$, AOA = 30˚, AR = 1.5, and Re = 1016. The Taguchi statistical analysis also gives an expected value for augmentation at this optimized condition, but a good expected value can only be found when linear dependencies on the parameters exist. Since the importance plots show nonlinear behavior for DFW, Re, and AOA, the expected result is not useable. Regardless, the Taguchi optimization differed from our hypothesized optimization. Extra tests were run to directly compare performance at AOA = 30˚ and 40˚ and DFW = $0.15L_p$ and $0.22L_p$. Comparisons were also made between Re = 615 and 1016 because the results were too close to choose an optimized condition.

Figure 4.24 shows the results of tests run to determine which DFW value would yield the highest augmentation. Both tests were run at Re = 615, AOA = 40˚, and AR = 1.5. The test with DFW = $0.15L_p$ shows a slightly higher heat transfer augmentation of 2.80%. A direct comparison of Re can be seen in Figure 4.25. The results in this plot are in terms of streamwise Nusselt augmentation, instead of the usual streamwise Nusselt number because the Nusselt numbers for two different Re cannot be directly compared. The constant conditions for these two tests were AOA = 40˚, DFW = $0.15L_p$, and AR = 1.5. The Re = 1016 case outperformed the

Re = 615 test by 2.65%. Finally, a direct comparison of AOA = 30˚ and 40˚ is shown in Figure 4.26. The constant test conditions for these trial were DFW = $0.15L_p$, AR = 1.5, and Re = 1016. Looking at Figure 4.26, there is not much difference in the two tests with the exception of the slightly higher Nusselt number at X = 0.125. The difference in augmentation between the two Re tests was a very small 0.34%.

The direct comparison trials for each of the parameter levels produced augmentation differences of less than 3%. Augmentation differences within experimental uncertainty, combined with the small number of comparison tests run did not allow for any strong generalizations to be made about the differences between these parameter levels. For these reasons, no optimized parameter set will be given until later in this chapter.

At this point in testing, there were still several effects that needed to be studied. First of all, the winglet setup used in the Taguchi trials had a mixed winglet orientation. It was still unknown what would happen if all VG-F or VG-B winglets were used. Second, no friction factor data had been collected. High heat transfer augmentation usually results in a higher friction factor. We wanted to know what ratios of heat transfer augmentation to friction factor augmentation we were getting with the winglets. The final effect that needed testing was winglet thickness. If the winglets were manufactured by stamping the louvers, then they would be the same thickness of the louvers. Tests needed to be run to compare winglets of louver thickness to the thin Inconel winglets used in all of the cases shown so far.

4.3 Backwards Vortex Generator and Rectangular Winglets Testing

To find which winglet orientation performed better with an alternating direction, a test was run where winglets upstream of the turnover were in the VG-F orientation while winglets oriented in the VG-B orientation were downstream of the turnover. This test, compared to the alternating winglet and direction case for Re = 1016, AOA = 30˚, DFW = $0.15L_p$, and AR = 1.5, can be seen in Figure 4.27. Notice that the VG-B orientation performs better than the mixed orientation from X = 0.675 to 0.825 while the VG-F orientation line falls below the mixed orientation line from X = 0.225 to 0.475. Since the VG-B orientation showed higher augmentation than the VG-F orientation, the test was rerun with all VG-B winglets. Figure 4.28 shows the results of this test once again compared to the mixed orientation test. The VG-B

winglets produced an average heat transfer augmentation of 34.40% which was 9.24% higher than the mixed winglets test.

Our hypothesis for why the VG-B winglets performed better than VG-F winglets has to do with the amount of winglet surface area immersed in subsequent hot and cold regions. If general flow redirection was the cause of increased heat transfer augmentation with the alternating winglet directions, then it would be beneficial for winglets directing cool air towards the wall to have more surface area in the center channel region. Conversely, it would also be better for the winglets that move the hot tube wall air to the center channel to have most of the surface area near the wall. Both of these situations occur with a full set of backwards winglets. When the winglets are in VG-F orientation, the smaller part of the winglet is in these critical areas, and the air has more of an ability to pass over the winglet and avoid redirection.

With these thoughts, rectangular winglets were added to the test matrix to get a better idea of what the results of a non-vortex generating shape would produce. Similar results to those of the VG-B orientation would support the general flow redirection hypothesis. As stated earlier, several tests were run with the high augmentation parameter levels, for both VG-B winglets and rectangular winglets, so direct comparisons between winglet shape and parameter levels could be made. The heat transfer results for these tests can be seen in Figure 4.29. Results are given in terms of average augmentation versus Re for easier comparison.

Looking at Figure 4.29, there are direct comparisons between AOA, DFW, and winglet shape shown for all Re. At Re = 230, all of the tests show near zero augmentation. At Re = 615, all three of the rectangular winglets tests were above 35% augmentation, while the only VG-B test near 35% was the one with AOA = 40˚ and DFW = $0.15L_p$. There is not enough separation between the various tests above 35% augmentation to make any generalizations about performance. The 30˚ VG-B cases showed augmentations of 24.86% and 24.57%, with the higher of the two corresponding with the DFW = $0.15L_p$ test. At Re = 1016, the highest heat transfer performer was the rectangular winglets at 40˚ and DFW = $0.15L_p$. All other test cases, with the exception of the VG-B winglets at AOA = 30° and DFW = $0.22L_p$ show similar heat transfer augmentations in the mid-30% range.

From this test set, several conclusions can be made about winglet shape, AOA, DFW, and Re. First, no matter how high the augmentations are for the higher Re tests, results for Re = 230 stay around zero percent. At higher Re, rectangular winglets showed better augmentation than

the VG-B winglets, and DFW = $0.15L_p$ was slightly better than DFW = $0.22L_p$. Also, the AOA = 40˚ winglets yielded higher heat transfer than the 30˚ winglets for VG winglets but results conflicted for rectangular winglets. There were also conflicting results for which Re produced the highest heat transfer augmentation. Three of the six lines showed increased augmentation from Re = 615 to Re = 1016 while the other three showed the opposite trend. Averaged over all three Reynolds numbers, the best heat transfer performer at all Re was the rectangular winglets at AOA = 40˚, DFW = $0.15L_p$, showing a maximum average augmentation of 38.54% at Re = 1016.

As mentioned earlier in this section, friction factor measurements were made for all of the VG-B and rectangular winglets cases. Friction factor data for the tests just described can be seen in Figure 4.30. Several of the friction factor trends match the heat transfer trends as well. The rectangular winglets yielded higher friction factor augmentations than the VG-B winglets and 40˚ winglets produced higher augmentations than 30º winglets. These trends hold true for Re = 615 and Re = 1016, but not for Re = 230 where the pressure drop measurements are misleading due to the large associated uncertainty. Nothing can be said about DFW though because $0.15L_p$ shows lower friction factor augmentation for rectangular winglets but higher for VG-B winglets. The optimized parameter levels for lowest friction factor were VG-B winglets at 30˚, with a DFW of $0.22L_p$, showing only a 6.9% augmentation over the baseline at Re = 1016. This number may seem very small when compared to friction factors shown in flat plat studies, but is normal when looking at the amount of flow that is actually affected by the winglets. For example, two winglets with AR = 1.5 on a louver at AOA = 40˚ only take up about 17.4% of the fin height. With the smaller winglet angle, there is less blockage to the flow, and therefore a smaller friction factor. There is a much larger flow area that is not affected by the winglets than is affected by the winglets, meaning the winglets only increase the pressure drop for a small portion of the flow.

As stated earlier, we wanted to know the ratio of heat transfer augmentation to friction factor augmentation. This ratio, given in the following equation,

$$\eta = \frac{\overline{Nu/Nu_0 - 1}}{f/f_0 - 1} \tag{4.1}$$

will be referred to as the efficiency index in the rest of the document. Combining the heat transfer and friction factor augmentation terms into the efficiency index was a good method to quantify a gain over penalty relationship. A large heat transfer augmentation may not be desirable if it corresponds to a large friction factor augmentation. With a radiator, extra pumping power is gained by increased vehicle speed. At the lower Re, where a fan is supplying the necessary convection, extra friction factor may cause the need for a larger and more costly fan. By defining efficiency index for the winglet studies, Modine was able to gauge the relative importance of heat transfer and friction factor augmentations in their design considerations.

The efficiency indexes for the direct comparison tests can be seen in Figure 4.31. On average, the VG-B winglets outperformed the rectangular winglets with the only exception being that the 40˚ VG-B winglets dropped below the results for the rectangular winglets at 30˚ and $0.15L_p$. At Re = 230, the efficiency index is nearly zero for all cases due to the very small heat transfer augmentation results that make up the numerator in the calculation. Re = 615 showed the highest efficiency index for all winglet setups because the heat transfer augmentations at Re = 615 were near those at Re = 1016, while the friction factor augmentation was several percent lower. At Re = 1016, it is worth mentioning the VG-B winglets at AOA = 30˚ and DFW = $0.15L_p$. This point is the one with the possibly erroneous results for heat transfer augmentation and therefore may be higher than the $0.22L_p$ winglets for this reason. Due to this, the optimization will go to the VG-B winglets at AOA = 30˚ and DFW = $0.22L_p$ with an efficiency index of 6.41 at Re = 615 and 4.14 at Re = 1016. Due to the fact that friction factor augmentations were more spread out than heat transfer augmentations, friction factor really set the shapes and AOAs apart. Since nearly equal heat transfer augmentation results were achieved with VG-B and rectangular winglets, but the friction factor was much higher for the rectangular winglets, the VG-B winglets were found to have a more efficient shape.

Winglet Thickness Testing

The final set of testing for the 100% louver length winglets involved a comparison of winglet thickness. All tests mentioned to this point were run with the thin Inconel winglets, but nothing was known about the effect of thickness on heat transfer and friction factor augmentation. To run the thick winglets tests, balsa winglets of louver thickness with AR = 1.5

were made and glued onto the thin winglets for support. The first test, which can be seen in Figure 4.32, was run with VG-B winglets at AOA = 30˚ and DFW = $0.15L_p$. The trends for Re = 1016 and Re = 615 are very similar, showing a slight augmentation between the entrance and turnover louver, below baseline augmentation at the turnover, and near baseline results between the turnover and exit louvers. The augmentations for Re = 1016 and 615 were 2.28% and 5.66% respectively. The Re = 230 test showed worse than baseline results through the whole test section, yielding an augmentation percentage of -7.78%. With thin winglets, this same configuration yielded 34.40%, 24.86% and -0.18% at Re = 1016, 615, and 230, respectively. These augmentation percentages show that winglet thickness had a strong adverse impact on heat transfer augmentation.

Friction factor augmentation data can be seen in Figure 4.33, compared to the same case with thin Inconel winglets. The friction factor augmentation increased by 5.8% at Re = 615 and 7.0% at Re = 1016 when the thickness was increased from thin to louver thickness winglets. Figure 4.34 shows the efficiency indexes of the thick and thin winglets cases just mentioned. With the combination of lower heat transfer augmentation and higher friction factor augmentation, the efficiency index for the thick winglets came out to about zero for all Reynolds numbers. With the thick winglets, there was minimal heat transfer augmentation combined with an increased friction factor, meaning that winglets of louver thickness in the VG-B orientation provided no benefit to the heat exchanger.

In an attempt to identify the cause of the decreased effectiveness of the winglets, two extra tests were run. In the first test, some of the extra winglet material was cut off in the downstream direction. In the second test, VG-F winglets were run in the same configuration. Cutting the winglets in the downstream direction was an attempt to make the thick and thin winglets look the same to the incoming flow (see Figure 4.35). Looking at Figure 4.35, a downstream cut would be directly into the page. In the cut winglets tests, every other winglet was cut to avoid damaging the Inconel winglets aimed away from the wall. The VG-F winglets test was run without cuts because VG-F winglets do not have a large piece of extra material like the VG-B winglets do.

Heat transfer augmentation results for thick winglets with and without cuts, and thin winglets can be seen in Figure 4.36. The tests were only run at Re = 1016, with AOA = 30˚, DFW = $0.15L_p$ and AR = 1.5. In order of best to worst heat transfer augmentation were thin VG-

B winglets (34.40%), thick VG-B winglets with cuts (15.72%), thick VG-F winglets (12.13%), and thick VG-B winglets (2.28%). By cutting every other VG-B winglet, the heat transfer augmentation rose to about halfway between the thick and thin VG-B winglets results. Placing the winglets in the VG-F orientation also improved heat transfer augmentation over thick VG-B winglets.

The friction factor augmentations and efficiency indexes for these tests can be seen in Figures 4.37 and 4.38. The friction factor augmentations shown in Figure 4.37 have the exact opposite trends as heat transfer augmentations shown in Figure 4.36. The thin VG-B winglets have the lowest friction factor augmentation at 7.77% while the thick VG-B winglets were the highest at 14.74%. The efficiency indexes shown in Figure 4.38 have the same trends as the heat transfer augmentation with thin VG-B winglets being far more efficient than any other winglet setup and the thick winglets being completely inefficient.

Although the exact cause of the poor performance with the thick winglets was not determined, reducing the extra material by cutting the winglets and placing them in VG-F orientation did seem to make the results closer to those for the thin winglets. Due to this, it is believed that the extra material that the flow sees, not the winglet thickness in general, is the main cause of the reduced efficiency. If the winglets were stamped from the louver material, the thickness would be a set value. These tests show that although thickness may not be able to be controlled, tube wall heat transfer is very sensitive to it.

4.4. Summary of Findings

Several different winglet parameters were tested with the 100% louvers, including AOA, DFW, AR, Re, winglet direction, winglet orientation, winglet shape, and winglet thickness. Using the Taguchi methodology and running tests to directly compare parameter level performance, general trends for each of these parameters were found. Also, optimizations were found for highest heat transfer augmentation, lowest pressure drop (for high heat transfer augmentation parameters), and highest efficiency index. In this section these trends and optimizations will be discussed generally based on the more detailed text in previous sections. As in Chapter 2, the parameters will be split into individual winglet parameters, overall winglet setup parameters, and flow parameters for discussions of trends and optimizations.

With respect to individual winglet parameter levels, the levels that produced high heat transfer augmentation generally produced high friction factor augmentation as well. This statement holds true for AOA, DFW, and winglet shape. Winglet thickness was the only parameter that showed opposite results with very low heat transfer augmentation and high friction factor augmentation. Friction factor tests were not run with any AR other than 1.5, however, it would make sense that increasing winglet size, and therefore heat transfer augmentation, would also increase friction factor augmentation as was true when switching from VG winglets to rectangular winglets.

Heat transfer augmentation increased with increasing AOA, increasing winglet size (decreasing AR), and decreasing DFW. For AOA = 20˚, results were poor, however, AOA = 30˚ and 40˚ performed very well, with the slight performance edge to the higher angle. The augmentation trend for AR in the VG winglet studies was linear with winglet length or surface area. An AR of 3 did not provide much benefit, AR = 2 results were average, and AR = 1.5 was the best producing high augmentations. Doubling the surface area of a VG winglet to make rectangular winglets also increased the heat transfer augmentation. Increasing winglet thickness was very detrimental to heat transfer augmentation, yielding significantly decreased augmentations compared to the thin winglets tests. The best heat transfer performer was the rectangular winglets at AOA = 40° and DFW = $0.15L_p$ with augmentations of 38.54%, 36.01%, and 3.36% at Re = 1016, 615, and 230 respectively.

As mentioned earlier, parameter levels that yielded higher heat transfer augmentations also produced higher friction factor augmentations. AOA = 30° had less associated pressure drop than the 40° winglets. Decreasing winglet size led to decreased friction factor augmentations. No generalizations can be made about the effect of DFW on friction factor augmentation because of conflicting results between the VG-B and rectangular winglets tests. Finally, increasing winglet thickness caused a large increase in friction factor augmentation. The optimized condition for lowest friction factor augmentation was the thin VG-B winglets with AOA = 30° and DFW = $0.22L_p$.

The best performers for efficiency index also had the lowest friction factor augmentations. This is true because all of the winglet setups had relatively close heat transfer augmentations while the friction factor augmentations were spread apart. The optimized case for

efficiency index was also the VG-B winglets with AOA = 30°, DFW = $0.22L_p$, showing results of 4.14, 6.41, and -0.61 at Re = 1016, 615, and 230 respectively.

There were three main overall winglet setups tested: VG-F winglets all aimed towards the wall, alternating winglet direction and orientation, and alternating winglet direction with VG-B winglets throughout. Of the three, friction factor data was only taken for the alternating winglet direction with VG-B winglets. Because of this, only a heat transfer augmentation optimization can be given. When all of the winglets were aimed towards the wall, the average heat transfer augmentations were always low with Nusselt numbers following the turnover louver below the baseline Nusselts. When winglet direction and orientation were alternated on every other louver, results were significantly improved with a maximum augmentation of 25.50% at Re = 1016, AOA = 40°, and DFW = $0.15L_p$. When all winglets were placed in the VG-B orientation with alternating direction, results improved once again, yielding augmentations of 33.41% at the same test conditions just mentioned. I believe it is safe to extend these results and say that if all winglets had been tested in the VG-F orientation with alternating direction that, Nusselt augmentation would be below the augmentation for the winglets with alternating orientation.

The ability of the winglets to augment heat transfer increased from Re = 230 to 615 but stayed fairly constant from Re = 615 to 1016. At Re = 230, none of the winglet setups produced augmentations greater than 4%. Augmentations at Re = 615 were much higher than at Re = 230 and only slightly different than those at Re = 1016. We believe that the increased augmentations at higher Re have to do with the higher flow rates reacting more to the blockage caused by the winglets. At Re = 230, the flow does not seem to get forced towards or away from the wall well enough to create good circulation. Friction factor augmentation also increased with Re. Most of the results in this chapter showed a fairly linear trend of friction factor augmentation with respect to Re, however, the large error associated with the Re = 230 friction factor measurements may be causing a misleading trend. Efficiency index increased sharply from Re = 230 to Re = 615 but dropped off from Re = 615 to Re = 1016. These results were mostly dominated by friction factor augmentation because friction factor varied more over the level range than heat transfer augmentation did.

Table 4.1 Winglet Setup, Nusselt Augmentation, Friction Factor, and Efficiency Index for all L_l/F_h = 100% Tests

Original Taguchi tests

Re	AOA	DFW	AR	Direction	Orientation	Thickness	Nu_{aug} [%]	f_{aug} [%]	η
625	40˚	$0.22L_p$	1.5	towards	VG-F	0.03t	3.76	N/A	N/A
230	20˚	$0.15L_p$	1.5	towards	VG-F	0.03t	-2.58	N/A	N/A
1016	40˚	$0.15L_p$	1.5	towards	VG-F	0.03t	2.60	N/A	N/A

Alternating winglet direction and orientation

Initial Tests

Re	AOA	DFW	AR	Direction	Orientation	Thickness	Nu_{aug} [%]	f_{aug} [%]	η
1016	40˚	$0.15L_p$	1.5	alternating	alternating VG-F/B	0.03t	25.50	N/A	N/A
625	40˚	$0.15L_p$	1.5	alternating	alternating VG-F/B	0.03t	22.85	N/A	N/A
230	40˚	$0.15L_p$	1.5	alternating	alternating VG-F/B	0.03t	1.74	N/A	N/A

Taguchi Tests (2nd attempt)

Re	AOA	DFW	AR	Direction	Orientation	Thickness	Nu_{aug} [%]	f_{aug} [%]	η
230	20˚	$0.15L_p$	1.5	alternating	alternating VG-F/B	0.03t	-5.65	N/A	N/A
625	30˚	$0.15L_p$	2	alternating	alternating VG-F/B	0.03t	15.90	N/A	N/A
1016	40˚	$0.15L_p$	3	alternating	alternating VG-F/B	0.03t	9.71	N/A	N/A
1016	20˚	$0.22L_p$	2	alternating	alternating VG-F/B	0.03t	6.47	N/A	N/A
230	30˚	$0.22L_p$	3	alternating	alternating VG-F/B	0.03t	-4.54	N/A	N/A
625	40˚	$0.22L_p$	1.5	alternating	alternating VG-F/B	0.03t	20.04	N/A	N/A
625	20˚	$0.29L_p$	3	alternating	alternating VG-F/B	0.03t	-0.11	N/A	N/A
1016	30	$0.29L_p$	1.5	alternating	alternating VG-F/B	0.03t	19.81	N/A	N/A
230	40˚	$0.29L_p$	2	alternating	alternating VG-F/B	0.03t	-2.17	N/A	N/A

Direct comparisons of Taguchi results

Re	AOA	DFW	AR	Direction	Orientation	Thickness	Nu_{aug} [%]	f_{aug} [%]	η
1016	30˚	$0.15L_p$	1.5	alternating	alternating VG-F/B	0.03t	25.16	N/A	N/A

Orientation changes

Initial Tests

Re	AOA	DFW	AR	Direction	Orientation	Thickness	Nu_{aug} [%]	f_{aug} [%]	η

1016	30˚	$0.15L_p$	1.5	alternating	VG-F front/VG-B back	0.03t	25.11	N/A	N/A
Backwards Vortex Generators									
Re	**AOA**	**DFW**	**AR**	**Direction**	**Orientation**	**Thickness**	**Nu_{aug} [%]**	**f_{aug} [%]**	**η**
1016	30˚	$0.15L_p$	1.5	alternating	VG-B	0.03t	34.40	7.77	4.43
615	30˚	$0.15L_p$	1.5	alternating	VG-B	0.03t	24.86	4.71	5.28
230	30˚	$0.15L_p$	1.5	alternating	VG-B	0.03t	-0.18	4.36	-0.04
1016	40˚	$0.15L_p$	1.5	alternating	VG-B	0.03t	33.41	13.11	2.55
615	40˚	$0.15L_p$	1.5	alternating	VG-B	0.03t	34.87	9.03	3.86
230	40˚	$0.15L_p$	1.5	alternating	VG-B	0.03t	3.86	7.67	0.50
1016	30˚	$0.22L_p$	1.5	alternating	VG-B	0.03t	28.72	6.93	4.14
615	30˚	$0.22L_p$	1.5	alternating	VG-B	0.03t	24.57	3.83	6.41
230	30˚	$0.22L_p$	1.5	alternating	VG-B	0.03t	-1.36	2.22	-0.61
Rectangular Winglets tests									
Re	**AOA**	**DFW**	**AR**	**Direction**	**Orientation**	**Thickness**	**Nu_{aug} [%]**	**f_{aug} [%]**	**η**
1016	30˚	$0.15L_p$	none	alternating	Rectangular	0.03t	36.07	13.54	2.66
615	30˚	$0.15L_p$	none	alternating	Rectangular	0.03t	36.37	9.27	3.93
230	30˚	$0.15L_p$	none	alternating	Rectangular	0.03t	1.19	7.46	0.16
1016	30˚	$0.22L_p$	none	alternating	Rectangular	0.03t	35.17	15.49	2.27
615	30˚	$0.22L_p$	none	alternating	Rectangular	0.03t	38.31	11.50	3.33
230	30˚	$0.22L_p$	none	alternating	Rectangular	0.03t	-0.53	6.66	-0.08
1016	40˚	$0.15L_p$	none	alternating	Rectangular	0.03t	38.54	22.75	1.69
615	40˚	$0.15L_p$	none	alternating	Rectangular	0.03t	36.01	16.85	2.14
230	40˚	$0.15L_p$	none	alternating	Rectangular	0.03t	3.36	10.64	0.32
Thick winglets									
Backwards Triangular Winglets									
Re	**AOA**	**DFW**	**AR**	**Direction**	**Orientation**	**Thickness**	**Nu_{aug} [%]**	**f_{aug} [%]**	**η**
1016	30˚	$0.15L_p$	1.5	alternating	VG-B	1.03t	2.28	14.74	0.15
615	30˚	$0.15L_p$	1.5	alternating	VG-B	1.03t	5.66	10.46	0.54

230	30˚	$0.15L_p$	1.5	alternating	VG-B	1.03t	-7.78	7.67	-1.01
Vortex Generator Winglets									
Re	**AOA**	**DFW**	**AR**	**Direction**	**Orientation**	**Thickness**	**Nu_{aug} [%]**	**f_{aug} [%]**	**η**
1016	30˚	$0.15L_p$	1.5	alternating	VG-F	1.03t	12.13	12.24	0.99
Thick with cuts									
Re	**AOA**	**DFW**	**AR**	**Direction**	**Orientation**	**Thickness**	**Nu_{aug} [%]**	**f_{aug} [%]**	**η**
1016	30˚	$0.15L_p$	1.5	alternating	VG-B	1.03t w/cuts	15.72	9.32	1.69

Table 4.2 Parameters for Delta Winglet Testing

	Parameter Levels		
Parameter	1	2	3
Angle of Attack (AOA)	20˚	30˚	40˚
Aspect Ration (AR)	1.5	2	3
Distance from Wall (DFW)	$0.15L_p$	$0.22L_p$	$0.29L_p$
Re	230	615	1016

Table 4.3 Taguchi Test Array

Test #	DFW	AOA	AR	Re
1	$0.15L_p$	20˚	1.5	230
2	$0.15L_p$	30˚	2	615
3	$0.15L_p$	40˚	3	1016
4	$0.22L_p$	20˚	2	1016
5	$0.22L_p$	30˚	3	230
6	$0.22L_p$	40˚	1.5	615
7	$0.29L_p$	20˚	3	615
8	$0.29L_p$	30˚	1.5	1016
9	$0.29L_p$	40˚	2	230

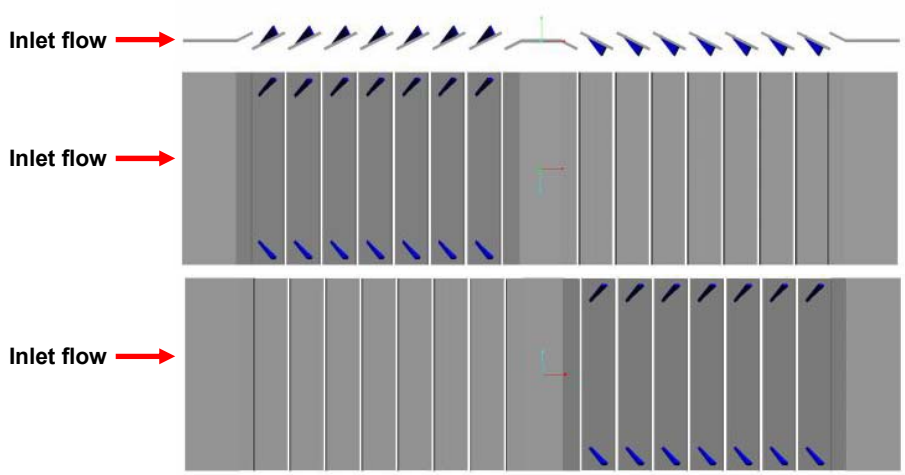

Figure 4.1 Side, top, and bottom view of VG-F winglets all aimed towards the wall.

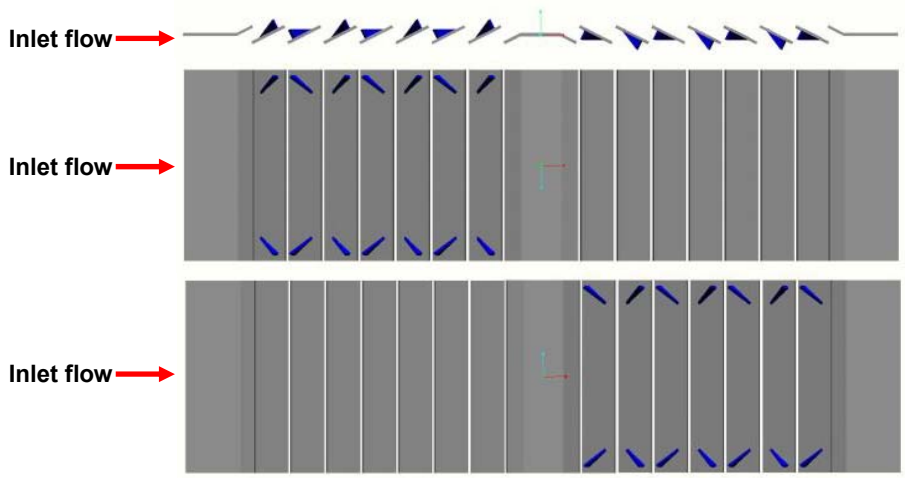

Figure 4.2 Side, top, and bottom view of alternating winglet direction and orientation.

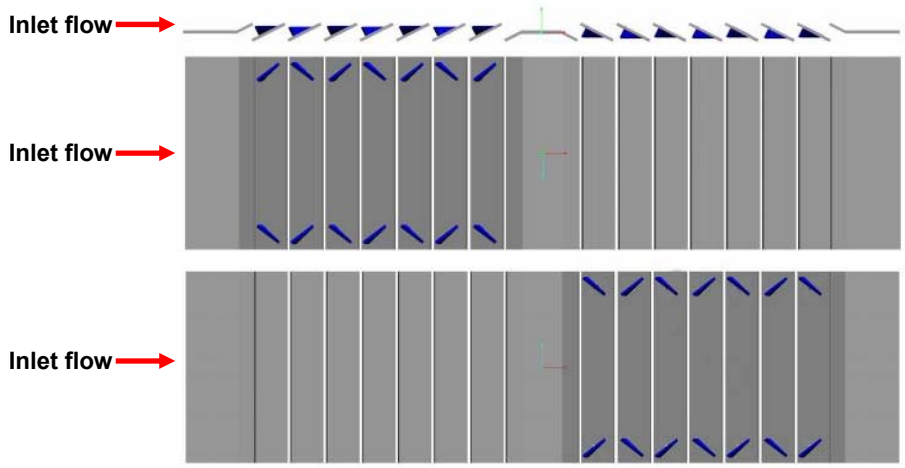

Figure 4.3 Side, top, and bottom view of VG-B winglets with alternating direction.

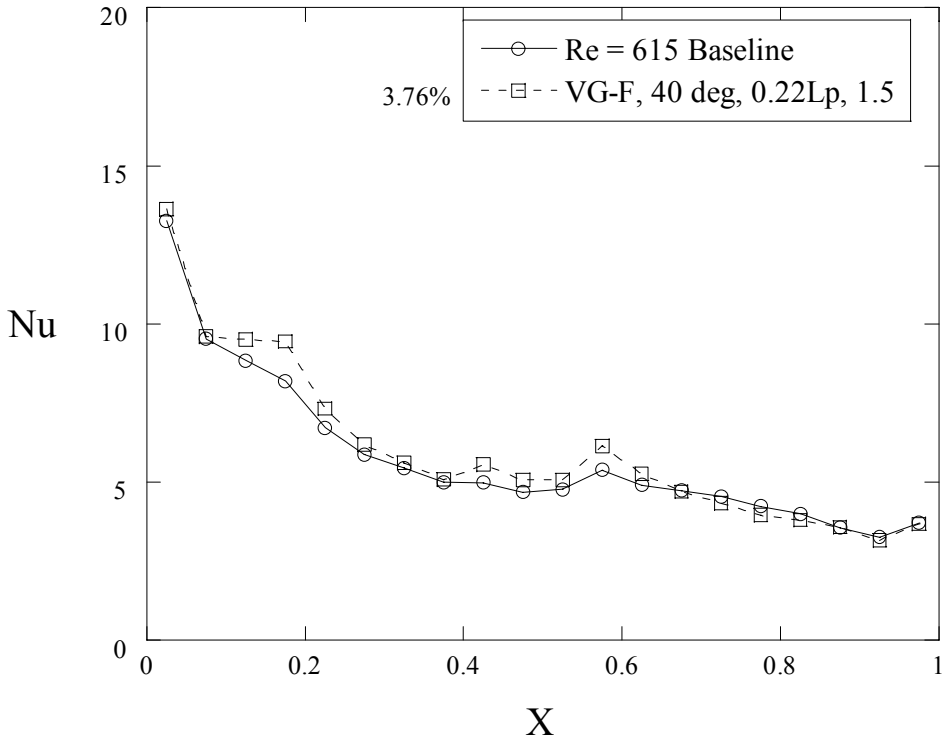

Figure 4.4 Taguchi test 6 with all winglets aimed towards wall in VG-F orientation for Re = 615.

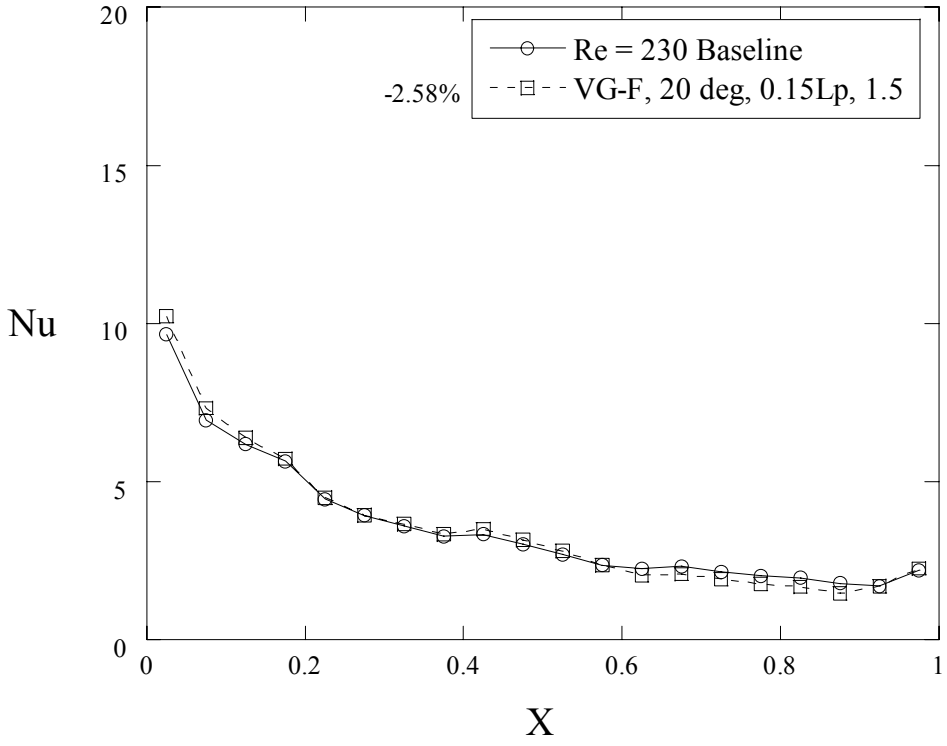

Figure 4.5 Taguchi test 1 with all winglets aimed towards wall in VG-F orientation for Re = 230.

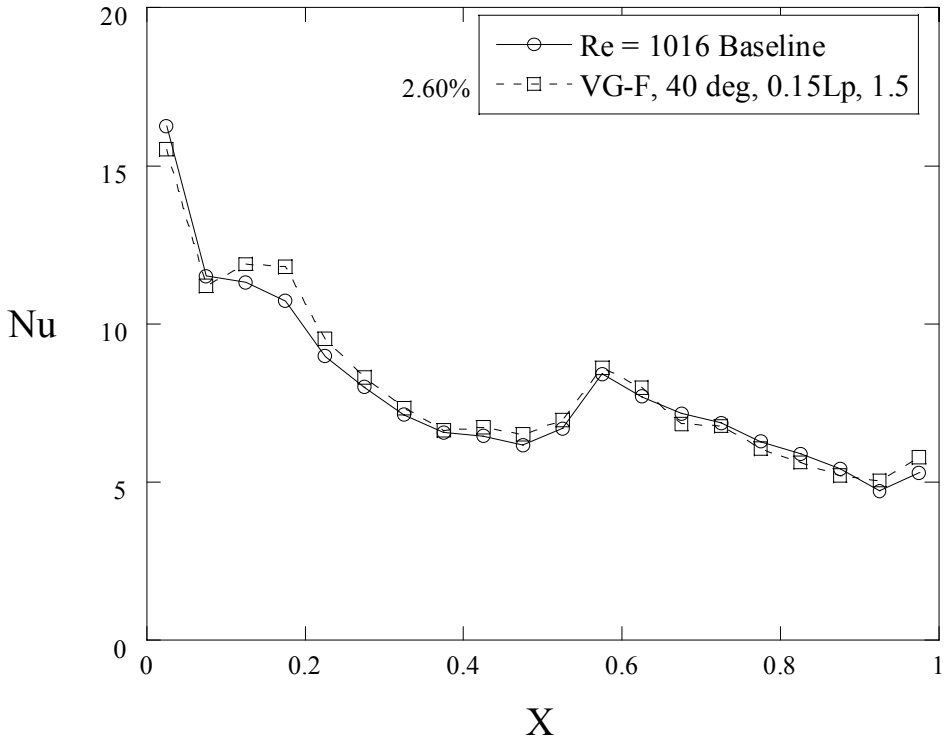

Figure 4.6 Hypothesized best case parameters with all winglets aimed towards wall in VG-F orientation for Re = 1016.

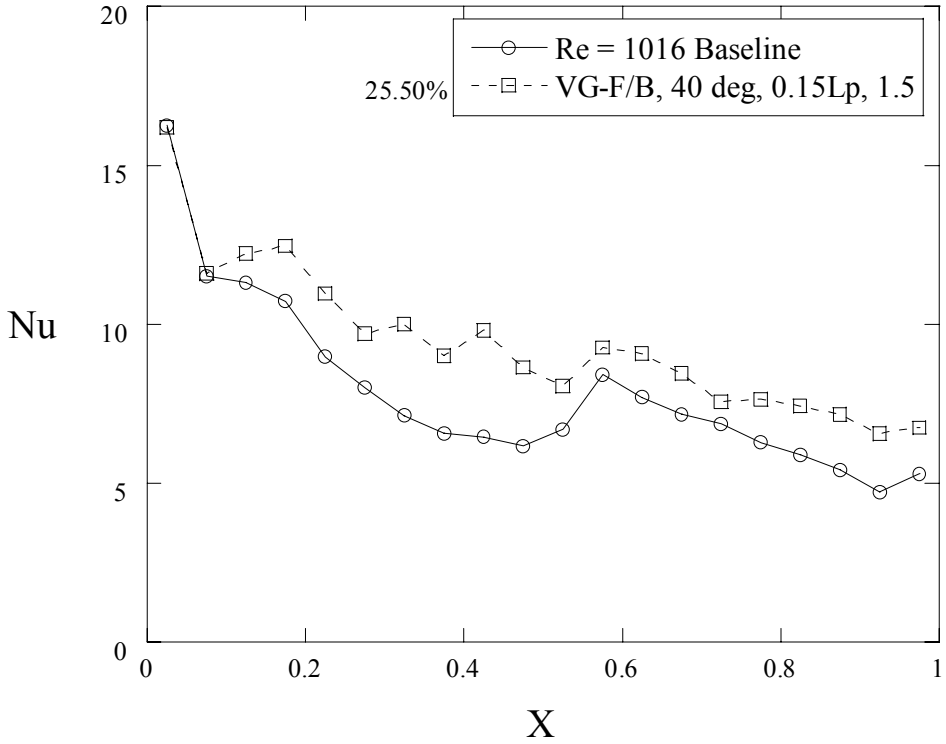

Figure 4.7 Hypothesized best case parameters with winglets with alternating orientation and direction for Re = 1016.

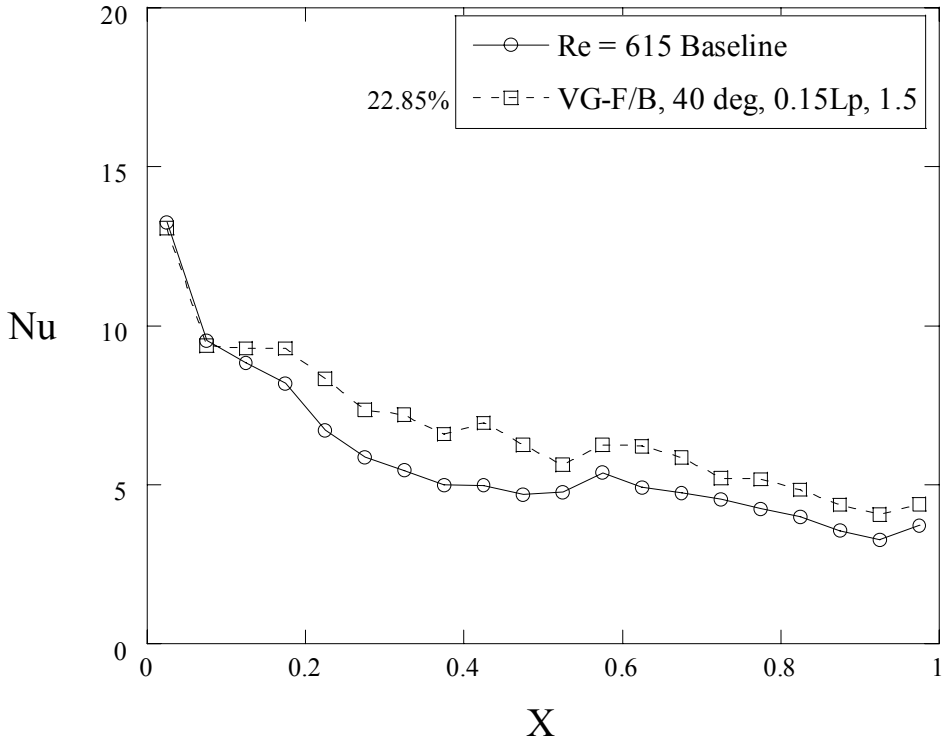

Figure 4.8 Hypothesized best case parameters with winglets with alternating orientation and direction for Re = 615.

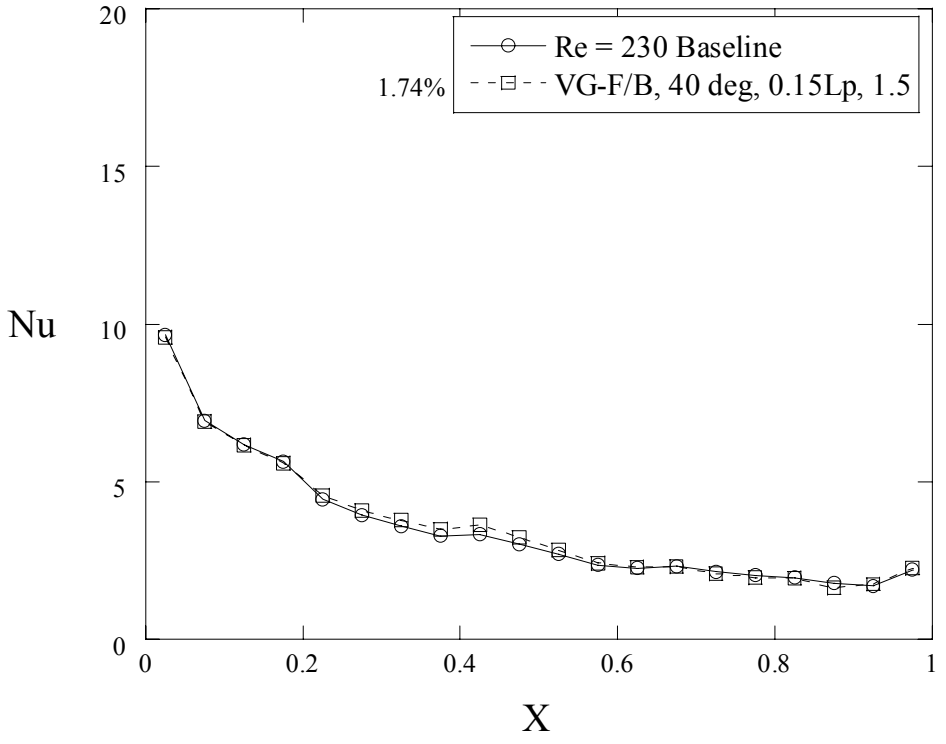

Figure 4.9 Hypothesized best case parameters with winglets with alternating orientation and direction for Re = 230.

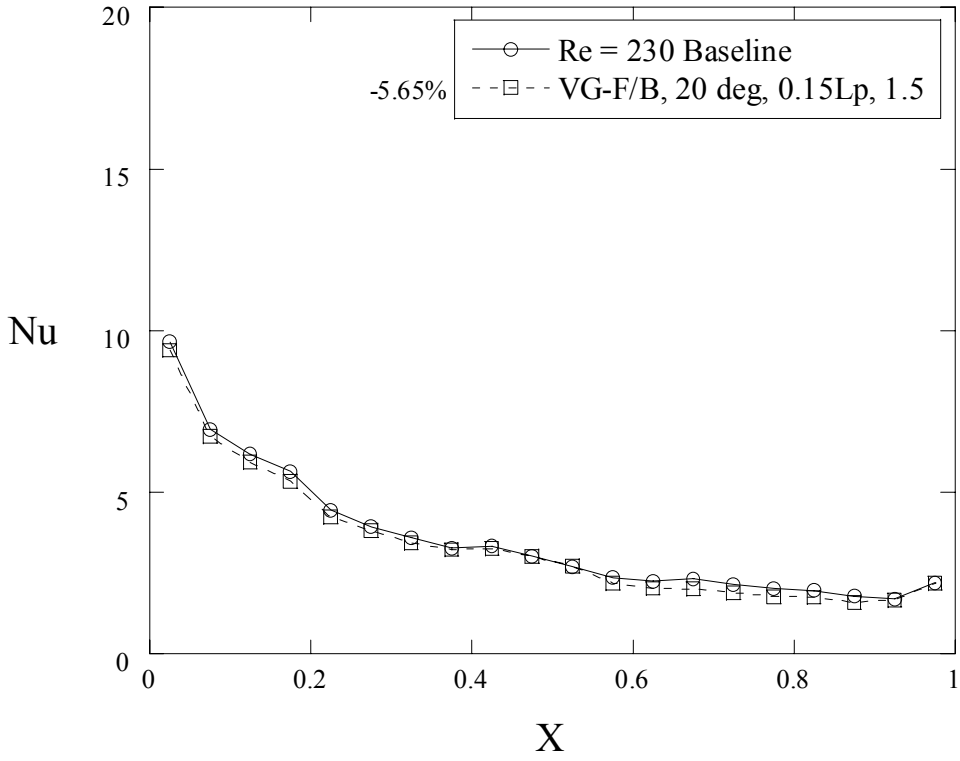

Figure 4.10 Taguchi test 1 with alternating winglet direction and orientation for Re = 230.

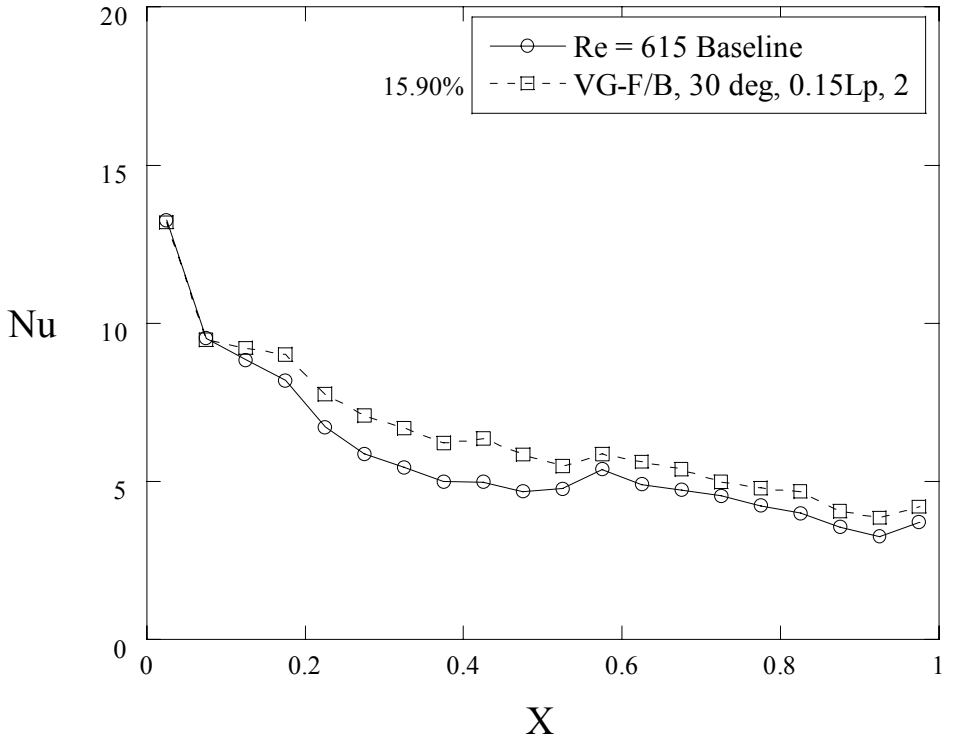

Figure 4.11 Taguchi test 2 with alternating winglet direction and orientation for Re = 615.

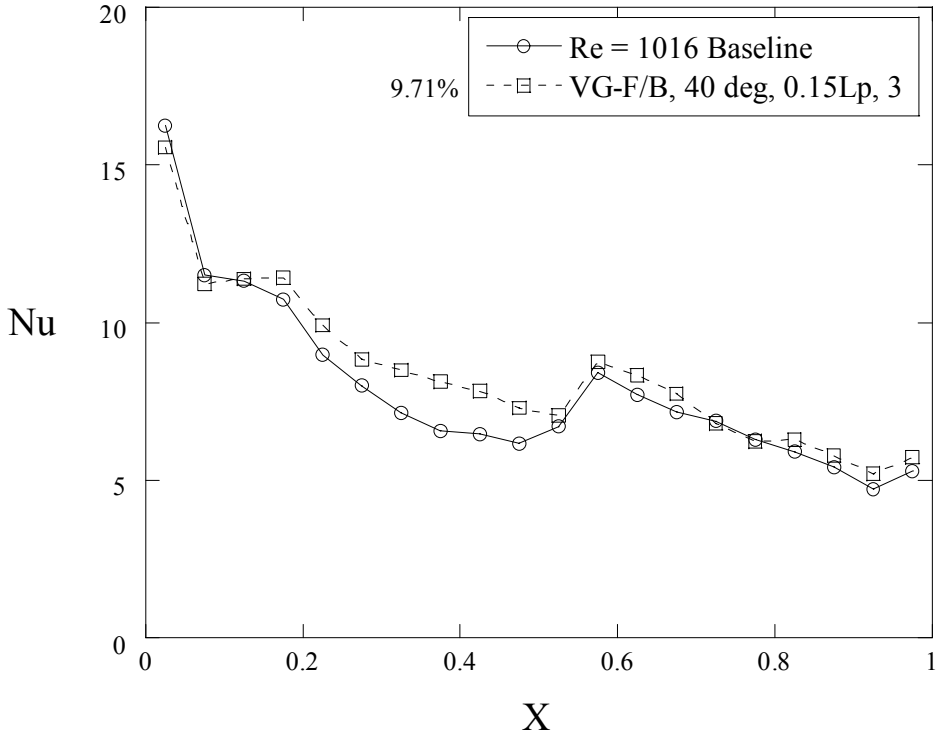

Figure 4.12 Taguchi test 3 with alternating winglet direction and orientation for Re = 1016.

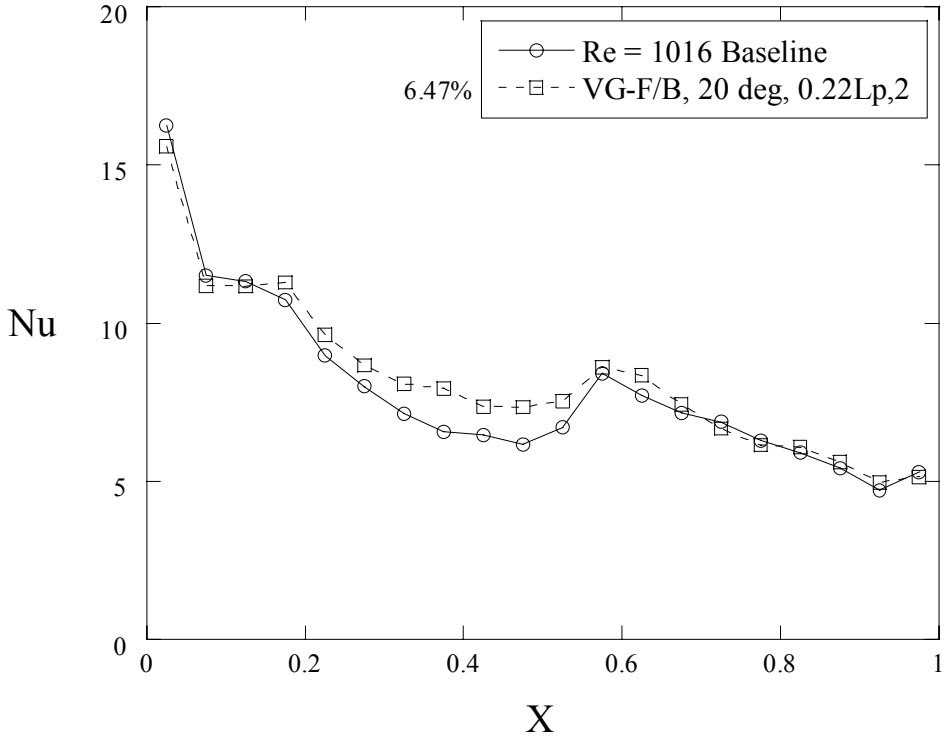

Figure 4.13 Taguchi test 4 with alternating winglet direction and orientation for Re = 1016.

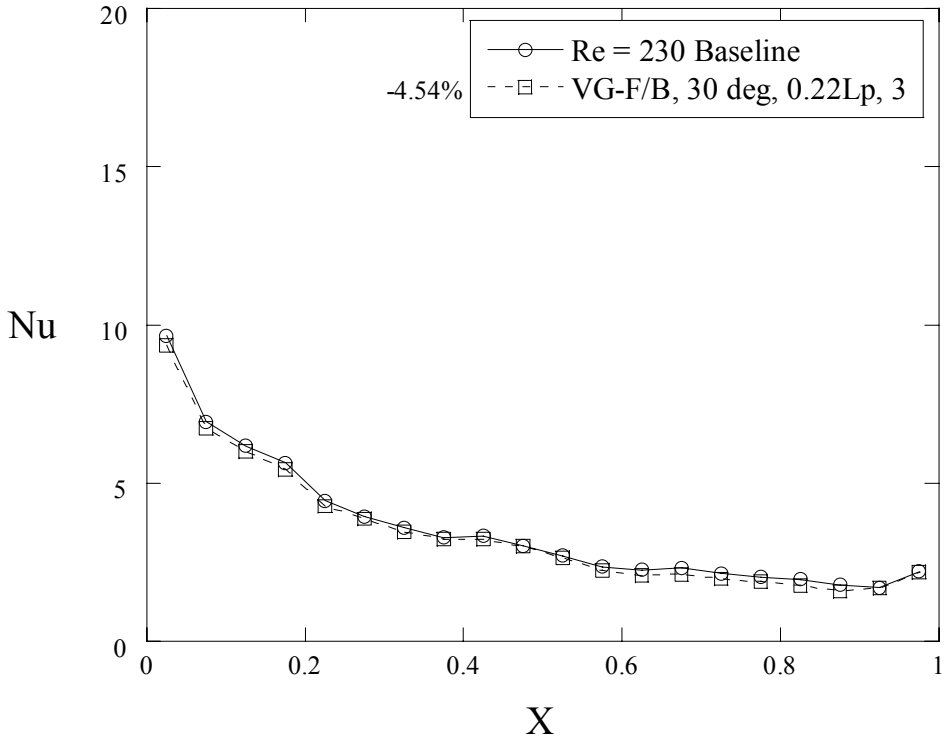

Figure 4.14 Taguchi test 5 with alternating winglet direction and orientation for Re = 230.

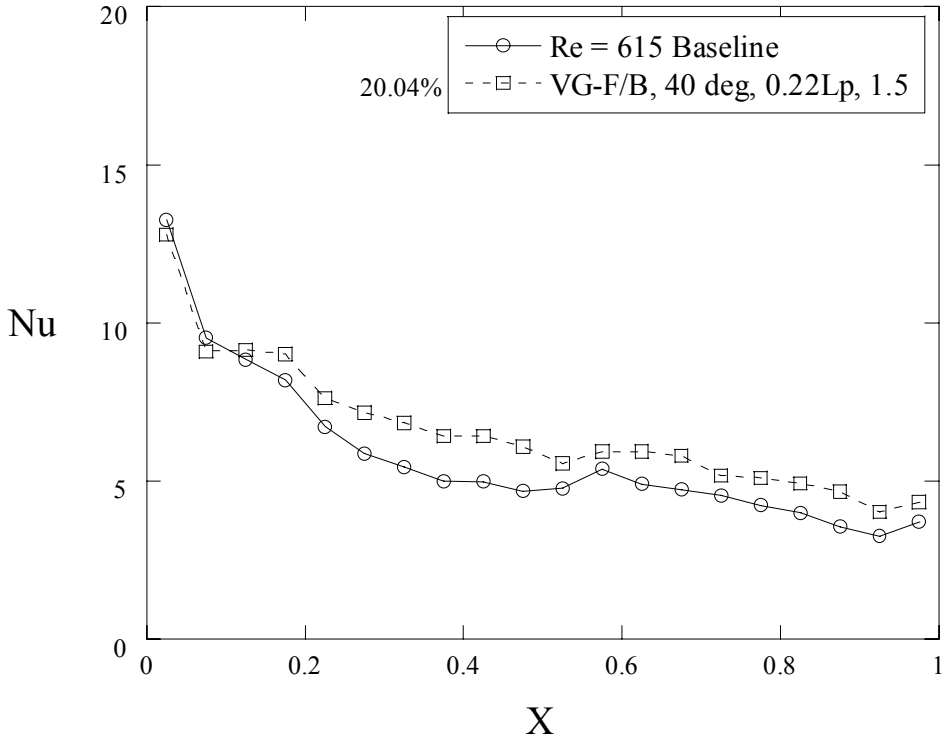

Figure 4.15 Taguchi test 6 with alternating winglet direction and orientation for Re = 615.

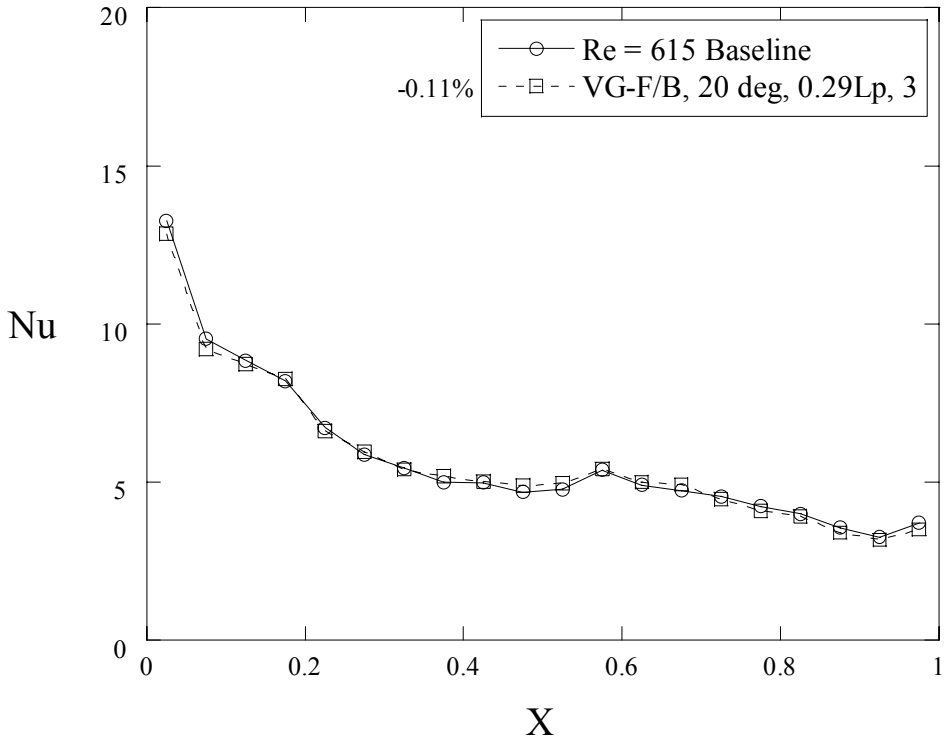

Figure 4.16 Taguchi test 7 with alternating winglet direction and orientation for Re = 615.

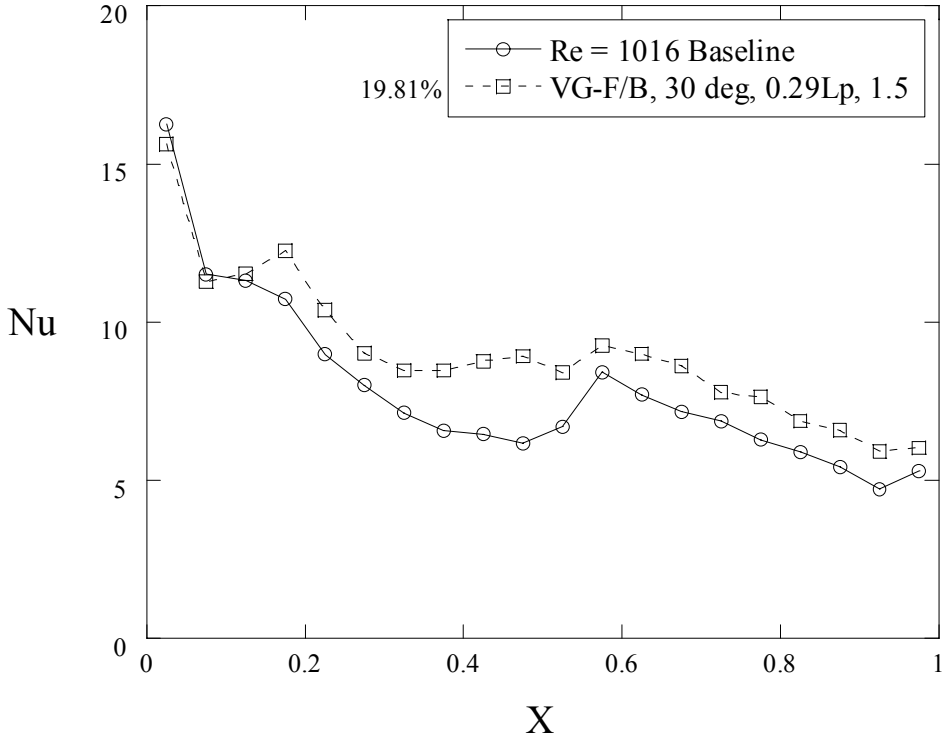

Figure 4.17 Taguchi test 8 with alternating winglet direction and orientation for Re = 1016.

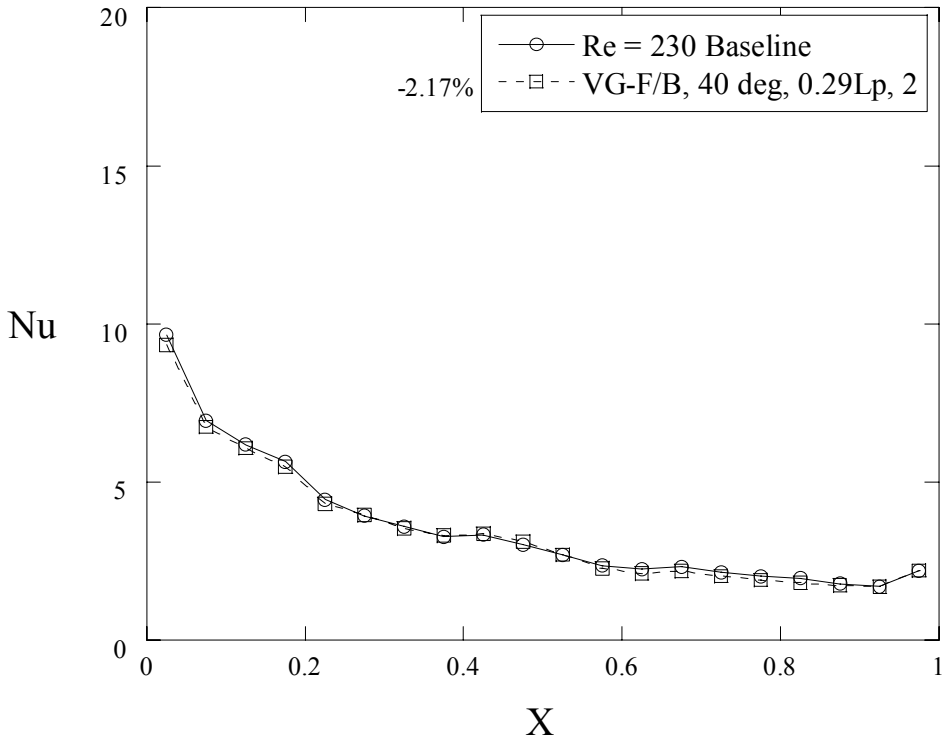

Figure 4.18 Taguchi test 9 with alternating winglet direction and orientation for Re = 230.

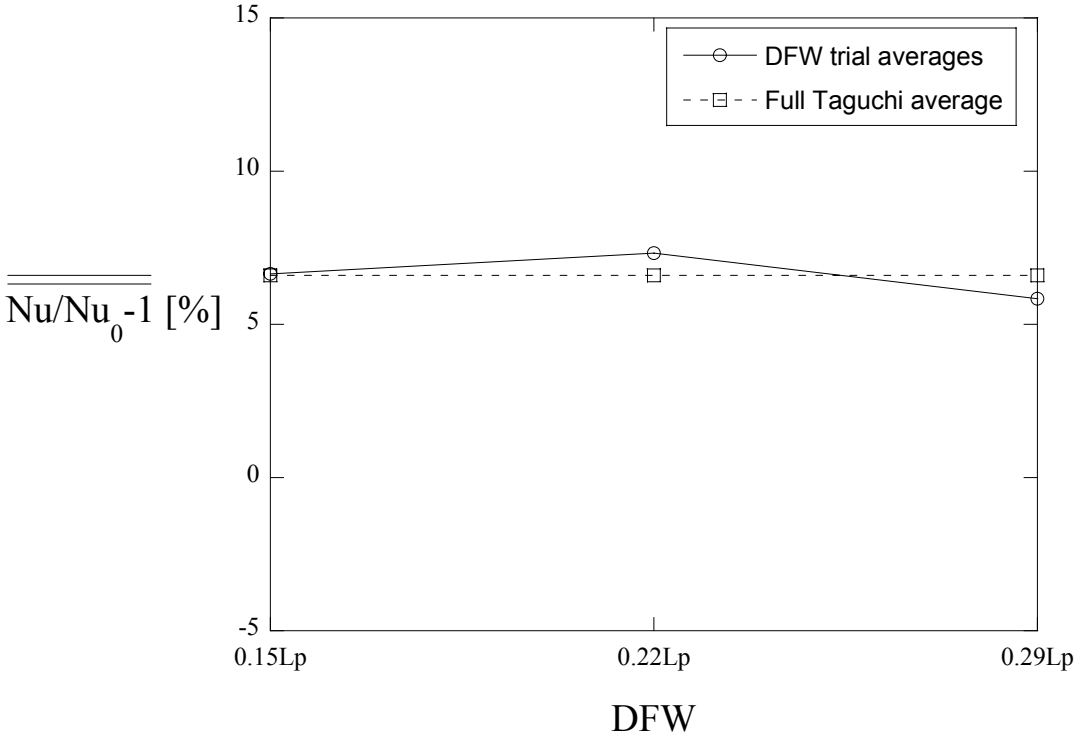

Figure 4.19 Taguchi parameter importance plot for DFW.

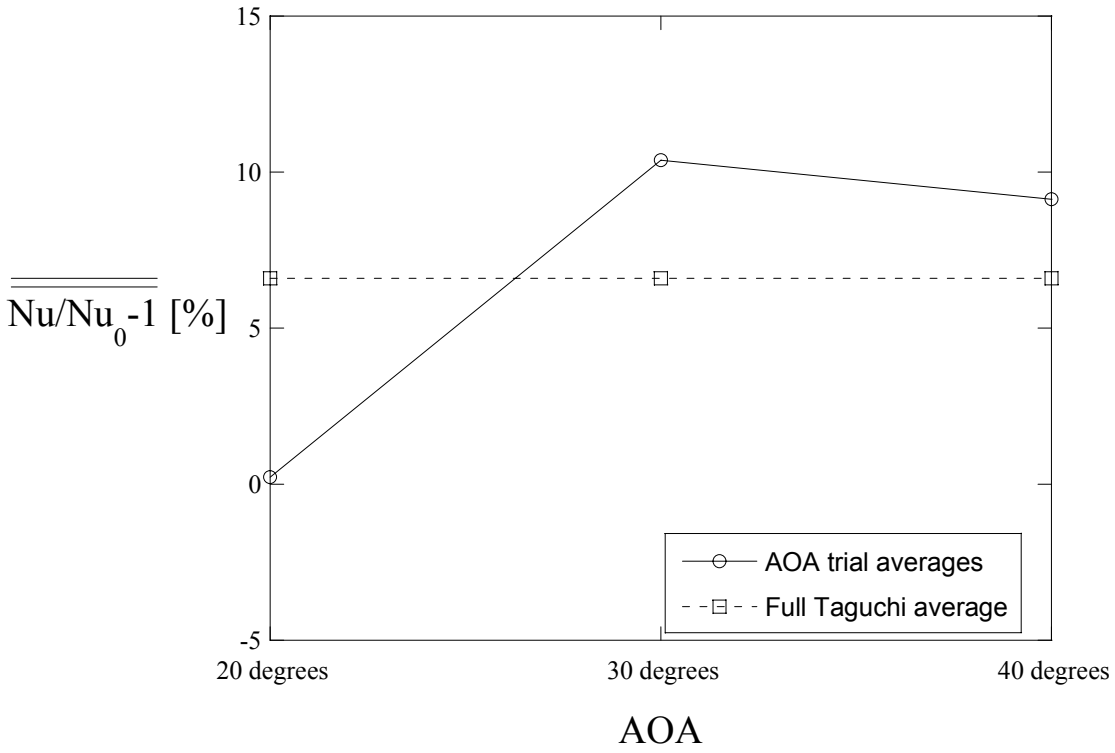

Figure 4.20 Taguchi parameter importance plot for AOA.

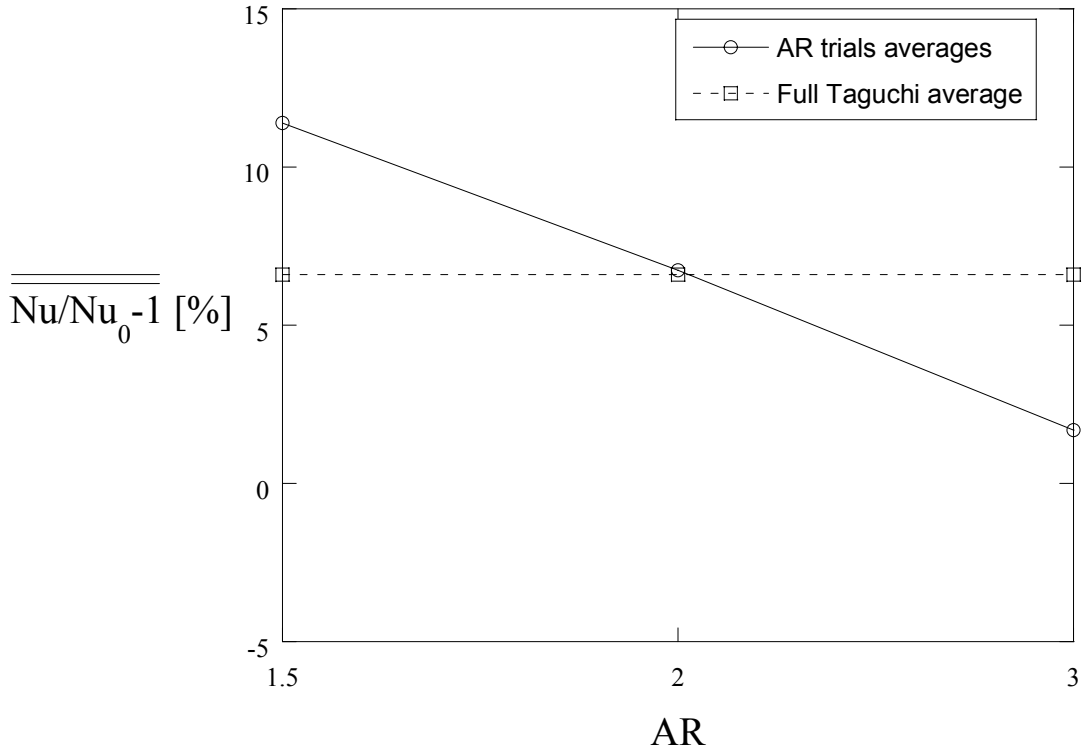

Figure 4.21 Taguchi parameter importance plot for AR.

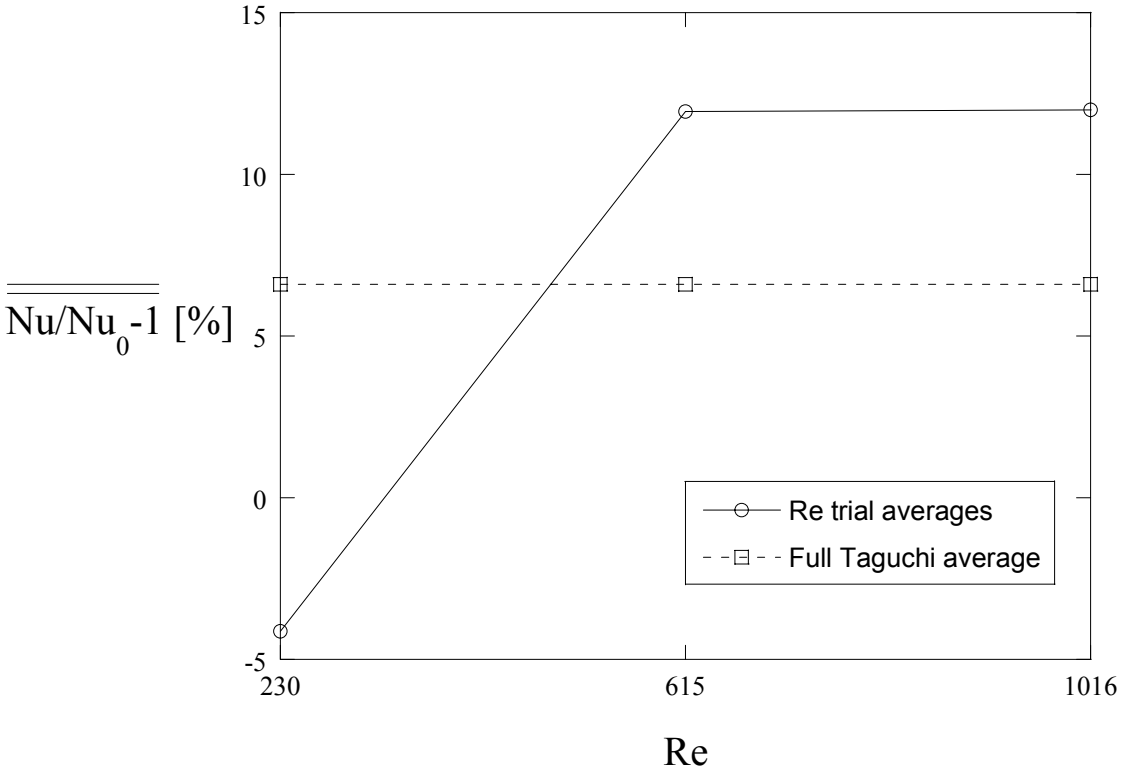

Figure 4.22 Taguchi parameter importance plot for Re.

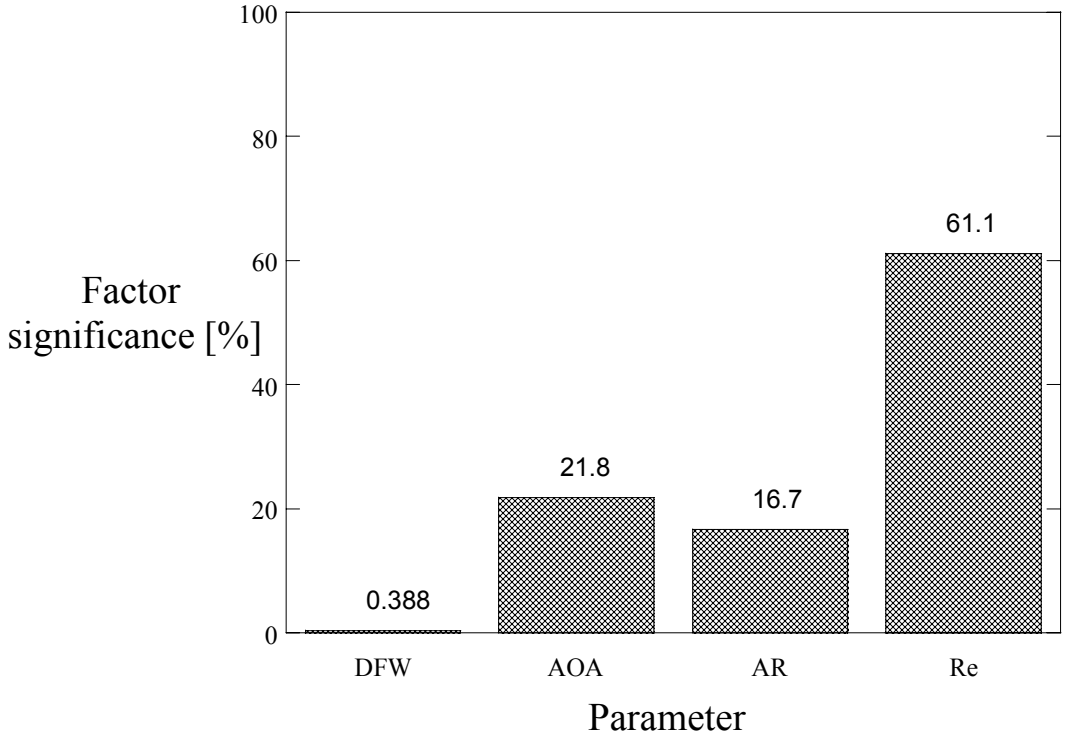

Figure 4.23 Taguchi factor significance plot.

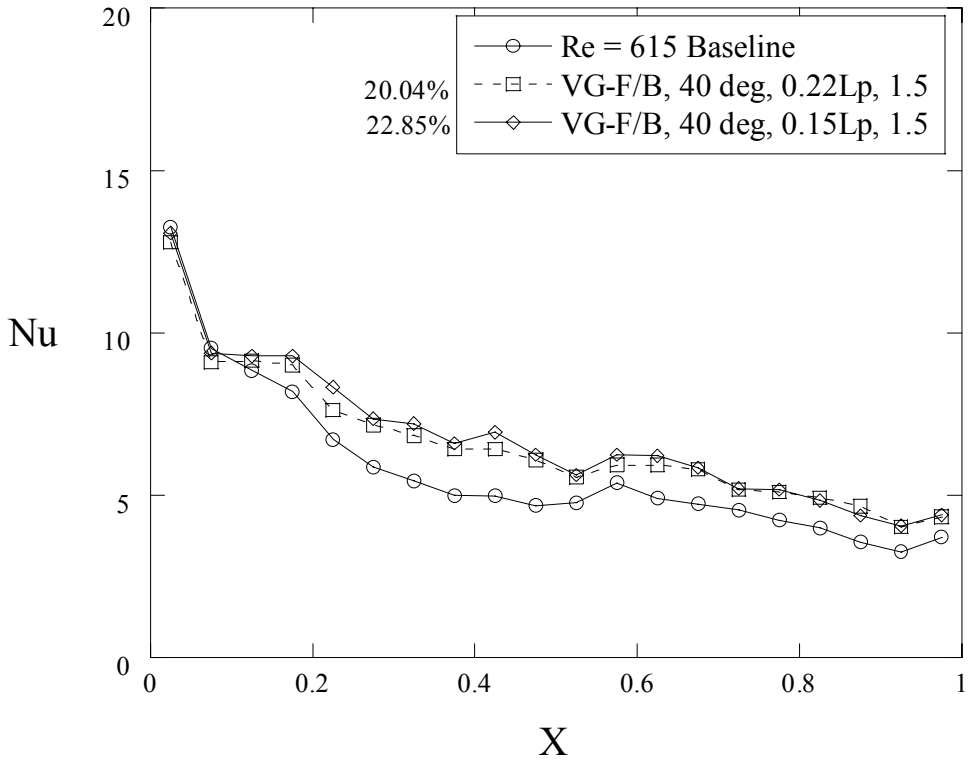

Figure 4.24 Comparison of DFW = $0.15L_p$ and $0.22L_p$ with alternating winglet orientation and direction, AOA = 40°, AR = 1.5, and Re = 615.

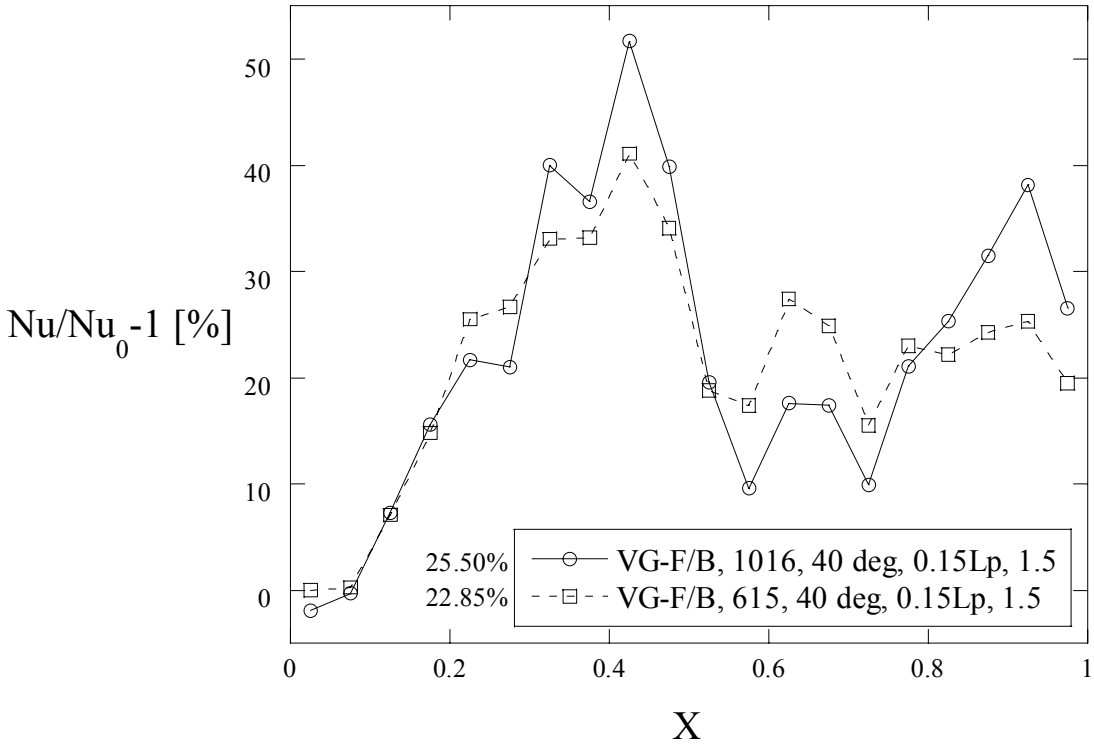

Figure 4.25 Comparison of Re = 615 and 1016 with alternating winglet orientation and direction, AOA = 40°, and AR = 1.5, DFW = $0.15L_p$.

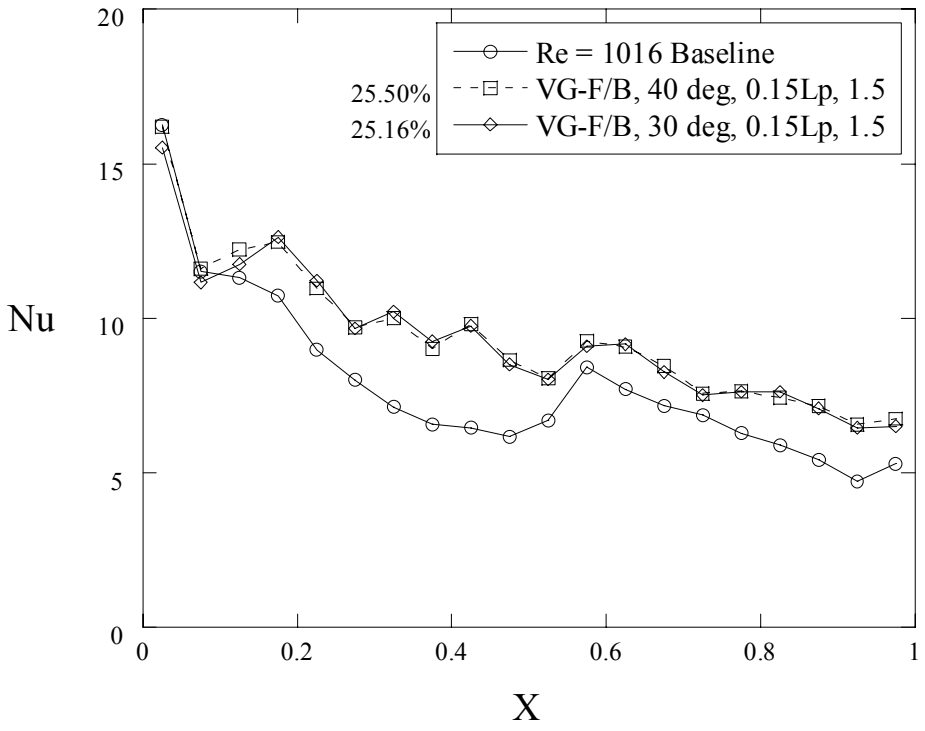

Figure 4.26 Comparison of AOA = 30° and 40° with alternating winglet orientation and direction, DFW = $0.15L_p$, AR = 1.5, and Re = 1016.

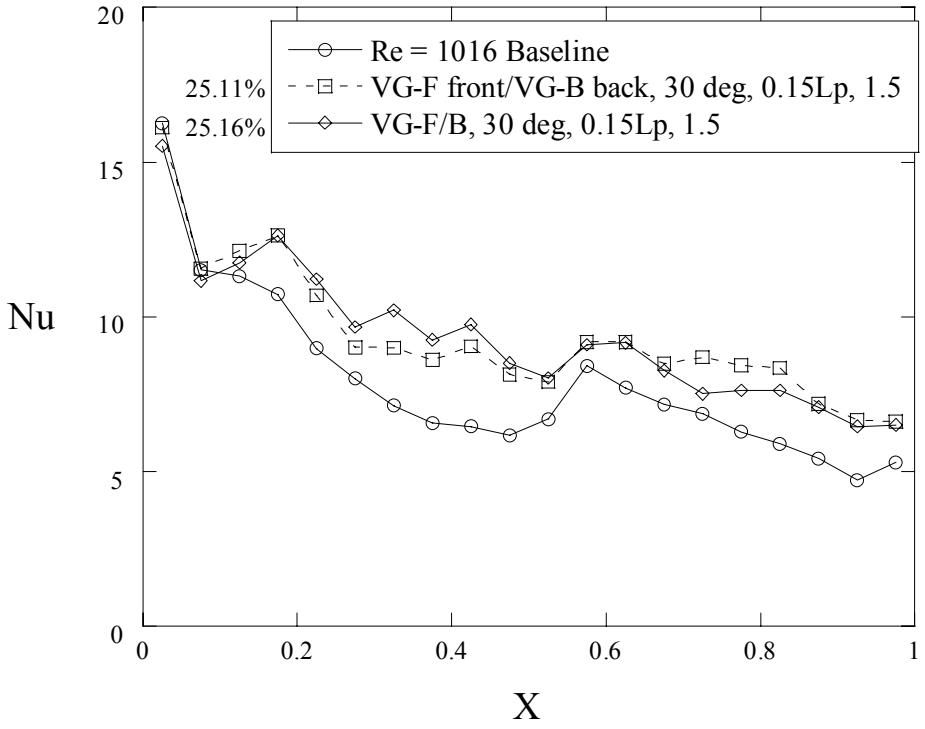

Figure 4.27 Comparison of winglet orientation, with winglets upstream of the turnover in VG-F orientation and winglets downstream of the turnover in VG-B orientation. Winglet direction is alternating and AOA = 30°, AR = 1.5, DFW = $0.15L_p$, and Re = 1016 for both cases.

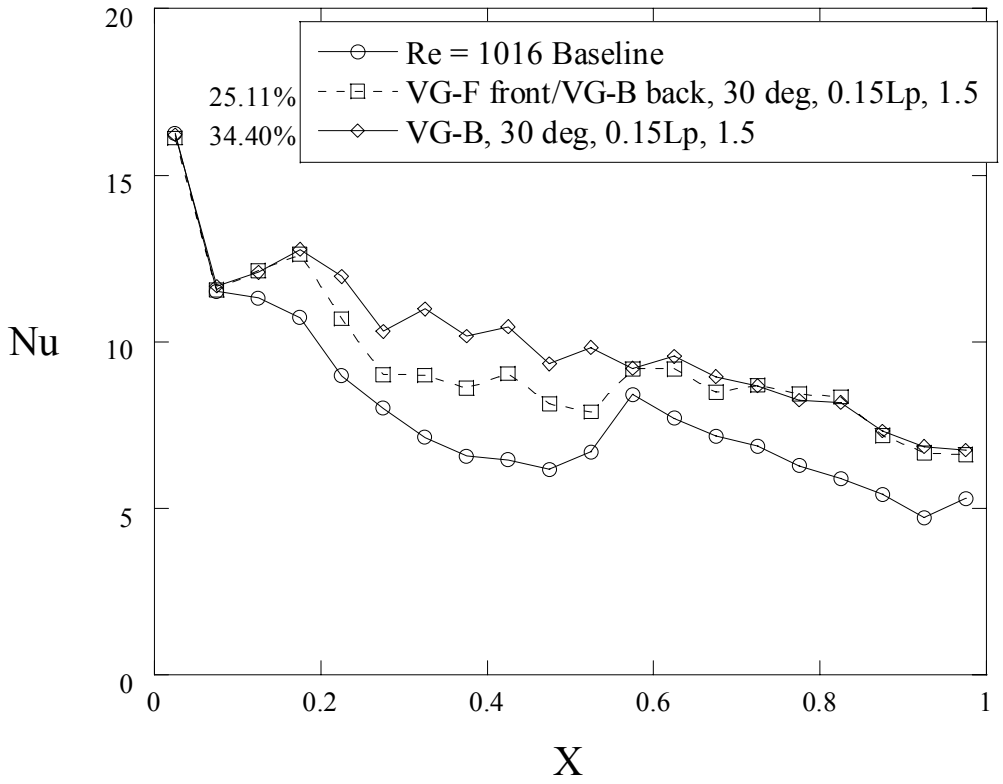

Figure 4.28 Comparison of winglet orientation with all winglets in VG-B orientation with alternating direction. AOA = 30°, AR = 1.5, DFW = 0.15L_p, and Re = 1016 for both cases.

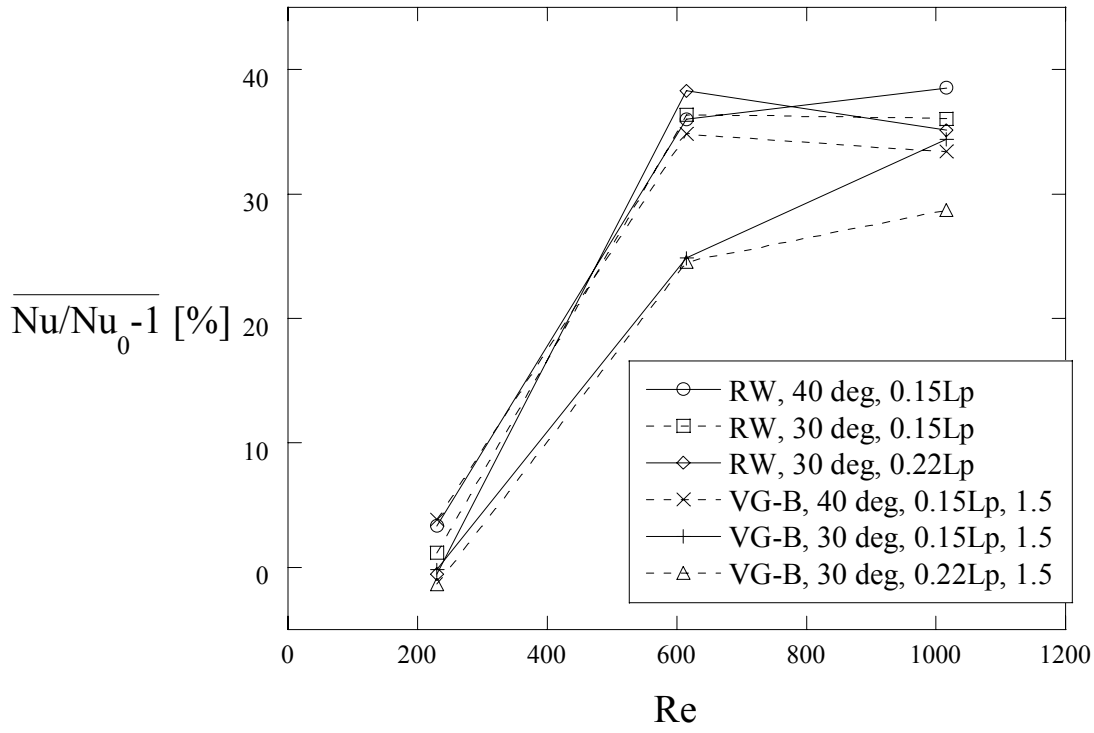

Figure 4.29 Heat transfer augmentation comparisons for winglet shape, AOA, and DFW at all Re.

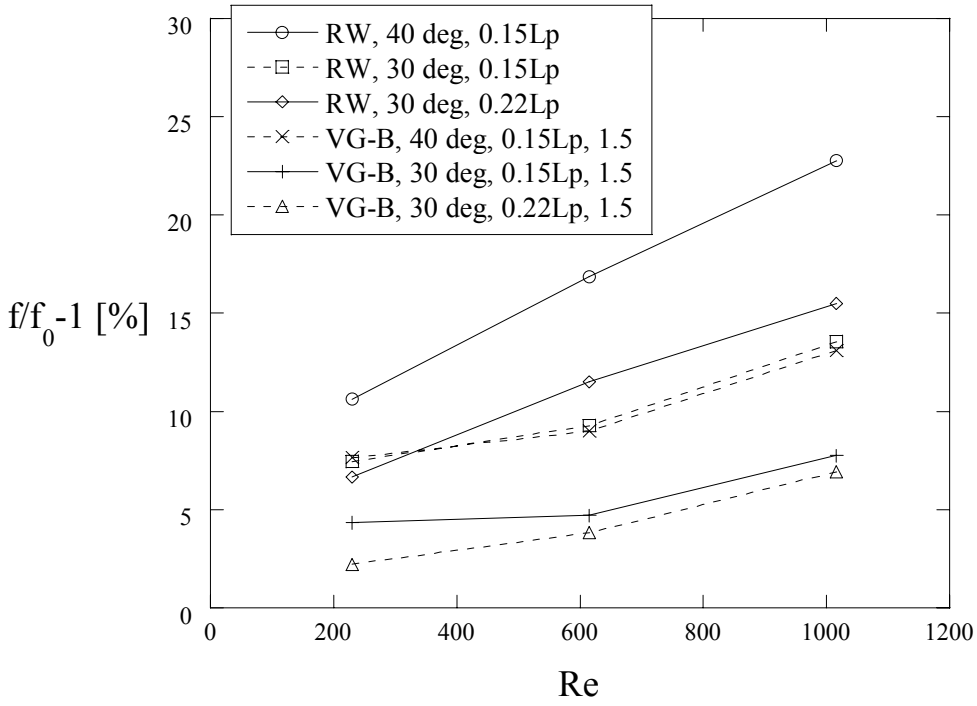

Figure 4.30 Friction factor augmentation comparisons for winglet shape, AOA, and DFW at all Re.

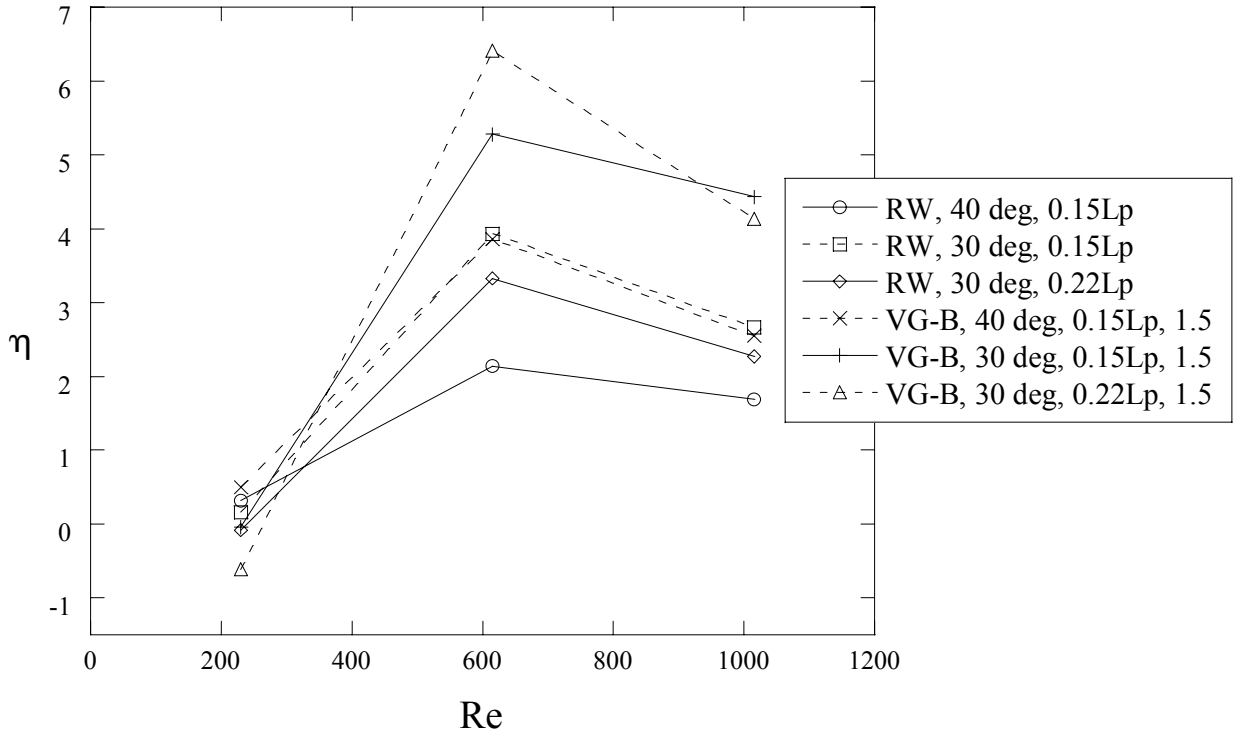

Figure 4.31 Efficiency index comparisons for winglet shape, AOA, and DFW at all Re.

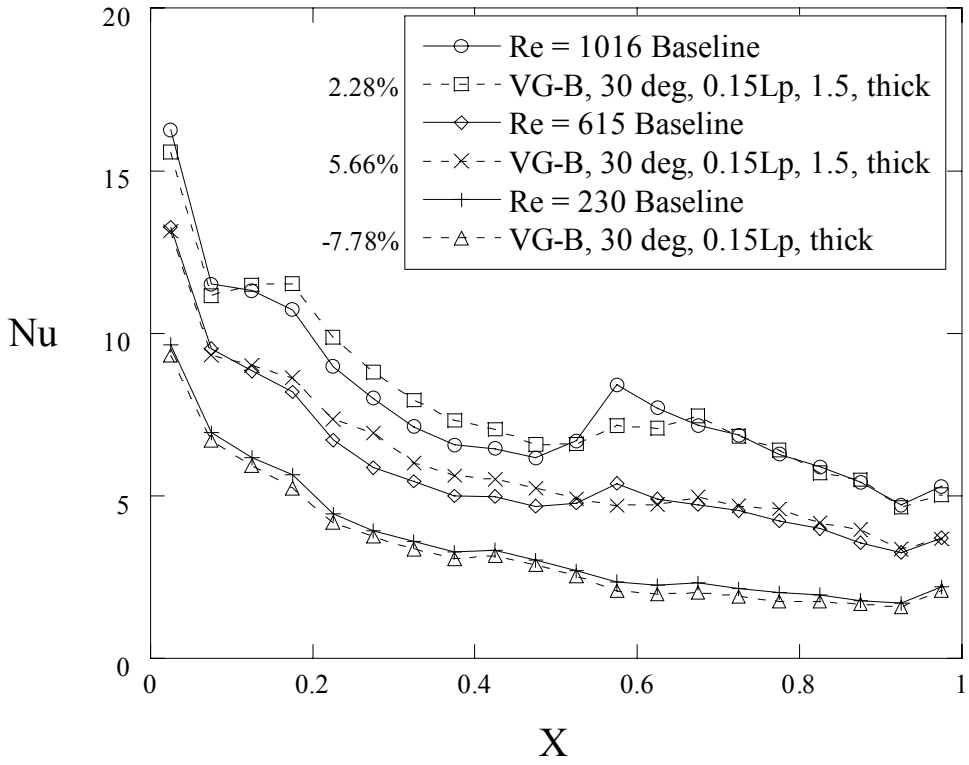

Figure 4.32 Heat transfer results for thick VG-B winglets with alternating direction with AOA = 30°, DFW = $0.15L_p$, and AR = 1.5 for all Re.

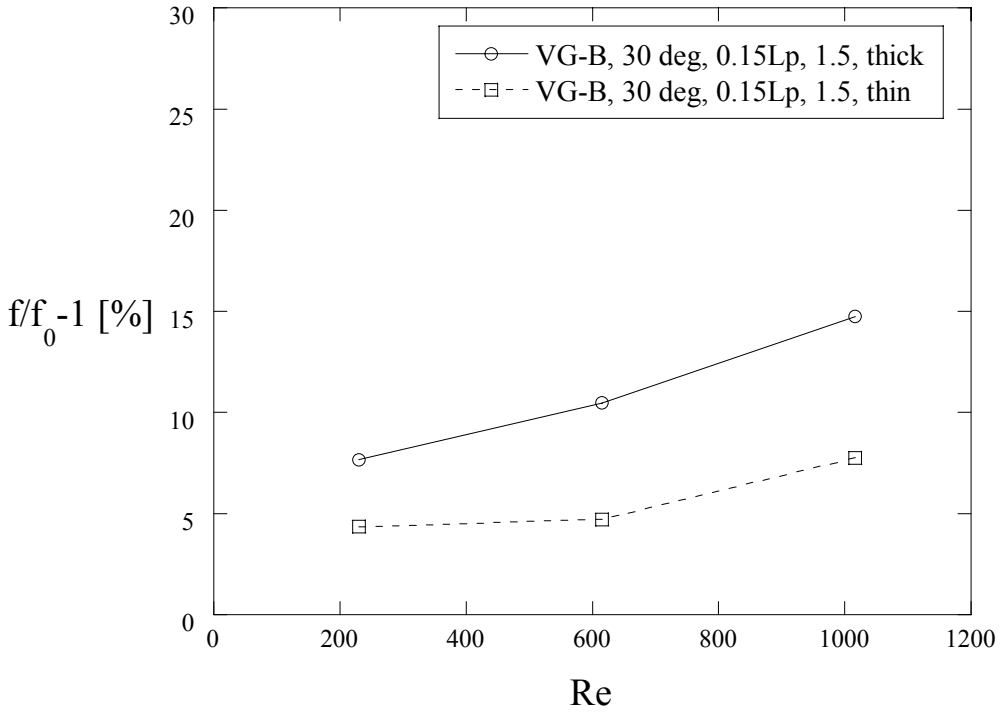

Figure 4.33 Comparison of friction factor augmentation for thick and thin winglets in VG-B orientation with alternating direction. AOA = 30°, DFW = $0.15L_p$, AR = 1.5, for both cases for all Re.

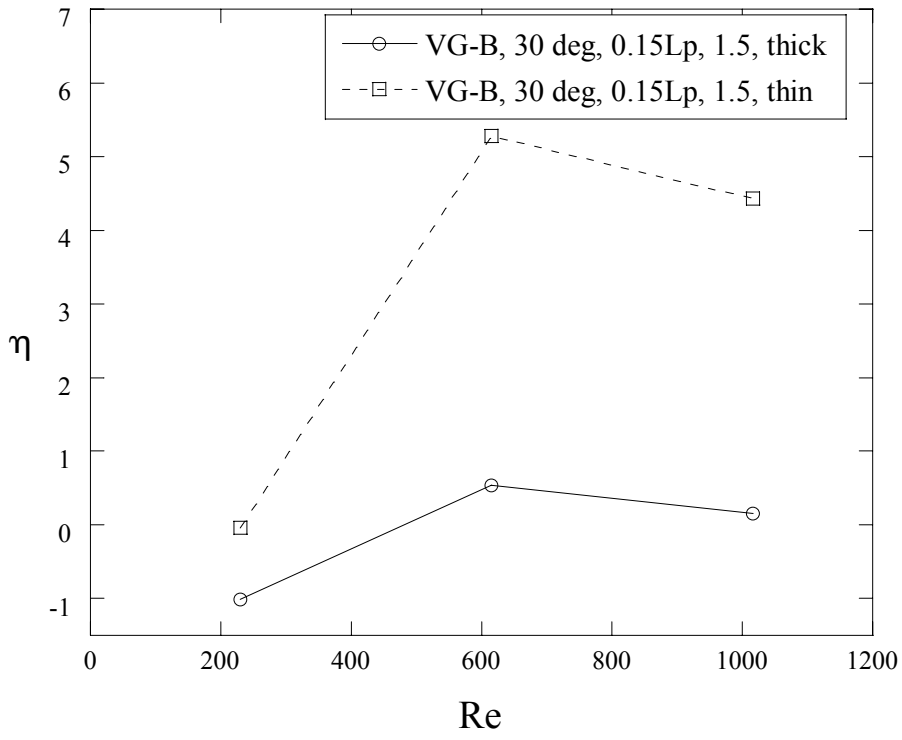

Figure 4.34 Efficiency index for thick and thin winglets in VG-B orientation with alternating direction. AOA = 30°, DFW = 0.15L_p, AR = 1.5, for both cases for all Re.

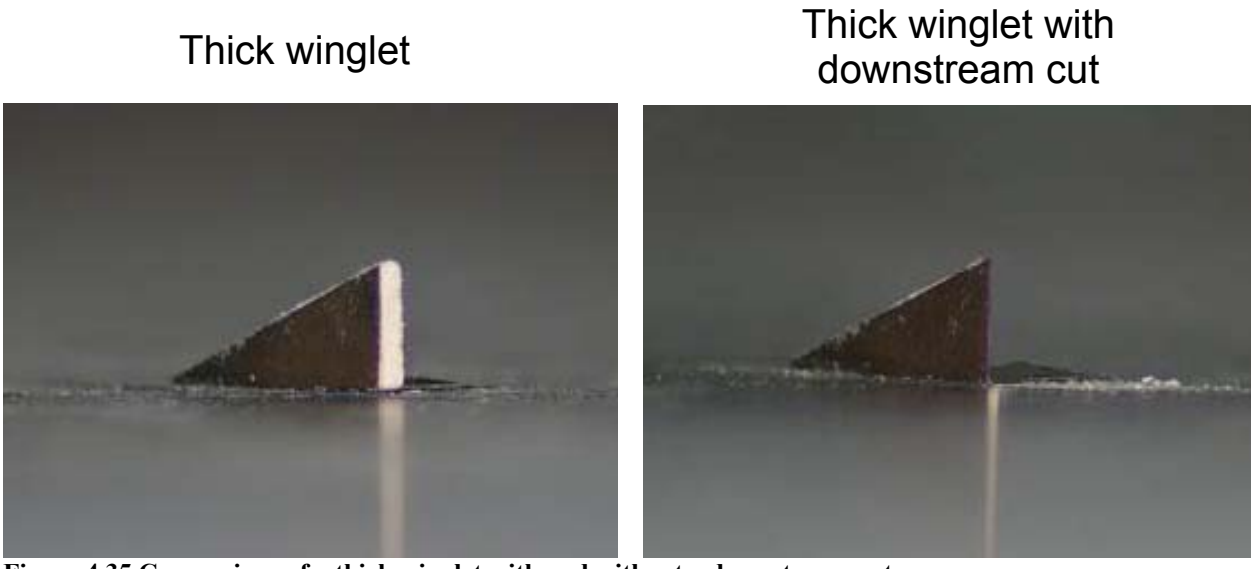

Figure 4.35 Comparison of a thick winglet with and without a downstream cut.

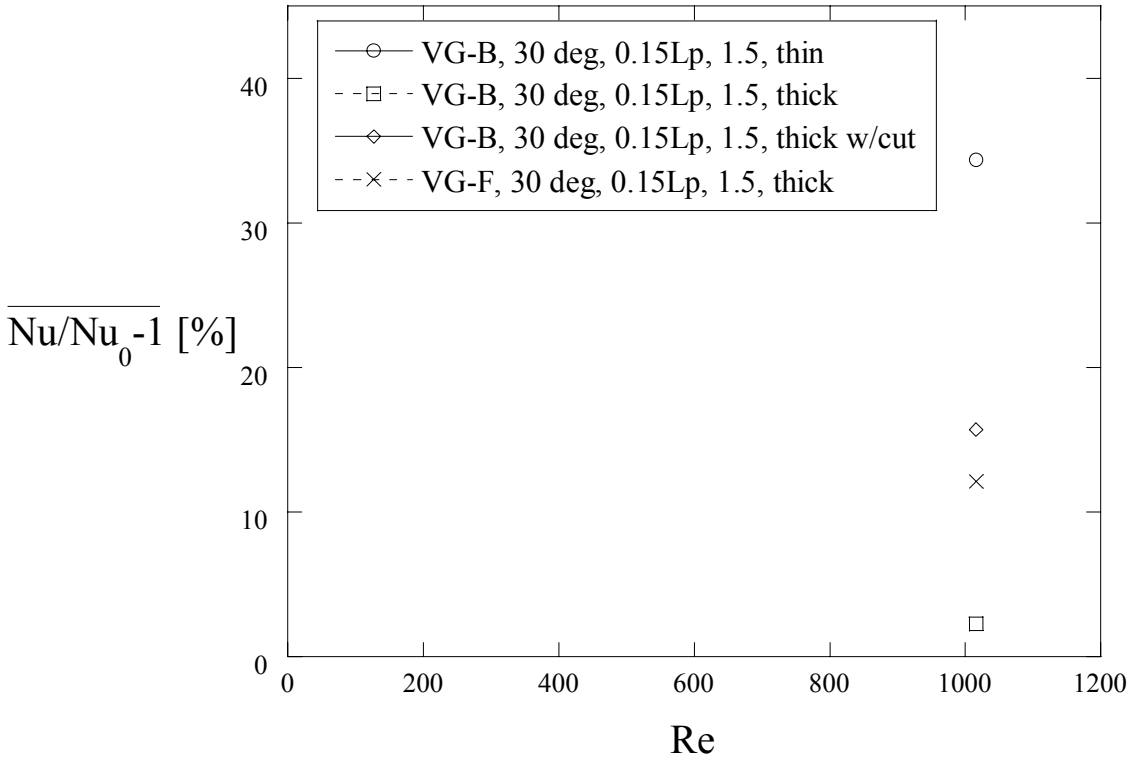

Figure 4.36 Heat transfer augmentation comparison for thick, thin, and thick with cut winglets at AOA = 30°, DFW = 0.15L_p, AR = 1.5, for Re = 1016. Results are shown for VG-B and VG-F winglets with alternating direction.

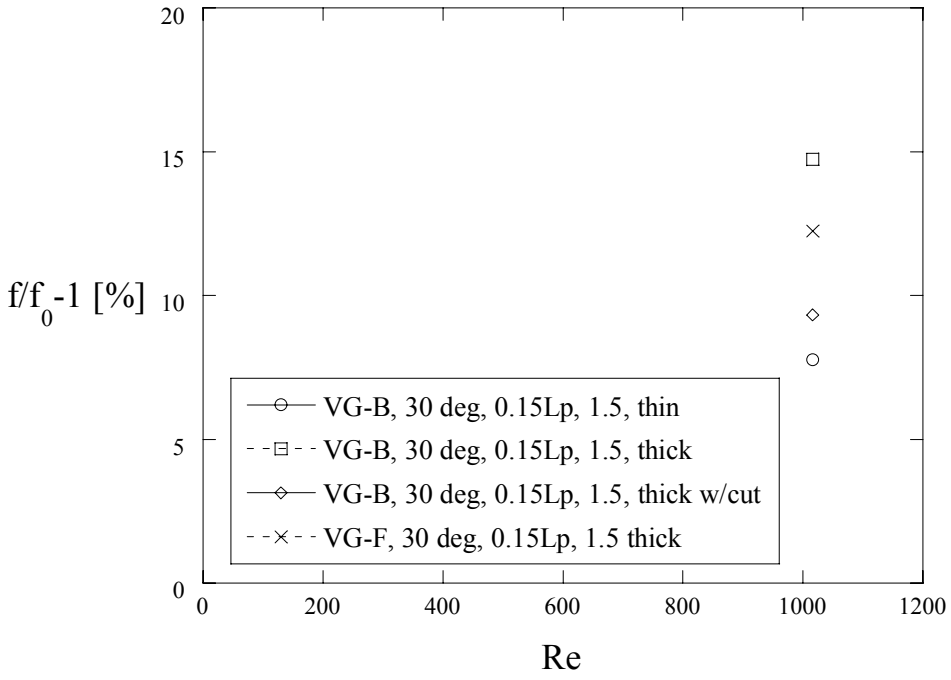

Figure 4.37 Friction factor augmentation comparison for thick, thin, and thick with cut winglets at AOA = 30°, DFW = 0.15L_p, AR = 1.5, for Re = 1016. Results are shown for VG-B and VG-F winglets with alternating direction.

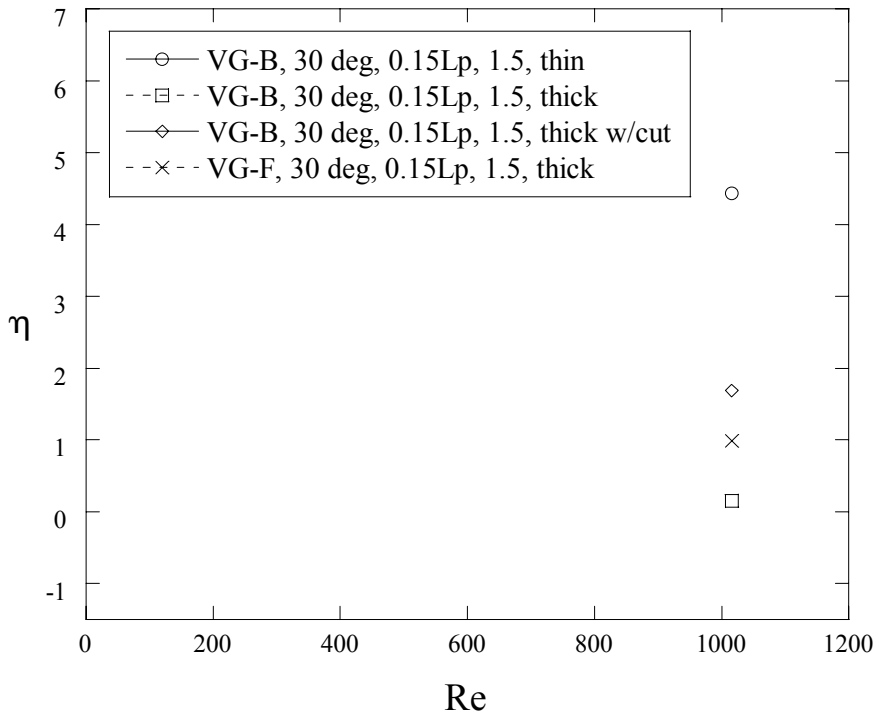

Figure 4.38 Efficiency index comparison for thick, thin, and thick with cut winglets with at AOA = 30°, DFW = 0.15L_p, AR = 1.5, for Re = 1016. Results are shown for VG-B and VG-F winglets with alternating direction.

Chapter 5 - Delta Winglet Studies for the L_l/F_h = 70% Louver Length

In Chapter 4, several different winglet parameters and levels were tested for the 100% louver length. The performance of the various winglet parameters was evaluated in three ways: heat transfer augmentation, friction factor augmentation, and efficiency index. In moving to the L_l/F_h = 70% louver length, we did not feel it was necessary to retest all of the parameters because it was expected that the same setups that worked well in the 100% louver length tests would continue to produce favorable results. For this reason, the number of test parameters was reduced in order to work with the parameters we felt would give the best results. In this chapter, all of the heat transfer, friction factor, and efficiency index data will be given for the L_l/F_h = 70% winglets tests, along with optimizations based on each.

5.1 Winglets Testing Overview

As with the 100% louver length tests, a strict test matrix was not followed for the 70% louver length winglet studies so that the best performing parameters could be investigated more freely. Once again, an overview of the parameters tested may help to orient the reader to the directions that were taken in this study to find the best performing parameters. For the 70% winglets tests, there was much more variation in the overall winglet setup than there was with individual winglet parameters. For all tests that will be shown, the following parameters remained constant: AOA = 40°, DFW = $0.15L_p$, and AR = 1.5. The winglets used throughout this segment of experimentation had a thickness of 0.063 in (1.59 mm, 0.69t). Although this is not the full louver thickness, tests run after the completion of this study showed that winglet thickness has a negligible effect on tube wall heat transfer results for the 70% louver geometry. Finally, all winglets were placed on the top side of the fins on the flat landing. This differed from the 100% louver length winglet setup where winglets downstream of the turnover louver were placed on the underside of the louvers to take advantage of the air contact on these surfaces. For the 70% louver length, the flow makes good contact on both the top and bottom of the flat landing, so we did not feel it would have any impact on tube wall heat transfer results.

As mentioned above, most of the variation in the test parameters dealt with the changes in the overall winglet setup on the fin. Initial testing began with the same alternating direction with

VG-B winglets configuration that ended the100% louver length studies. This configuration was tested with and without cuts yielding poor results for both. Winglets aimed towards the wall through the whole channel were tested in the VG-B and VG-F orientation. Unlike the 100% results, this configuration showed high augmentation, so the majority of the remaining tests were run with winglets aimed towards the wall in both orientations. Several tests were also run with 16 winglets on a full fin row instead of the 34 usually tested to determine the effect of winglet spacing on heat transfer augmentation. Winglets were as well tested on the turnover louver because it became geometrically possible to do so with the flat landings. The final set of testing involved winglet configurations that would be more realistic for manufacturing. More details will be given for each of these setups as the results are discussed.

Table 5.1 shows all of the tests that were completed in the setups just described, as well as average Nusselt augmentation, friction factor augmentation, and efficiency index. Also, since there were several different configurations tested for the 70% studies, and the wording used to describe them can be very long, diagrams of the winglet setups are given next to every streamwise Nusselt plot. For each of the diagrams, the flow direction is towards the top of the page as shown by the arrows. Finally, next to the legend in each streamwise Nusselt plot, average augmentation values are given for each test.

In each of the friction factor augmentation plots, the vertical axis starts at zero because below zero augmentations are not possible. However, because of the large associated uncertainty for the Re = 227 friction factor measurements, augmentation values ranged from -56% to 44% over the course of winglet testing. To avoid making the plot range too large for the sake of the Re = 227 data, the bounds were set so that all of the Re = 1001 and 606 data could be seen. Therefore, if there are no data points shown at Re = 227 in the friction factor augmentation plots, it is because they showed augmentations below 0% or above 35%. Efficiency index plots start at -1 on the vertical axis because this axis extension does not distort the plots too much.

5.2 Heat Transfer, Friction Factor, and Efficiency Index Results

As stated earlier, 70% louver length winglet testing began with alternating winglets in the VG-B orientation. For the 100% louver length, this combination of parameters produced the highest heat transfer augmentation for the delta winglets without a large friction factor

augmentation. We believed that VG-B winglets produced higher heat transfer than the VG-F winglets because of the larger winglet area in alternating hot and cold regions producing circulation of the air towards and away from the tube wall. Heat transfer augmentations for AOA = 40°, DFW = $0.15L_p$, and AR = 1.5 and thin Inconel winglets were 33.41%, 34.87%, and 3.86% at Re = 1016, 615, and 230 respectively for the 100% case. The same setup (but with thick winglets), for which results can be seen in Figure 5.1, was run for the 70% louver length at Re = 1001 and Re = 227. Although the Re = 1001 case shows positive augmentation between the entrance and exit louvers, the average augmentation only came out to 6.04%. The Re = 227 case is below the baseline over the entire fin depth, showing an augmentation of -11.26%. There were similar problems obtaining good augmentation with the thick winglets in the 100% louver length studies. However, cutting the winglets in the downstream direction seemed to remedy this.

The next test that was conducted had the same configuration as seen in Figure 5.1 but the winglets were all cut in the downstream direction (Figure 5.2). Looking at Figure 5.2, the heat transfer results were worse than those shown with no cuts. Average augmentations for these tests were the worst for all of the winglet tests run yielding -3.08% and -13.54% at Re = 1001 and 227 respectively. Since cutting the winglets did not help, we were led to believe that the alternating direction configuration and not the winglet thickness was the major contributor to the poor heat transfer performance. We believe the alternating winglets did not perform well for the 70% louver length because the flow in the region near the wall is more like a channel flow than a flat plate flow. How exactly the flow types affect winglet air circulation is not known.

Friction factor augmentations for VG-B winglets with alternating direction, with and without cuts, were 16.70% and 14.26% respectively at Re = 1001. Once again, these values are dissimilar to those measured for the 100% winglet tests in which the cuts reduced the friction factor augmentation by about 8%. The efficiency index plot seen in Figure 5.3, shows values of 0.42 and 0.35 for the alternating winglets without cuts at Re = 1001 and 227 respectively. The value of 0.35 at Re = 227 is misleading because both the heat transfer augmentation and the friction factor were negative, producing a positive number. In actuality this setup was very inefficient. The alternating winglets with cuts produced efficiency index values of -0.18 and -0.31 at Re = 1001 and 227 respectively, also performing very poorly.

With several different trends in the 70% and 100% winglet results, it became clear that more extensive testing, at least with regard to overall winglet setup, needed to be performed.

Testing switched back to configurations with winglets aimed towards the wall. The first of such tests was run with VG-B winglets with cuts in the downstream direction at Re = 1001 and 227. Heat transfer results for this test can be seen in Figure 5.4. For Re = 1001, there is a very large augmentation in heat transfer starting just downstream of the turnover (X = 0.125) and continuing through the exit louver. At X = 0.325 there is a spike in the data leading to an immediate trough at X = 0.375. The Nusselt numbers reach another peak at X = 0.425 and then decrease linearly until X = 0.625. From X = 0.625 to 0.775, the Nusselt numbers rise again and then decrease as they approach the exit. There is one final spike at X = 0.975, but this increase is believed to be cause by the conduction losses as mentioned in Chapter 3. Since the augmentation decreases near around the turnover and exit louvers, these louvers seem to be adversely contributing to the winglets ability to augment tube wall heat transfer. Average heat transfer augmentations for the tests shown in Figure 5.4 were 52.57% at Re = 1001 and 0.61% at Re = 227. This was the highest heat transfer augmentation achieved at Re = 1001 for any winglet configuration in this study.

In Chapter 3, the point was made that dips in the 70% and 82% louver length baseline heat transfer results at X = 0.375and X = 0.625 seemed to have some significance in the winglet tests as well. A quick look at Figure 5.4 and all of the remaining heat transfer results shown in this chapter at Re = 606 and 1001 will show that winglet performance also declines at these same locations. Once again, the cause of this has yet to be determined.

Figure 5.5 shows the results for winglets aimed towards the wall in the VG-F orientation at all Re. The heat transfer trends seen in and Figure 5.5 are very similar but weaker than those seen for the VG-B winglets in Figure 5.4. In Figure 5.5, the Re = 606 data looks much like the data at Re = 1001, but the Re = 227 data remains near baseline levels throughout the test section. The average heat transfer augmentations at Re = 1001, 606, and 227 were 44.42%, 29.48%, and 1.14%. The 100% winglet tests showed that nearly equal augmentation percentages were possible at Re = 615 and 1016, but for the 70% winglets tests, Re = 606 augmentation values are substantially lower Re = 1001 values.

The VG-B winglets showed slightly higher friction factor augmentation at Re = 1001 than the VG-F winglets, with augmentations for the two cases of 21.23% and 19.13%. No data was collected for the VG-B winglets at Re = 606, however, for the VG-F winglets, a friction factor augmentation of 21.32% was measured at Re = 606 which was higher than the

augmentation at Re = 1001. The efficiency index plot seen in Figure 5.6 shows that efficiency indexes for the VG-F and VG-B winglets are very similar at Re = 1001 and 227 with the slight performance advantage to the VG-B winglets. Efficiency index values of 2.48 and 0.06 were achieved with the VG-B winglets at Re = 1001 and 227 respectively. The VG-F winglets had efficiency index values of 2.32, 1.38, and -0.03 from high to low Re. These results differ from the results for the 100% louver length tests where efficiency indexes at Re = 615 were always higher than those at Re = 1016

In one of our semi-annual meetings with Modine, they raised concerns about the structural integrity of a fin with winglets stamped at every louver position. If less winglets could be used without a large performance reduction, fin strength could be vastly improved. With this in mind, tests were conducted to determine the sensitivity of wall heat transfer to winglet spacing. To run these tests, winglets were placed on louvers 1, 3, 5, 7, 8, 10, 12, and 14, not counting the entrance turnover and exit louvers. A diagram will be given next to the first set of heat transfer results presented. With winglets on either side of the louvers, this amounted to a total of 16 winglets on a fin row instead of the 34 used in all of the heat transfer results given to this point. For all of the results that will be shown from this point forward, the reduced number of winglets was used.

The first test was run with all winglets aimed towards the wall in the VG-B orientation. Figure 5.7 shows the heat transfer results for this test at Re = 1001 and 227 as well as the diagram that shows where the winglets were placed for the 16 winglets configuration. The results for 16 winglets seen in Figure 5.7 are very similar to the results seen in Figure 5.5 with all 34 winglets. The only exceptions are that in Figure 5.7, values between X = 0.425 and 0.625 curve off slowly instead of decreasing linearly and values from X = 0.825 to 0.925 increase slowly while they decreased for the full number of winglets. The average heat transfer augmentation values for the tests with 16 winglets were 42.18% and -0.11% at Re = 1001 and 227 compared to 44.42% and 1.14% for 36 winglets. Using close to half of the winglets, average heat transfer augmentation was reduced a mere 2.2% at Re = 1001.

A test with 16 winglets was also completed for the VG-B orientation with all winglets aimed towards the wall. The results for this test at Re = 1001, 606, and 227 can be seen in Figure 5.8. The trends seen in this plot are not significantly different than those shown for the VG-F orientation with double-spaced winglets. Heat transfer augmentations were 39.8%, 26.2%,

and -0.87% from high to low Re. The same test with 36 winglets produced 52.57% and 0.61% at Re = 1001 and 227, showing that heat transfer augmentation is far more sensitive to the number of winglets used for the VG-B orientation than the VG-F orientation.

Since all of the heat transfer results given in this chapter have shown a reduction in augmentation just downstream of the turnover louver, winglets were applied to the turnover louver in an attempt to stop the Nusselt numbers from dropping in this region. Continuing to use the 16 winglets at the usual louver positions, two extra winglets were added on either side of the turnover louver (because the turnover louver is $2L_p$ wide). Tests were run with VG-F winglets at Re = 1001 and 227, for which heat transfer results and a descriptive diagram can be seen in Figure 5.9. In Figure 5.9, a distinctive dome shape can be seen from X = 0.375 to 0.625 and the Nusselt numbers from X = 0.625 to 0.925 are fairly constant. Figure 5.10 shows a direct comparison of the VG-F winglets at double spacing with and without turnover winglets. In Figure 5.10, although the turnover winglets do increase heat transfer in the turnover region, results from X = 0.675 to the end of the channel are below those without the turnover winglets. The average Nusselt augmentations for the case with turnover winglets were 39.64% and 0.13% at Re = 1001 and 227 respectively, which at Re = 1001 was about 2.5% lower than the augmentation without turnover winglets. It was mentioned in Chapter 3 that augmentation gains upstream of the turnover louver usually coincide with augmentation losses downstream of the turnover louver. This is one of the few observations that held true in both the 100% louver length and 70% louver length winglet studies.

Plots of friction factor and efficiency index can be seen for 16 winglets in the VG-B orientation and the VG-F orientation, with and without turnover winglets, in Figures 5.11 and 5.12. In Figure 5.11, Re = 1001 provides the only point to directly compare the friction factor augmentations for the cases just mentioned. At Re = 1001, the highest friction factor augmentation (21.23%) was produced by the VG-B orientation, followed by the VG-F orientation with turnover winglets (17.99%) and finally the VG-F orientation with no turnover winglets (8.59%). The VG-F orientation with 16 winglets had the lowest friction factor augmentation measured for any of the 70% louver length winglet tests. Just adding the turnover winglets produced a friction factor augmentation at Re = 1001 that was only 1.1% less than the friction factor augmentation measured for the VG-F test with all 34 winglets. Since heat transfer augmentations drop significantly over the turnover louver region and turnover winglets account

for a large portion of the friction factor augmentation for the VG-F winglets, I believe there is a very interesting flow phenomenon that occurs over the turnover louver to cause these occurrences. This is an area where more investigation is needed so that winglets can be applied in a manner that yields high heat transfer augmentation with reduced friction factor augmentation. The efficiency indexes seen in Figure 5.12 show that the VG-F orientation without turnover winglets was the most efficient with a value of 4.91 at Re = 1001, while efficiency indexes of the VG-F orientation with turnover winglets and the VG-B winglets were 2.20 and 1.87 respectively. As in the 100% louver length studies, the spread of these results was mostly determined by friction factor augmentation. Efficiency indexes shown for all three cases at Re = 227 were zero.

Although most of the Re = 230 heat transfer data has been ignored because of near baseline results, several of the plots show slight augmentations starting and ending at different points upstream of the turnover. One case was run specifically to see if heat transfer in this region could be augmented while avoiding below baseline results commonly associated with the region downstream of the turnover louver. VG-F winglets were aimed towards the wall at the louver positions shown in Figure 5.13. The heat transfer results, also seen in Figure 5.13, show some slight augmentation from X = 0.325 to X = 0.625, but the Nusselt numbers from X = 0.825 to X = 0.975 are below the baseline. The average Nusselt augmentation for this test was 0.24%, which was not any higher than the augmentations shown earlier in this chapter, and did not warrant continued study. Because the results were so poor, friction factor data was not collected for this setup.

At this point the direction of testing changed again so that manufacturability of the winglets was taken more into account. Winglets were tested in a mirrored configuration (winglets upstream of the turnover louver were mirrored downstream of the turnover) so that they could be placed in a radiator in either direction and provide equal performance. For all of the tests run up to this point, it would matter which end was facing the front of the car. It would be difficult to orient the fins in a plant, and if the fins were placed in the radiator backwards, there would be serious performance ramifications. A comparison of a mirrored winglet setup compared to one that is not mirrored can be seen in Figure 5.14. In Figure 5.14, (a) shows VG-F winglets aimed towards the wall, (b) shows configuration (a) turned 180˚ as if flow were entering in from the opposite direction in (a). Notice how the portion of (a) that is below the dotted line is

not the same as the portion of (b) that is below the dotted line (the same applies to portions above the dotted line). The winglets in (b) are in the VG-B orientation aimed away from the wall. Figure 5.14 (c) and (d) show a mirrored configuration where either way the fins are placed in the heat exchanger produces the same conditions for the flow. Notice how (c) and (d) are the same above and below the dotted line. From now on, this configuration will be called the mirrored configuration. It requires that the direction and the orientation of the winglets change at the turnover louver to the opposite direction and orientation.

The first test with the mirrored configuration had VG-B winglets aimed towards the wall upstream of the turnover, and therefore, VG-F winglets aimed way from the wall downstream of the turnover. Heat transfer results for this test can be seen in Figure 5.15. Upstream of the usual trough at X = 0.625, the Nusselt numbers have the same trends as most of the other plots shown in this chapter, however, downstream of this position, there is a new trend. At Re = 1001, the Nusselt numbers drop steadily and almost reach baseline levels. At Re = 606 and 227, the winglet results do fall below baseline levels at X = 0.825 and X = 0.475 respectively. It is obvious from these results that the winglets aimed away from the wall adversely affect tube wall augmentation. Average Nusselt augmentations for Re = 1001, 606, and 227 were 30.15%, 15.6%, and -6.58%. A test with 16 VG-F winglets aimed towards the wall can be seen in Figure 5.16. The results seen in Figure 5.16 are nearly the same as those in Figure 5.15, with heat transfer augmentations of 28.61%, 13.9% and -1.99% at Re = 1001, 606, and 227. By mirroring these two cases, heat transfer augmentations at Re = 1001 and 606 were 10% to 12% lower than the same cases with all winglets aimed towards the wall. Results at Re = 230 were also worsened as the mirrored winglets produced large negative augmentations in the rear half of the test section.

Friction factor results for both of the mirrored winglets tests can be seen in Figure 5.17 at all Re. Both cases showed nearly equal friction factor augmentations at Re = 1001 and 615 with the VG-B winglets upstream of the turnover only yielding 1.5% and 2% higher augmentations at each Re. Friction factor augmentations values were in the mid-20% range at Re = 1001 which was about 5% higher than the non-mirrored augmentations. Efficiency indexes for the mirrored tests can be seen in Figure 5.18. The efficiency indexes produced essentially the same values of 1.15 and 0.70 at Re = 1001 and 615 respectively. At Re = 227, the VG-B winglets upstream for

the turnover yielded an efficiency index of -0.39 because of the largely negative heat transfer augmentation, while the efficiency index for the VG-F winglets was 0.11.

5.3 Summary of Results and Optimization

In order to better compare and discuss the heat transfer, friction factor, and efficiency index trends, plots of each comprised of results for most of tests already shown will be given. The only results excluded from these plots correspond to the alternating winglets tests and the test focused on increasing Re = 227 heat transfer. Their exclusion was based on poor performance or lack of sufficient data points.

Having said this, the summary will start with the poor performers and will move to direct comparisons of the other tests. The alternating winglets cases for the 100% louver length worked very well, providing high heat transfer with relatively low friction factor augmentation. However, when placed on the 70% louver length fins, heat transfer performance was significantly decreased. Cutting the winglets in the downstream direction unexpectedly reduced heat transfer augmentation even further. The results with and without cuts at Re = 1001 were 6.04% and -3.08%. This -3.08% augmentation was the only negative result obtained at Re = 1001, where augmentations are usually high. At Re = 227, results were very poor showing augmentations for winglets with and without cuts of -11.26% and -13.54%. Although, no substantial augmentation has been achieved for any setup at Re = 227, these results were well below than the usual Re = 227 results of -2% to 2%. It is believed that the channel flow near the tube wall hinders the circulation of the air with the alternating winglets, but it is not know how.

The only test aimed specifically at augmenting heat transfer augmentation at Re = 227, also produced poor results. Augmentations upstream of the turnover louver led to negative augmentations downstream of the turnover louver. Although this gain and loss relationship is commonly seen at other Re, it is especially costly at Re = 227, where even the slightest decrease in performance downstream of the turnover louver results in a negative augmentation. The average heat transfer augmentation of this test was 0.24%, cementing the belief that augmentation at Re = 227 with the use of winglets is not possible.

A comparison of the heat transfer results for all other tests can be seen in Figure 5.19. Since all tests were not run at Re = 606, and the tests that were run at Re = 606 show the same

trends at Re = 1001, only the Re = 1001 comparisons will be given. In Figure 5.19, the highest augmentations at Re = 1001 were from the tests where winglets were aimed towards the wall at every louver position. The VG-B winglets showed the highest augmentation achieved in any winglet test in this study at 52.57%. The VG-F winglets showed an augmentation value of 44.42%. Looking back at the L_l/F_h = 100% results, the VG-F orientation did not produce high augmentation values. It is believed that results are significantly improved for the 70% louver length because vortices are bound by the channel near the wall and are not interrupted by louver surfaces as they were for the 100% louver length. Keeping the winglets contained in the channel also allows for each winglet to boost and strengthen the vortex from the upstream winglet. As far as the reason that the VG-B winglets perform so well, we have no explanation because the nature of the flow coming off of the VG-B winglet is not known.

The next highest heat transfer performers were from the tests with 16 winglets aimed towards the wall. All three of these 16 winglets tests had augmentations within 2.5 % of each other at Re = 1001. In order from high to low heat transfer augmentation were the VG-F orientation (42.18%), the VG-B orientation (39.8%), and the VG-F orientation with turnover winglets (39.64%). The first point to make is that the reduced number of VG-F winglets only produced a difference in average augmentation of 2.2% at Re = 1001 from the same case with the full number of winglets. For the VG-B winglets, this difference was 12.8%, showing that winglet spacing has a stronger influence on VG-B augmentation than VG-F augmentation. The next point is that although turnover winglets did produce local augmentations that were higher than tests without turnover winglets, the results downstream of X = 0.675 were below them. This ended up producing a slightly lower heat transfer augmentation than the case without turnover winglets.

The mirrored winglets tests showed the lowest augmentations seen in Figure 5.19. With average augmentations around 30% at Re = 1001 for both tests, these results are by no means poor, but heat transfer performance following X = 0.625 was greatly reduced from the tests where winglets were aimed towards the wall through the entire channel. Results at both Re = 606 and 227 dropped below the baseline yielding negative augmentations in this region. Although average augmentation is still fairly high for Re = 606 and 1001, the test with VG-B winglets aimed towards the wall upstream of the turnover louver produced an augmentation of -6.58% at Re = 227, which is one of the lowest in all winglet studies.

As mentioned earlier, the parameters that performed best at Re = 1001 also performed the best at Re = 606. The only point to make about the data at Re = 606 is that is it significantly below the data at Re = 1001. In the 100% louver length tests, winglet performance at Re = 615 and 1016 were very similar in many cases. This is yet another difference between the winglet behavior for the two different louver lengths. At Re = 227, most of the data was around 0% with only the one mirrored winglets test falling significantly below that. The optimization for highest heat transfer augmentation went to the VG-B winglets aimed towards the wall at every louver position. This setup produced a heat transfer augmentation 52.57% at Re = 1001.

With the 100% louver length winglets studies, the parameters that provided the most heat transfer benefit generally produced the highest friction factor augmentations as well. This was not the case at all for the 70% winglet tests, as Figure 5.20 shows. The two tests run in the mirrored configuration yielded the highest friction factor augmentation with values of 26.09% and 25.12%. These setups showed the lowest heat transfer augmentations in Figure 5.19. This is probably because the flow around the winglets has to change direction following the turnover louver. The next highest friction factor augmentations belonged to the VG-B winglets aimed towards the wall through the whole channel, with 34 and 16 winglets. Both winglet spacings produced the same friction factor augmentation of 21.32% at Re = 1001, showing that winglet spacing did not affect pressure drop through the channel for the VG-B orientation. This was not the case with 34 and 16 winglets in the VG-F orientation. The VG-F case with the full number of winglets produced the next highest friction factor augmentation of 19.13%, while augmentation for 16 VG-F winglets dropped to 8.59%. This value of 8.59% was the lowest measured for the 70% winglet studies. When turnover winglets were added to the double-spaced VG-F setup, friction factor augmentation jumped to 17.99%. Just as the turnover louver has a strong influence over heat transfer augmentation, it also seems to have a strong effect on friction factor augmentation.

All of the trends at Re = 606 were the same as they were for Re = 1001 with the exception of the data point for VG-F winglets at every louver position aimed towards the wall. All of the other friction factor augmentations decreased from Re = 1001 to Re = 606, but this point did not. Because it is the only point that strays from the trend of decreasing augmentation with decreasing Re, more investigation in needed. Data at Re = 227 is widely varying. No conclusions can be made about the Re = 227 friction factor data.

Based on the results seen in Figure 5.20, the optimized condition for lowest friction factor belongs to the case with 16 VG-F winglets aimed towards the wall through the whole channel. Decreasing the number of winglets did not affect the VG-B cases, but for the VG-F winglets, friction factor was reduced from 19.13% to 8.59%.

Overall, the friction factor augmentations seen in the 70% winglet studies were higher than those seen in the 100% studies. Unfortunately, there were no friction factor measurements made for the winglets towards the wall setup run for the 100% louver length, and only two measurements were made for the alternating winglets configuration for the 70% louver length. The friction factor augmentations made for the alternating winglets configuration were very similar between the louver lengths. It could be possible that aiming the winglets towards the wall in general yields higher friction factors, but not enough data was collected at both louver lengths to make a strong statement about this. It is also possible that the thicker winglets in the 70% louver length studies caused the increase.

Efficiency indexes based on the results shown in Figures 5.19 and 5.20 can be seen in Figure 5.21. The case with 16 VG-F winglets aimed towards the wall produced the highest efficiency index of 4.91 at Re = 1001, nearly double the next highest point. This configuration showed heat transfer augmentations just below the VG-F case with winglets at every louver position but friction factors were less than half shown by the second lowest point. The next three points on the efficiency index plot are grouped very closely. They are in order from highest to lowest efficiency index at Re = 1001, VG-B winglets at every louver position aimed towards the wall (2.48), VG-F winglets at every louver position aimed towards the wall (2.32), and 16 winglets in the VG-F orientation with turnover winglets aimed towards the wall (2.20). Double-spaced VG-B winglets aimed towards the wall yielded an efficiency index of 1.87 at Re = 1001. The mirrored winglets produced the lowest efficiency indexes of 1.16 and 1.14 at Re = 1001, due to their low heat transfer augmentation and high friction factor augmentation.

At Re = 606, the trends match the Re = 1001 data with the exception of the VG-F winglets at every louver position aimed towards the wall which had the questionable data point. It is expected that this point should produce the highest efficiency index of the Re = 606 tests. Just like heat transfer augmentation, values at Re = 227 are clustered around zero. The low point is from the mirrored configuration with VG-B winglets aimed towards the wall upstream of the turnover louver which showed -6.58% heat transfer augmentation.

The optimized condition for maximum efficiency index was double-spaced VG-F winglets aimed towards the wall through the entire channel. This case showed a heat transfer augmentation of 42.18% and a friction factor augmentation of 8.59% at Re = 1001. I believe that the results of this test should lead to further testing of winglet spacing, at least for the VG-F configuration. If high heat transfer augmentations are possible with even less winglets, this would be advantageous in terms of reduced friction factor augmentation and more fin rigidity. I think the issue of winglet spacing is mainly determined by how long a strong vortex can be sustained. In flat plate studies, vortices spread and lift from the surface producing less heat transfer benefit with distance. However, with the vortices bounded in the side channels of the 70% louver length, they might weaken, but they cannot possibly spread or lift from the surface.

In a comparison of efficiency indexes between the two louver lengths, values were very similar at Re = 227 and 1001. However, the efficiency indexes at Re = 606 were much lower than those at Re = 615 for the 100% louver length. The 70% louver length tests all showed increasing efficiency index with increasing Re while the 100% louver length showed maximum values at Re = 615 which then dropped off at Re = 1016.

Table 5.1 Winglet Setup, Nusselt Augmentation, Friction Factor, and Efficiency Index for all L_l/F_h = 70% Tests

Alternating Winglet Direction Tests										
Re	AOA	DFW	AR	Direction	Orientation	Thickness	Special	Avg. Nu_{aug} [%]	f_{aug}[%]	η
1001	40	0.15Lp	1.5	alternating	VG-B	0.67t	N/A	6.04	14.26	0.42
227								-11.26	-32.57	0.35
1001	40	0.15Lp	1.5	alternating	VG-B	0.67t w/cut	N/A	-3.08	16.7	-0.18
227								-13.54	44.26	-0.31
Winglets Towards Wall Tests										
Re	AOA	DFW	AR	Direction	Orientation	Thickness	Special	Avg. Nu_{aug} [%]	f_{aug}[%]	η
1001	40	0.15Lp	1.5	towards	VG-B	0.67t w/cut	N/A	52.57	21.23	2.48
227								0.61	9.84	0.06
1001	40	0.15Lp	1.5	towards	VG-F	0.67t w/cut	N/A	44.42	19.13	2.32
606								29.48	21.32	1.38
227								1.14	-37.81	-0.03
16 Winglets Tests										
Re	AOA	DFW	AR	Direction	Orientation	Thickness	Special	Avg. Nu_{aug} [%]	f_{aug}[%]	η
1001	40	0.15Lp	1.5	towards	VG-F	0.67t w/cut	16 winglets	42.18	8.59	4.91
227								-0.11	-56.15	0.00
1001	40	0.15Lp	1.5	towards	VG-B	0.67t	16 winglets	39.8	21.23	1.87
606								26.2	17.73	1.48
227								-0.87	25.56	-0.03
1001	40	0.15Lp	1.5	towards	VG-F	0.67t w/cut	16 + turnover winglets	39.64	17.99	2.20
227								0.13	22.57	0.01
227	40	0.15Lp	1.5	towards	VG-F	0.67t w/cut	winglets on 6, 8, 10, 12	0.24	N/A	N/A
Mirrored Winglets Tests										
Re	AOA	DFW	AR	Direction	Orientation	Thickness	Special	Avg. Nu_{aug} [%]	f_{aug}[%]	η
1001	40	0.15Lp	1.5	towards front/ away back	VG-B front/ VG-F back	0.67t	16 winglets, mirrored	30.15	26.09	1.16
606								15.6	21.55	0.72
227								-6.58	16.85	-0.39
1001	40	0.15Lp	1.5	towards front/ away back	VG-F front/ VG-B back	0.67t	16 winglets, mirrored	28.61	25.12	1.14
606								13.9	20.05	0.69
227								-1.99	-18.66	0.11

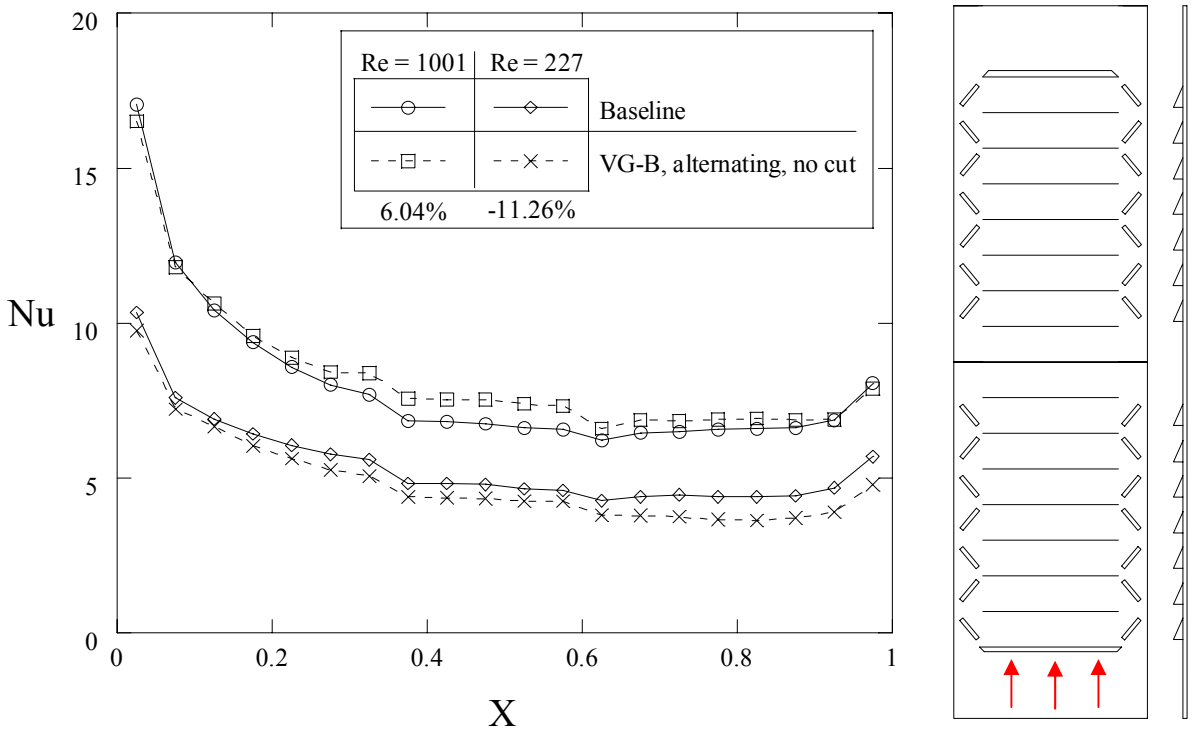

Figure 5.1 Streamwise Nusselt numbers for VG-B winglets with alternating direction at Re = 1001 and 227. AOA = 40°, DFW = 0.15L_p, AR = 1.5, winglet thickness is 0.67t, no cuts on winglets.

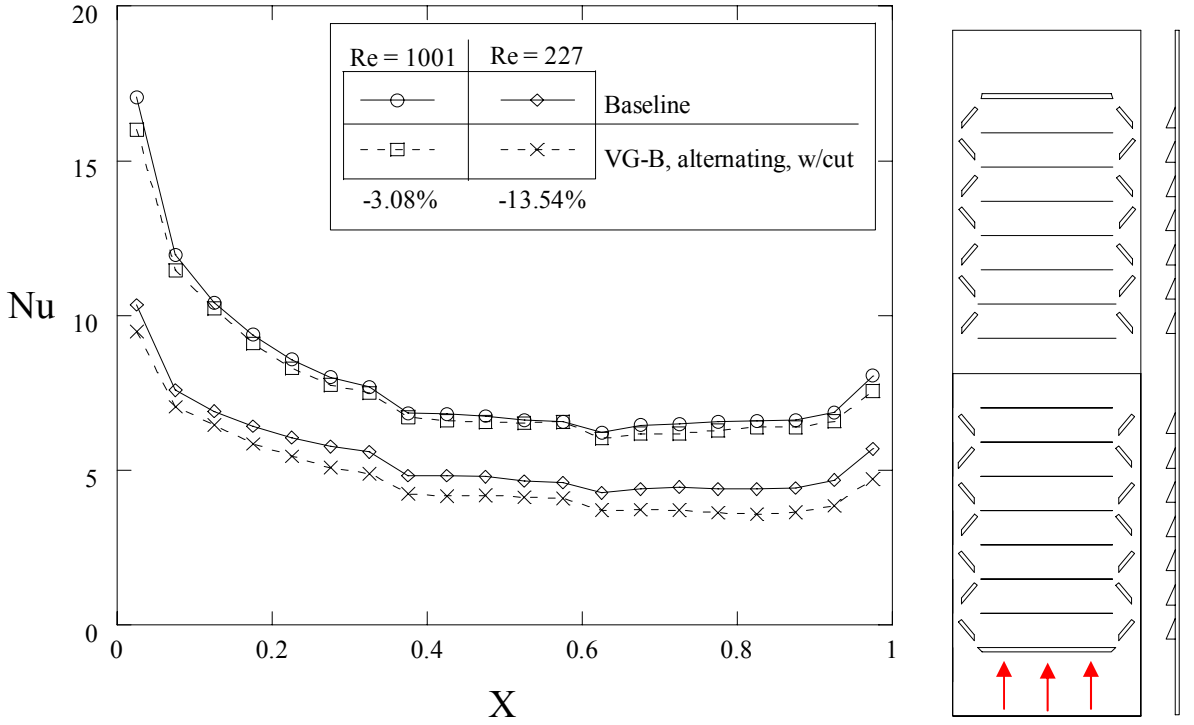

Figure 5.2 Streamwise Nusselt numbers for VG-B winglets with alternating direction at Re = 1001 and 227. AOA = 40°, DFW = 0.15L_p, AR = 1.5, winglet thickness is 0.67t, winglets are cut.

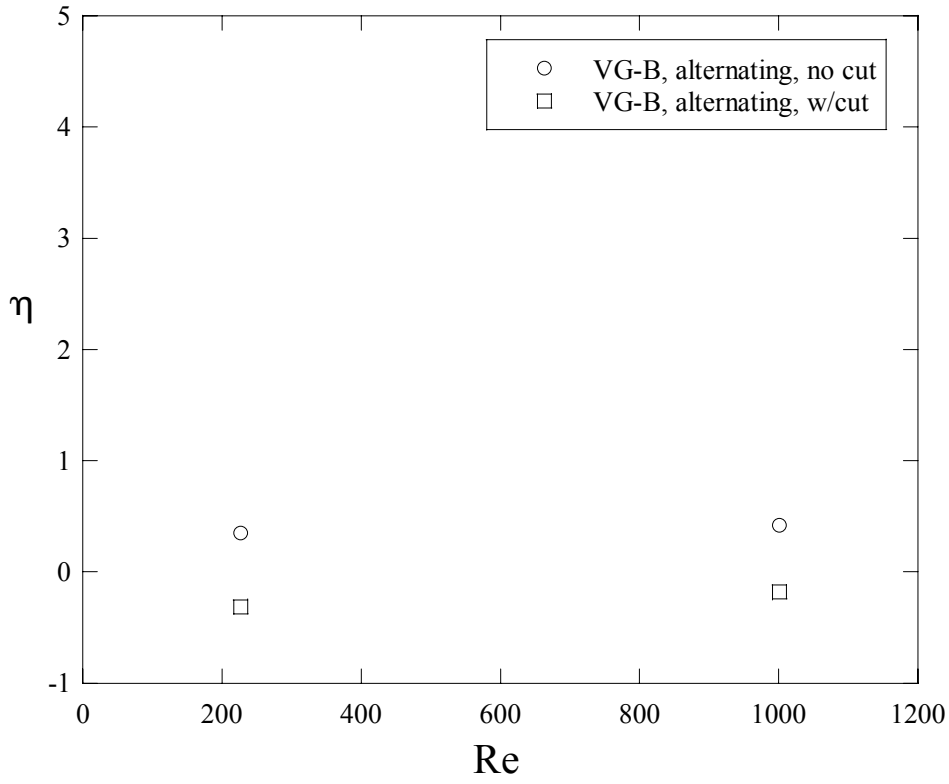

Figure 5.3 Efficiency indexes for VG-B winglets with alternating direction at Re = 1001 and 227. AOA = 40°, DFW = 0.15L_p, AR = 1.5, winglet thickness is 0.67t. Results are for cut and uncut winglets.

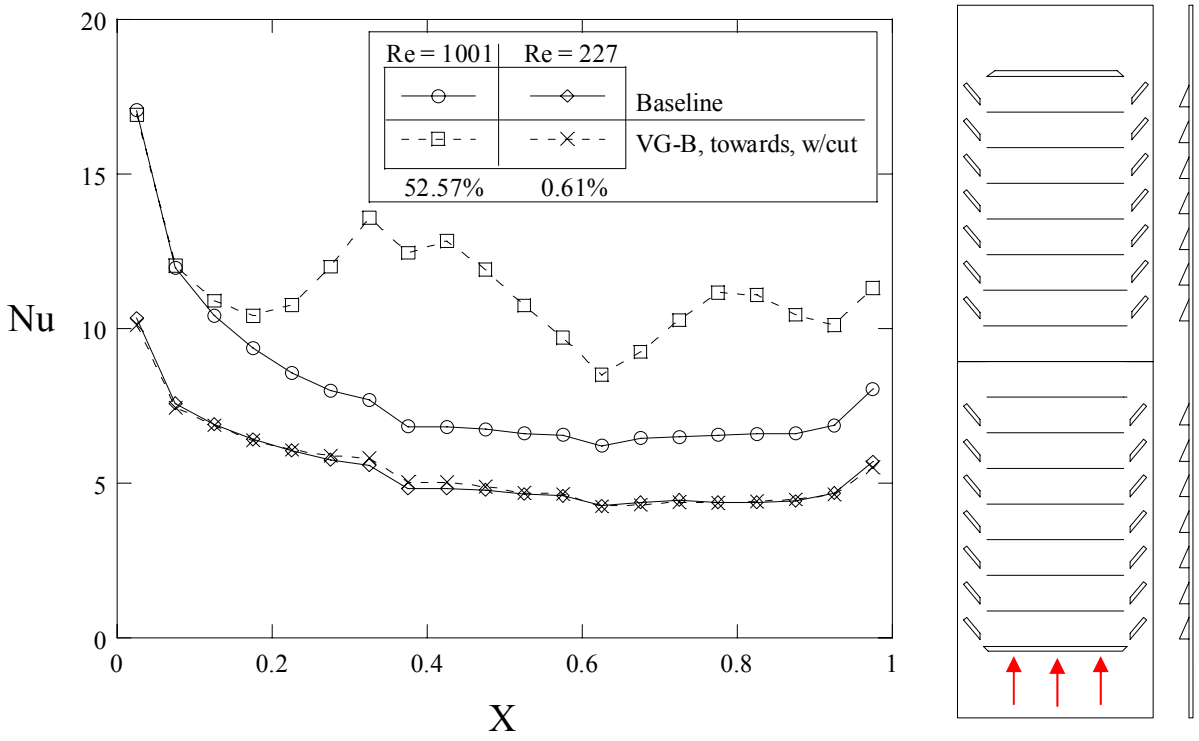

Figure 5.4 Streamwise Nusselt numbers for VG-B winglets aimed towards wall at Re = 1001 and 227. AOA = 40°, DFW = 0.15L_p, AR = 1.5, winglet thickness is 0.67t, winglets are cut.

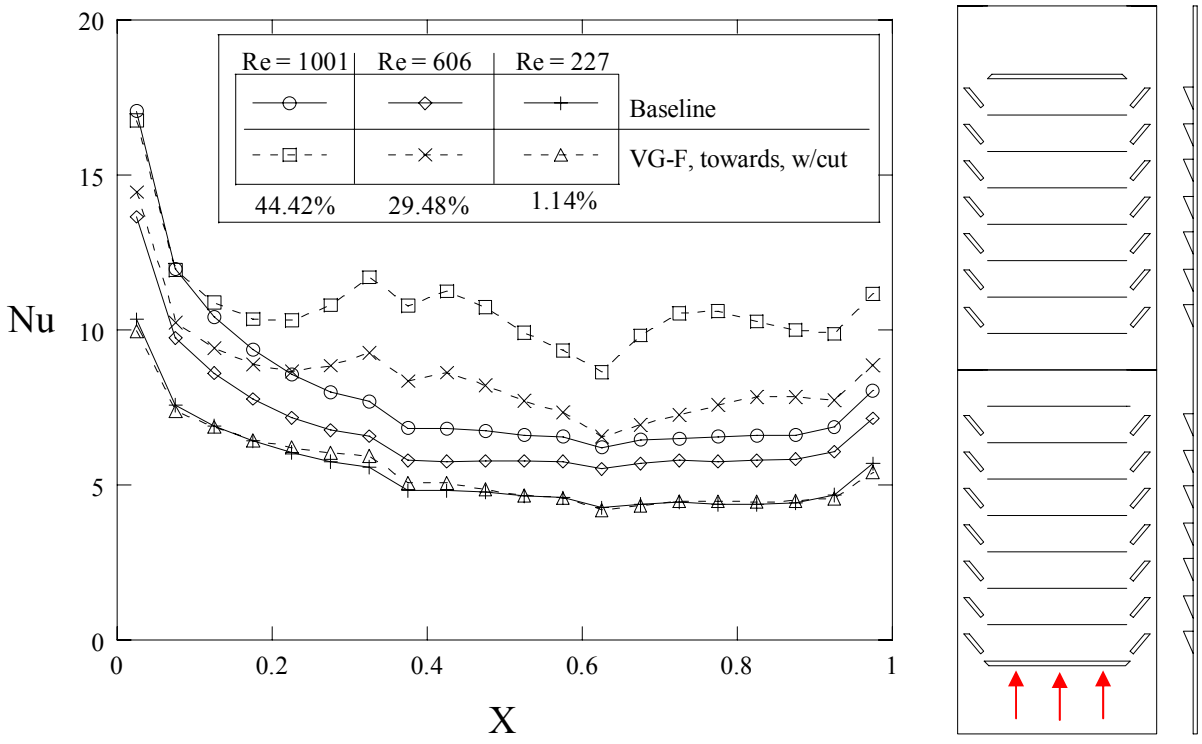

Figure 5.5 Streamwise Nusselt numbers for VG-F winglets aimed towards wall at Re = 1001, 606, and 227. AOA = 40°, DFW = 0.15L_p, AR = 1.5, winglet thickness is 0.67t, winglets are cut.

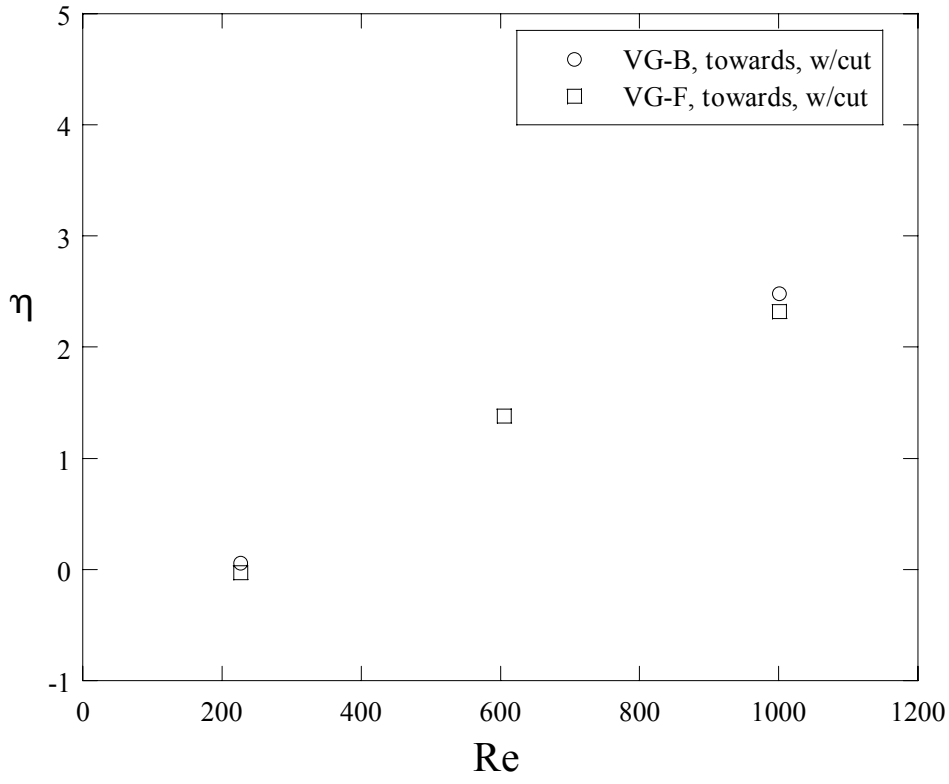

Figure 5.6 Efficiency indexes for both VG-F and VG-B winglets aimed towards wall at Re = 1001, 606, and 227. AOA = 40°, DFW = 0.15L_p, AR = 1.5, winglet thickness is 0.67t, winglets are cut.

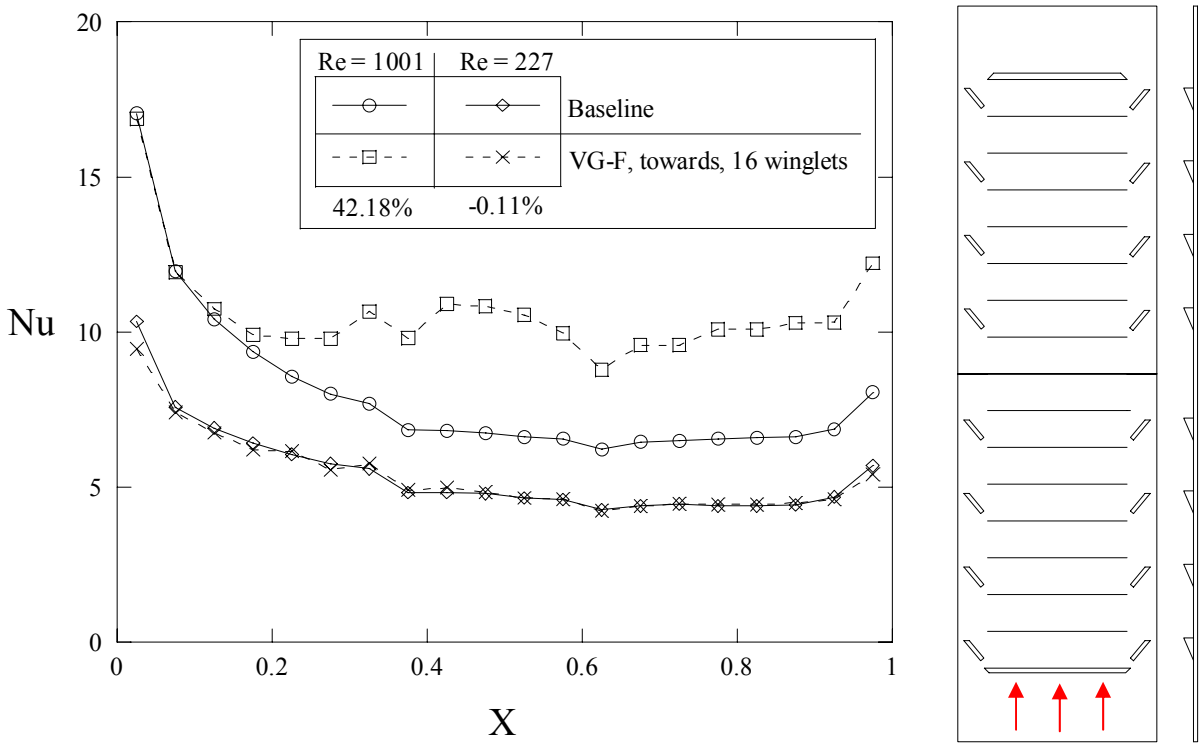

Figure 5.7 Streamwise Nusselt numbers for 16 VG-F winglets aimed towards wall at Re = 1001 and 227. AOA = 40°, DFW = 0.15L_p, AR = 1.5, winglet thickness is 0.67t, winglets are cut.

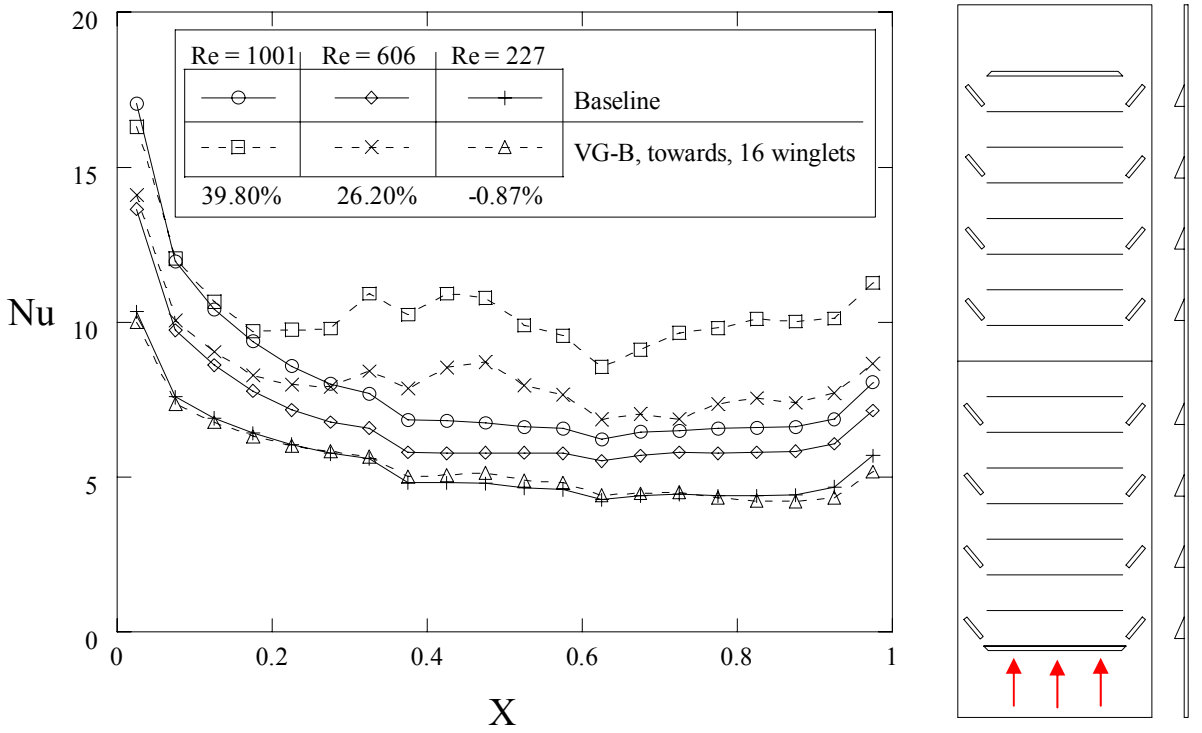

Figure 5.8 Streamwise Nusselt numbers for 16 VG-B winglets aimed towards wall at Re = 1001, 606, and 227. AOA = 40°, DFW = 0.15L_p, AR = 1.5, winglet thickness is 0.67t, no cuts on winglets.

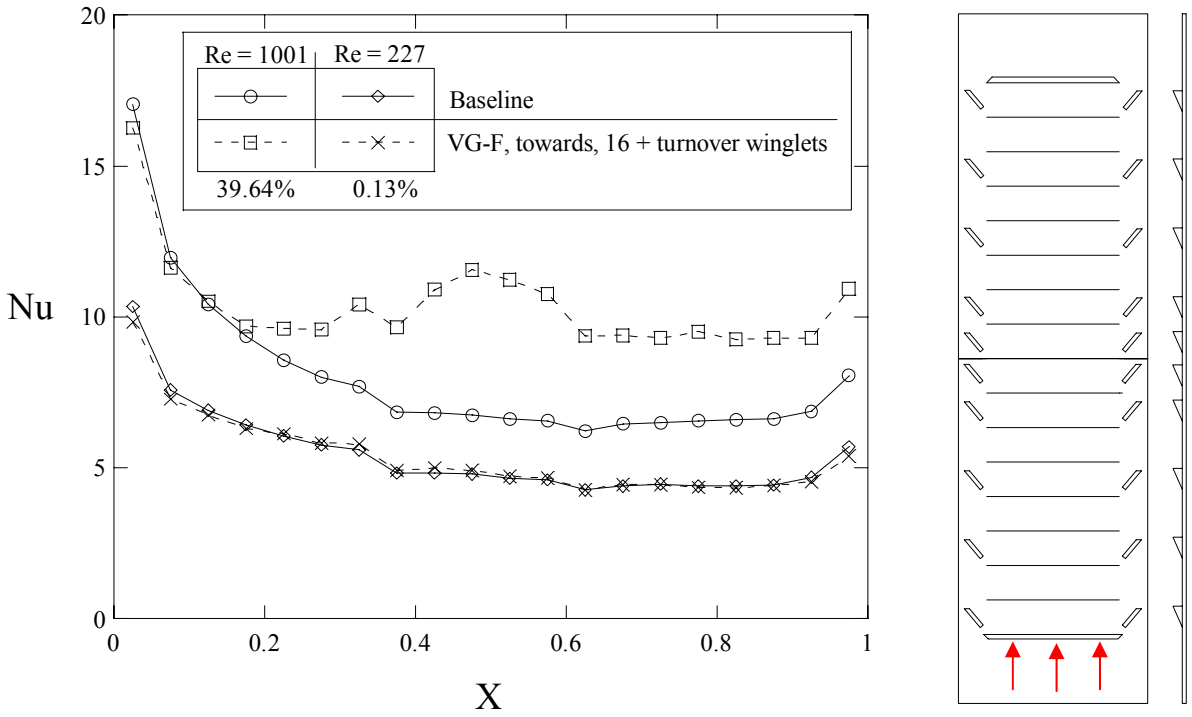

Figure 5.9 Streamwise Nusselt numbers for 16 plus turnover VG-F winglets aimed towards wall at Re = 1001 and 227. AOA = 40°, DFW = 0.15L_p, AR = 1.5, winglet thickness is 0.67t, winglets are cut.

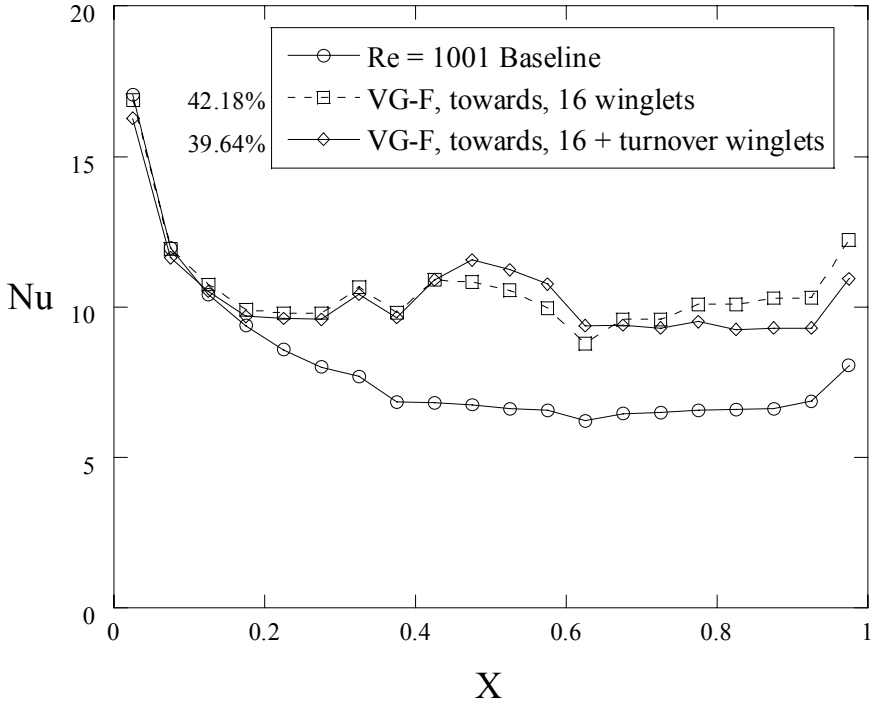

Figure 5.10 Comparison of streamwise Nusselt numbers for 16 VG-F winglets with and without turnover winglets at Re = 1001. AOA = 40°, DFW = 0.15L_p, AR = 1.5, winglet thickness is 0.67t, winglets are cut.

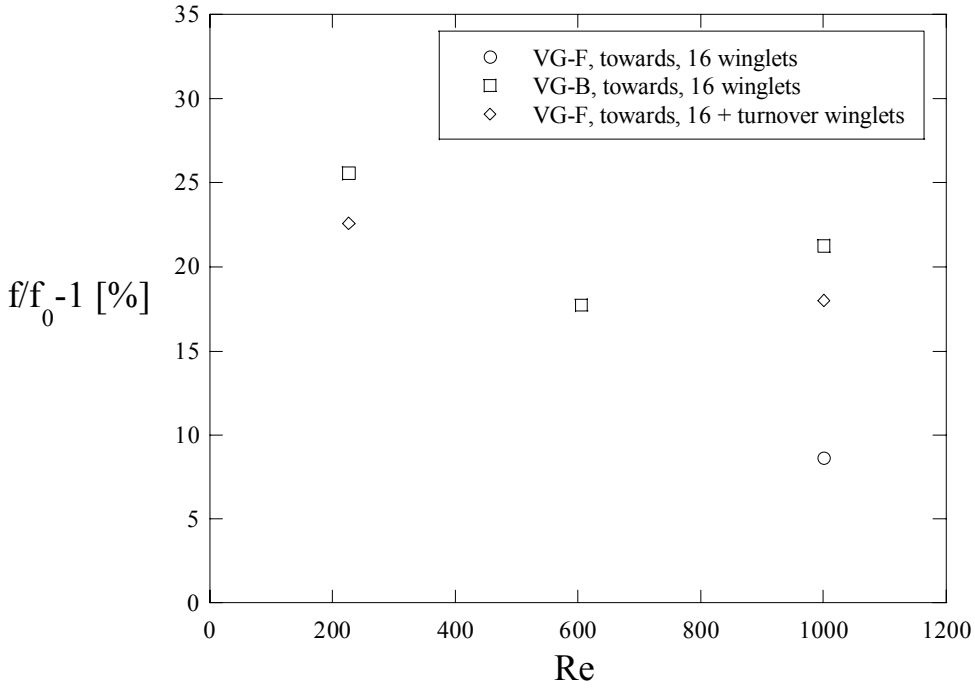

Figure 5.11 Friction factor augmentations for 16 VG-F winglets with and without turnover winglets as well as 16 VG-B winglets aimed towards wall at Re = 1001, 606, and 227. AOA = 40°, DFW = 0.15L_p, AR = 1.5, winglet thickness is 0.67t, winglets are cut.

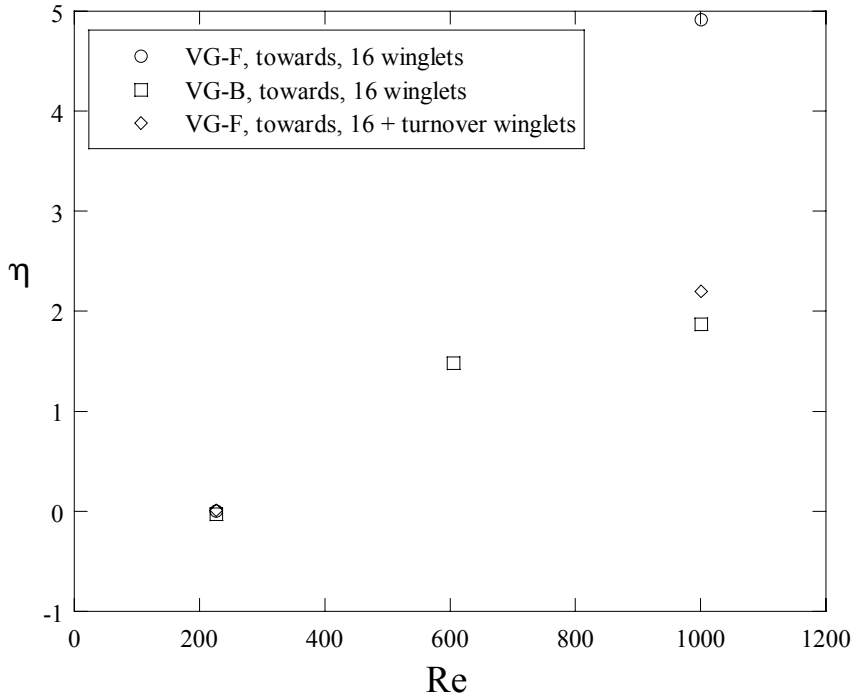

Figure 5.12 Efficiency indexes for 16 VG-F winglets with and without turnover winglets as well as 16 VG-B winglets aimed towards wall at Re = 1001, 606, and 227. AOA = 40°, DFW = 0.15L_p, AR = 1.5, winglet thickness is 0.67t, winglets are cut.

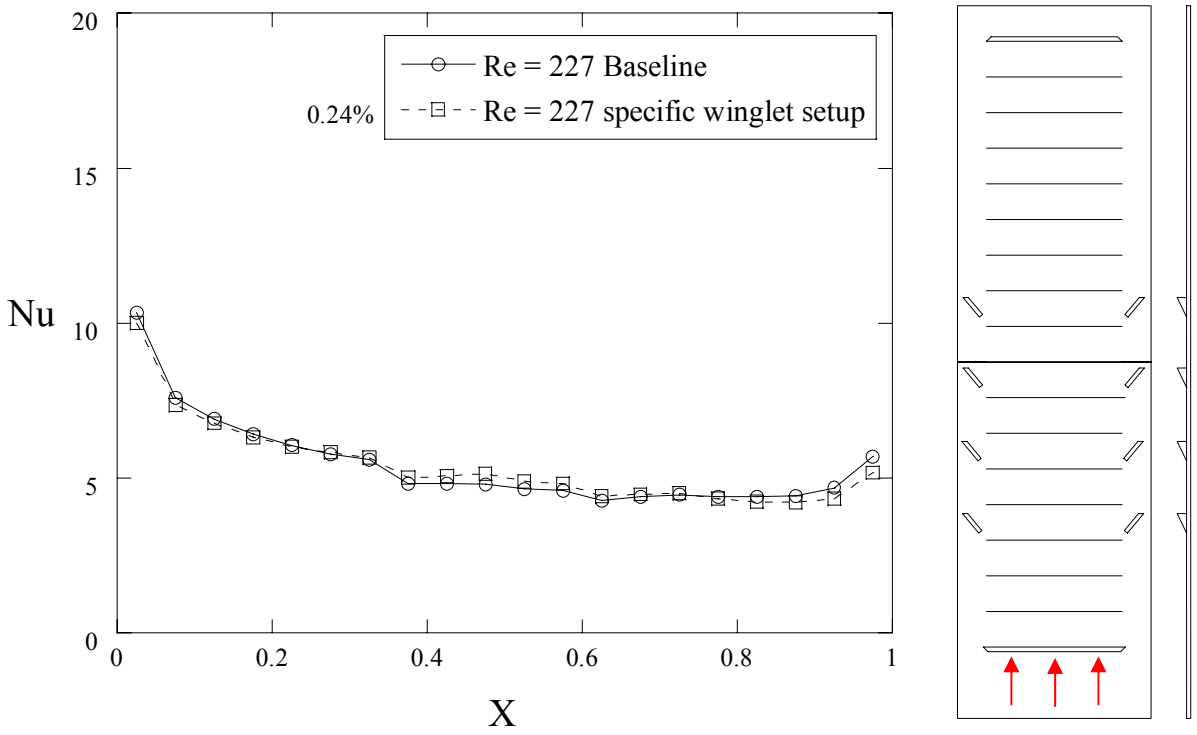

Figure 5.13 Streamwise Nusselt numbers for Re = 227 specific VG-F winglets, aimed towards wall at Re = 227. AOA = 40°, DFW = 0.15L_p, AR = 1.5, winglet thickness is 0.67t, winglets are cut.

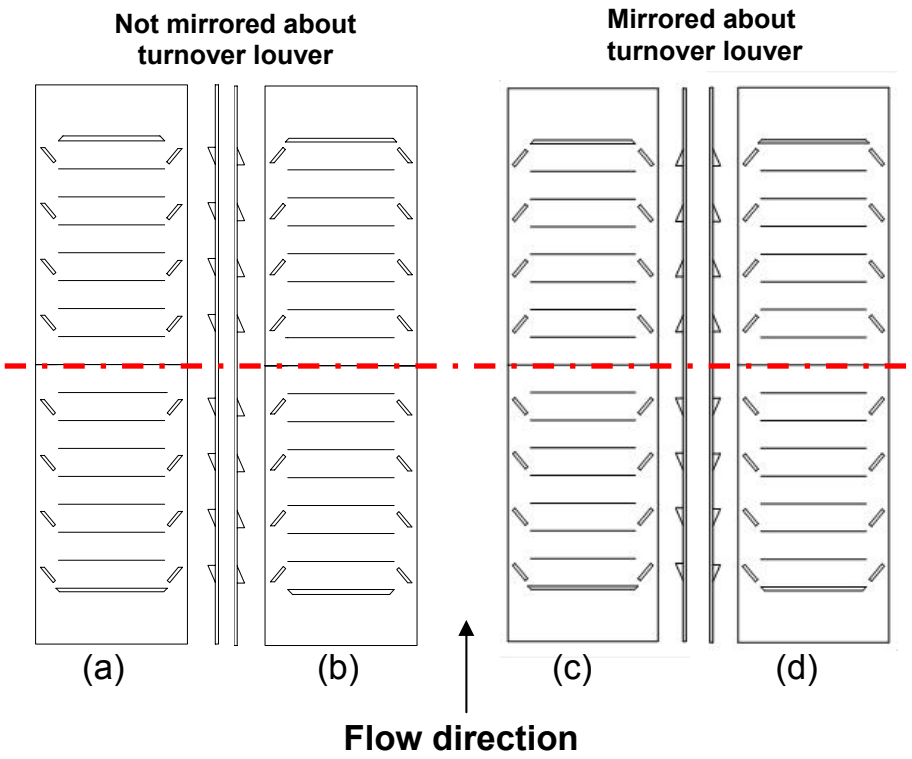

Figure 5.14 Comparison of mirrored and non-mirrored winglet configurations.

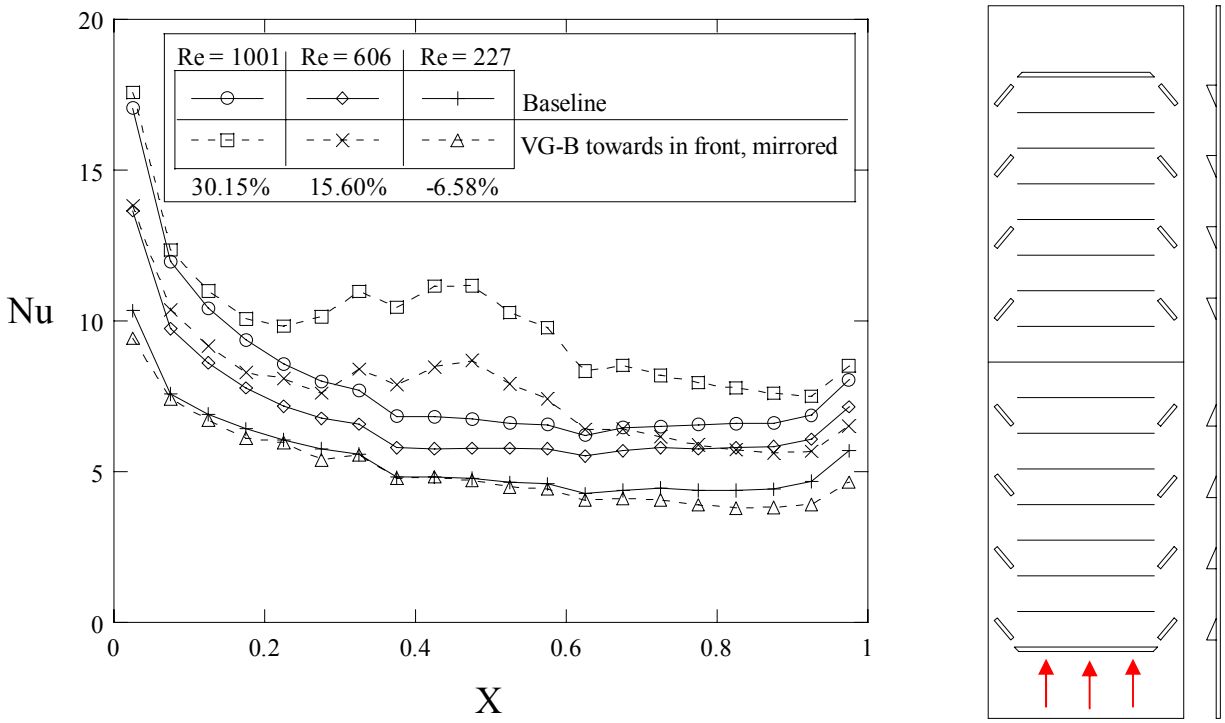

Figure 5.15 Streamwise Nusselt numbers for mirrored winglets in VG-B orientation aimed towards wall upstream of the turnover at Re = 1001, 606, and 227. AOA = 40°, DFW = 0.15L_p, AR = 1.5, winglet thickness is 0.67t, no cuts on winglets.

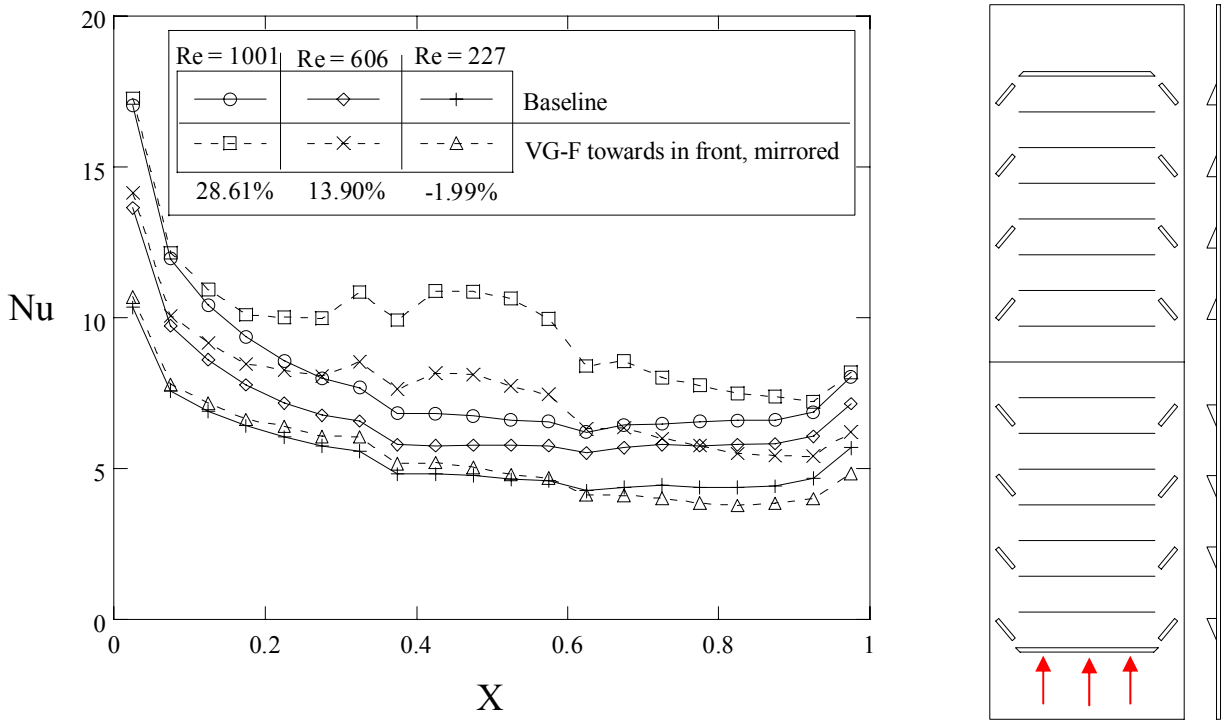

Figure 5.16 Streamwise Nusselt numbers for mirrored winglets in VG-F orientation aimed towards wall upstream of the turnover at Re = 1001, 606, and 227. AOA = 40°, DFW = 0.15L_p, AR = 1.5, winglet thickness is 0.67t, no cuts on winglets.

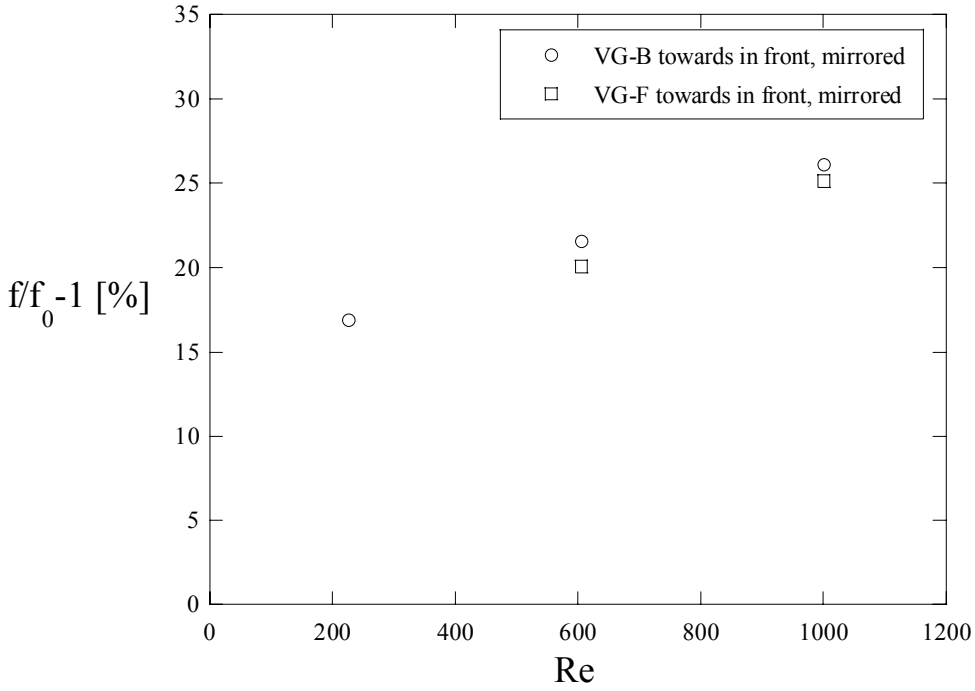

Figure 5.17 Friction factor augmentations for mirrored winglets in VG-F and VG-B orientation aimed towards wall upstream of the turnover at Re = 1001, 606, and 227. AOA = 40°, DFW = 0.15L_p, AR = 1.5, winglet thickness is 0.67t, no cuts on winglets.

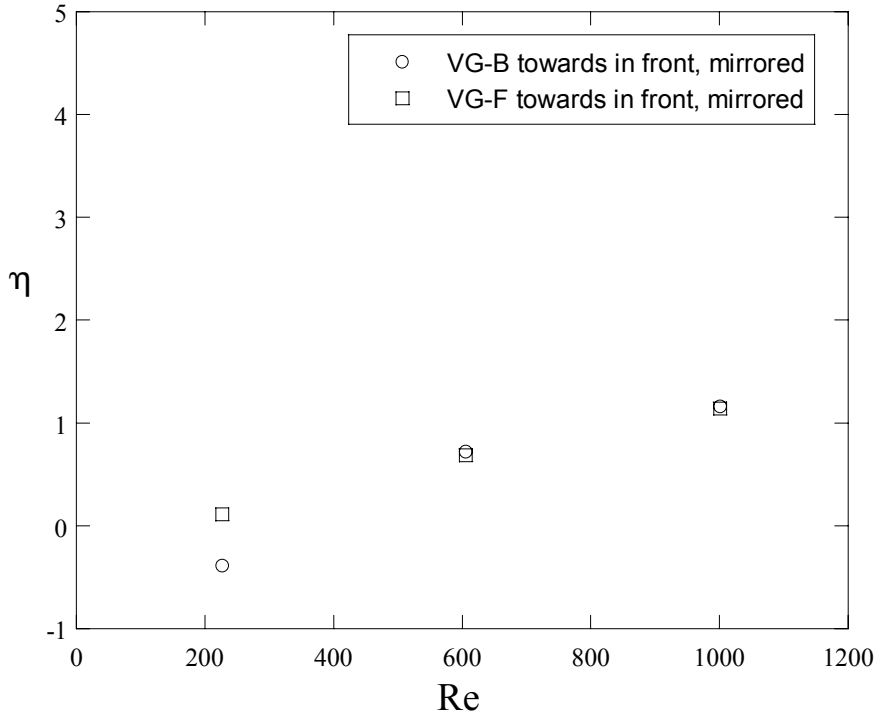

Figure 5.18 Efficiency indexes for mirrored winglets in VG-F and VG-B orientation aimed towards wall upstream of the turnover at Re = 1001, 606, and 227. AOA = 40°, DFW = 0.15L_p, AR = 1.5, winglet thickness is 0.67t, no cuts on winglets.

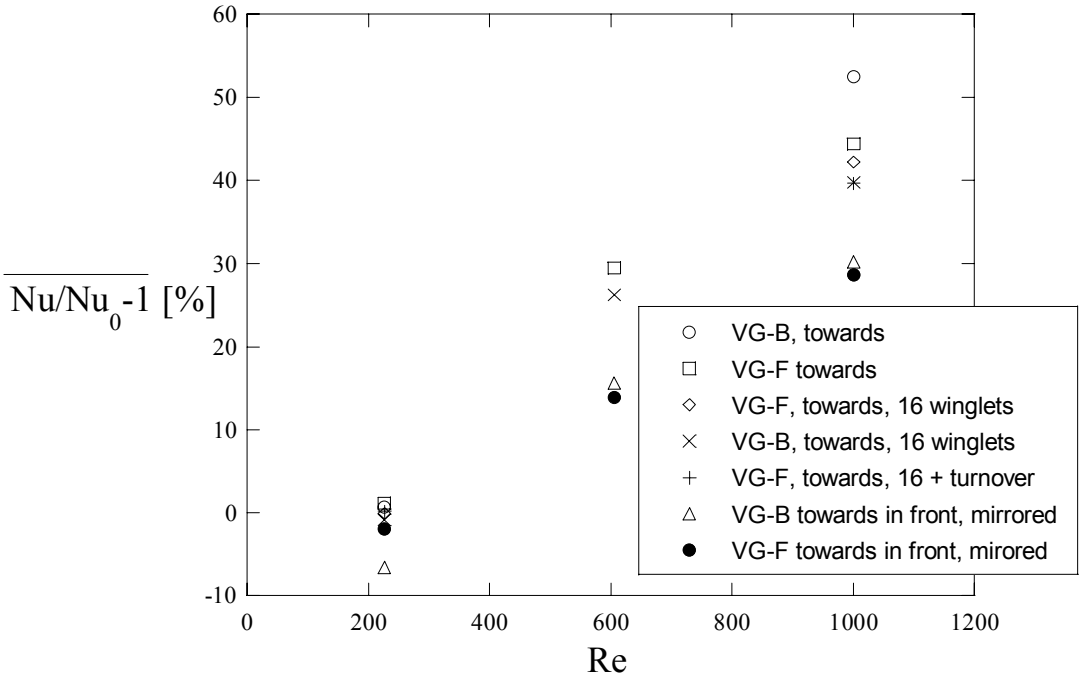

Figure 5.19 Comparison of average heat transfer augmentations for most of the tests shown in this chapter at Re = 1001, 606, and 227. AOA = 40°, DFW = 0.15L_p, AR = 1.5, winglet thickness is 0.67t, some winglets are cut.

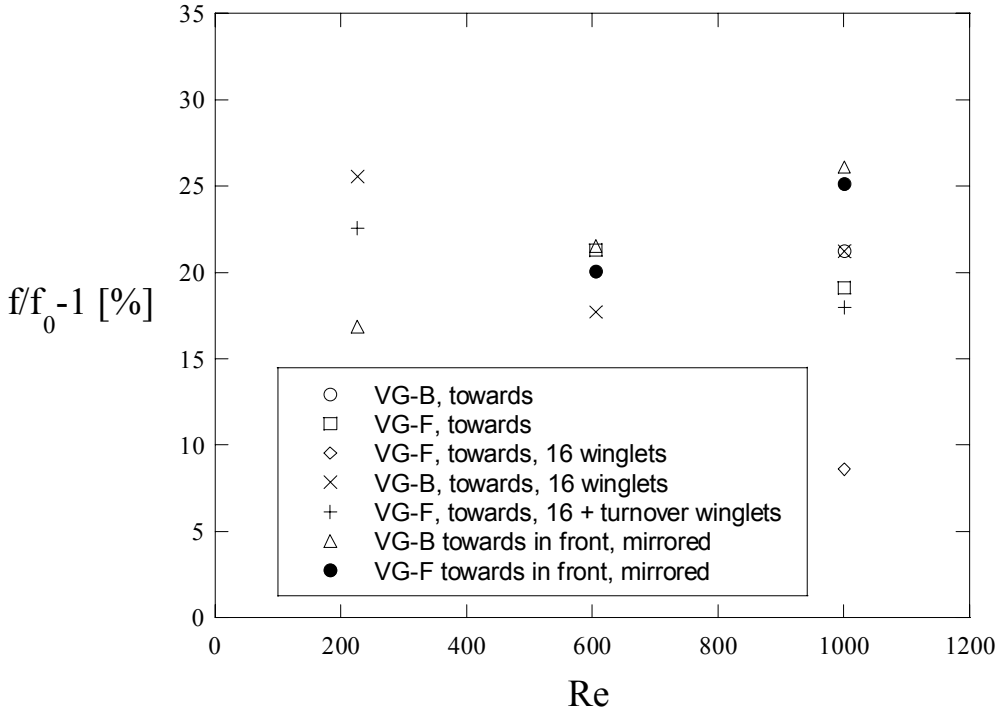

Figure 5.20 Comparison of friction factor augmentations for most of the tests shown in this chapter at Re = 1001, 606, and 227. AOA = 40°, DFW = 0.15L_p, AR = 1.5, winglet thickness is 0.67t, some winglets are cut.

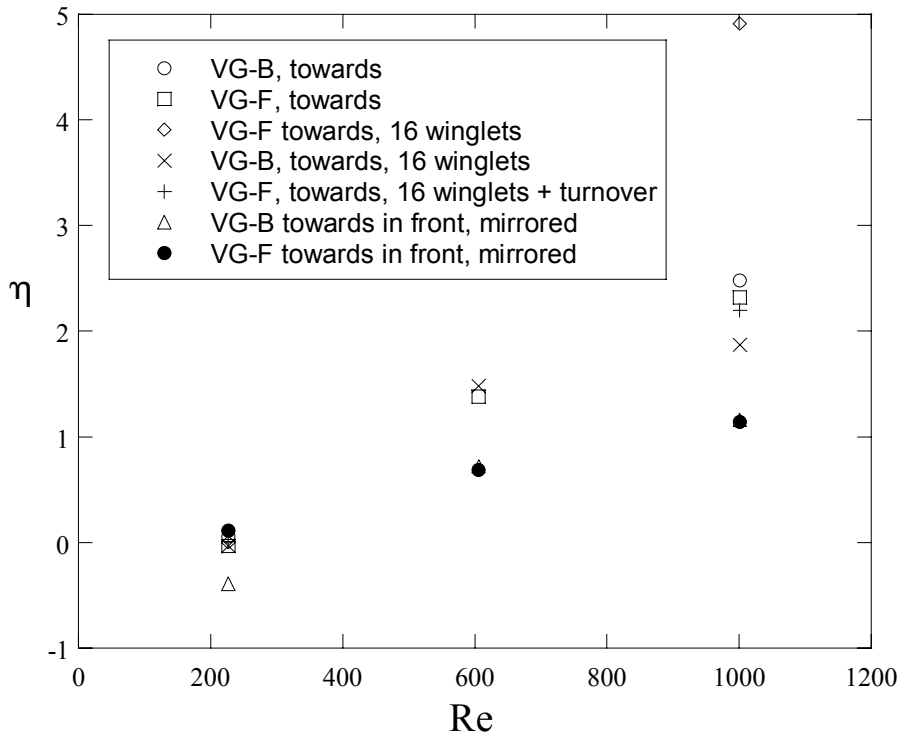

Figure 5.21 Comparison of efficiency index for most of the tests shown in this chapter at Re = 1001, 606, and 227. AOA = 40°, DFW = 0.15L_p, AR = 1.5, winglet thickness is 0.67t, some winglets are cut.

Chapter 6 – Conclusions and Recommendations for Future Work

An experimental study to determine the effect of louver length and delta winglets on friction factor and tube wall heat transfer was conducted. Both segments of this study were completed using 20X scale models of a louvered fin heat exchanger that was representative of a geometry used in radiator applications. Reynolds numbers based on louver pitch of 230, 615, and 1016 were studied based on a range of typical conditions a radiator might experience. Heat transfer studies were conducted with a constant heat flux surface that modeled the tube wall in an actual exchanger. Thermocouples were imbedded behind the heater in 20 streamwise locations so that local Nusselt numbers could be calculated. Friction factor measurements were made through pressure taps placed upstream of the entrance louver and downstream of the exit louver. Louver length studies were completed for three louver length to fin height ratios: 70%, 82%, and 100%. Winglet studies were conducted for louver lengths of 70% and 100% of the fin height. Several individual winglet parameters and overall winglet setups were studied and evaluated on the basis of heat transfer augmentation, friction factor augmentation, and efficiency index. This chapter summarizes the important findings of this study and also provides suggestions for future work in this area of research.

6.1 Louver Length Conclusions

Heat transfer and friction factor measurements were made for L_l/F_h = 100%, 82%, and 70% louver lengths to determine the mechanisms of heat transfer on the tube wall while also finding the pressure drop penalty related to the different geometries. Although the 100% louver length is an idealized case, it acts as a good comparator to the more realistic louver lengths of 70% and 82%. The trends for tube wall heat transfer were somewhat different for the 100% louver length when compared to the short louver lengths. Flow through the L_l/F_h = 100% array was like flat plate flow with large augmentations in heat transfer occurring in the regions of the entrance, turnover, and exit louvers at the higher Reynolds numbers. At Re = 230, the flow was unaffected by the special louvers which is related to low fluid momentum for this Re. In general, flow over the tube wall for the 100% louver length looked similar to flat plate flow, however, due to small interruptions in the boundary layer caused the leading edge of the louvers, heat

transfer results were higher than normal flat plate values. Of all of the louver lengths, the 100% louver length showed the highest friction factor caused by the extra blockage to the flow from the angled portion of the louver near the tube wall.

Heat transfer results for the short louver lengths were very similar showing almost no reaction to the entrance, turnover, and exit louvers as was seen in the 100% case. Nusselt values at all Reynolds numbers flattened off upstream of the turnover louver and remained nearly constant through the rest of the channel, leading to the belief that some type of mixed channel and flat plate flow was being set up in the side channels created by the tube wall and the fins. Over the Reynolds number range tested, the short louver lengths provided a higher heat transfer benefit to the tube wall because the values flattened off while the values for the 100% louver cases dropped following the turnover louver. The short louver lengths also produced lower friction factors than the 100% case with the 70% case being the lowest. This reduction in friction factor penalty can be attributed to the length of the flat landing, or the amount of the fin that is in line with the flow direction. Due to the high heat transfer results on the tube wall combined with the lowest friction factor, the 70% louver length was deemed the most beneficial for tube wall enhancement caused by louver length. However, it should be kept in mind that this study did not take into account any changes in fin efficiency related to changes in louver length.

6.2 Winglet Conclusions

In an attempt to augment the heat transfer on the tube wall, delta winglets were placed on the louver or fin surfaces. Delta winglets are a passive means of augmenting heat transfer by creating a surface feature that produces a longitudinal vortex which thins the thermal boundary layer and mixes the bulk flow. Several different delta winglet configurations were studied for 100% and 70% louver lengths. The parameters investigated were winglet aspect ratio, angle of attack, distance from heated wall, direction, orientation, shape, thickness, spacing related to the louvers, and overall setup on the fins. Heat transfer and friction factor measurements were made in the same manner as for the baseline louver length tests, however, performance was based on augmented values compared to the baseline results.

The effects of the individual winglet parameters were mainly tested on the 100% louver length showing increases in heat transfer and friction factor augmentations with increasing aspect

ratio, angle of attack, and Reynolds number, with varying dependencies on each. For the 100% louver length winglet studies, winglet thickness played a vital role in heat transfer and friction factor performance, with increasing thickness leading to poor results for both. It was also shown that VG-B winglets were better for heat transfer augmentation than VG-F winglets, and alternating winglet direction provided superior results to winglets all aimed towards the wall.

For the 70% louver length, winglet aspect ratio, distance from wall, angle of attack, and thickness were not varied, while more attention was paid to the effect of changes in overall winglet setup. It was shown for the 70% louver length that winglets aimed towards the wall provided a much higher benefit to tube wall heat transfer than winglets with alternating direction which was a completely different result than the 100% case. It is believed that the difference is due to the side channels for the 70% case allowing the vortices to maintain a straight course that is not interrupted by the leading edges of the louvers as they are with the 100% louver length. It was also shown that decreasing the number of winglets on a fin row produced substantially lower friction factors while providing heat transfer results similar to those with the full number of winglets. Also, when half of the winglets were used, the orientation of the winglets proved to be less consequential on heat transfer results than with the full number of winglets. When winglets in either orientation were aimed away from the wall, as they were downstream of the turnover louver in the mirrored setup, heat transfer results degraded quickly and friction factor increased.

For both louver lengths, high heat transfer augmentations were found at the higher Reynolds numbers with a relatively small friction factor increase. The highest heat transfer augmentation found for the 100% winglets was 38% using rectangular winglets in an alternating direction configuration with AOA = 40°, DFW = $0.15L_p$, and Re = 1016. The friction factor increase for this case was 23%. However, by just reducing the angle of attack and keeping the other parameters constant, heat transfer and friction factor augmentations of 36% and 14% were obtained. For the 70% louver length, the highest heat transfer obtained was 52% with alternating VG-B winglets at AOA = 40°, DFW = $0.15L_p$, and AR = 1.5 at Re = 1001. The friction factor augmentation for this case was 21%. For both louver lengths tested, Re = 615/606 results were typically high as well while no substantial augmentation was ever found at Re = 230/227.

It has been shown through several careful experiments that large tube wall heat transfer augmentations with a relatively small pressure drop increase can be achieved with the use of vortex generators. Also, as delta winglets can be produced by the same stamping process used to

shape the louvers, this is not a purely academic exercise, but a viable method to be incorporated into actual production louvered fin exchangers.

6.3 Future Recommendations

Although several effects related to louver length and delta winglets were found in this study, there are several others to be looked at in further study. I believe the most important extension of this study at this point is to make detailed flow field measurements in the regions around the winglets. We have shown that winglet direction, orientation, size, and shape have a large influence on the heat transfer of the tube wall, but it is not known what physical flow mechanisms are causing these differences. This knowledge would not only quell the curiosity, but would provide huge benefits for future winglet designs.

I believe the next most important step would be to put conductive metal fins in the test section and heat them from both sides. This could be done simply and cheaply and provide information on how changes in louver length and winglet setup influence the overall heat transfer of the exchanger. After all, an increase in overall exchanger performance is what really matters. Initial tests following this study have been aimed at testing winglets with the holes that would be left in the fin after a stamping process. I can imagine that the number and size of holes cut into the fin could strongly influence conduction from the tube wall to the louvers, having possibly very large effects in overall heat transfer performance that would not been seen in tube wall specific tests. Also, as was shown by Gentry and Jacobi (2002), the vortices coming off of the winglets have influences on other surrounding surfaces. In the current setup, there is a potential to produce augmentation on three surfaces (tube wall, fin above winglet, fin the winglet is on). There is also a double benefit on each fin surface because the vortices in the channels above or below a given channel are also augmenting the fins. None of these effects can be studied without a fully heated test section.

Finally, much more attention needs to be given to winglet spacing. It was shown in the 70% winglet studies that reducing the number of winglets by nearly half resulted in lower friction factors but similar heat transfer augmentations to the full number of winglets. What would happen if only a quarter or an eighth of the winglets were used? This study would show how long a vortex can be sustained in the side channel region without needing a boost from another winglet. If high augmentations can be achieved with even less winglets, I believe the

friction factor reductions alone would make this worthwhile. This type of study could have especially large benefits to the more realistic mirrored winglets setup. As seen in Chapter 5, the winglets aimed away from the wall downstream of the turnover cause large decreases in tube wall heat transfer, showing below baseline results for Re = 606 and 227. If the number of winglets aimed away from the wall could be reduced, overall tube wall augmentation might increase. In an extreme example, let us say that one winglet placed at the first louver position could produce a vortex that remained strong through the front half of the test section. This means that the corresponding winglet aimed away from the wall in the rear of the section, as necessary in the mirrored winglets setup, would be placed on the last louver position. The flow would be nearly out of the test section before the winglet aimed away from the wall could decrease heat transfer results. It may be beneficial to gain less heat transfer enhancement upstream of the turnover louver as to lose less downstream of the turnover louver. Only a complete understanding of winglet spacing can lead to optimized placement on the fin surface.

References

Achaicha, A. and Cowell, T. A. (1988) "Heat Transfer and Pressure Drop Characteristics of Flat Tube and Louvered Plate Fin Surfaces," *Experimental Thermal and Fluid Science*, Vol. 1, pp. 147-157.

Atkinson, K. N., Draulic, R., Heikal, M. R., and Cowell, T. A. (1998) "Two- and Three-Dimensional Numerical Models of Flow and Heat Transfer Over Louvered Fin Arrays in Compact Heat Exchangers," *International Journal of Heat and Mass Transfer*, Vol. 41, pp. 4063-4080.

Chen, Y., Fiebig, M., Mitra, N. K. (1998) "Heat transfer enhancement of a finned oval tube with punched longitudinal vortex generators in-line," *International Journal of Heat and Mass Transfer*, Vol. 41, pp. 4151-4166.

Cui, J. and Tafti, D. K. (2002) "Computations of flow and heat transfer in a three-dimensional multilouvered array fin geometry," *International Journal of Heat and Mass Transfer*, Vol. 45, pp. 5007-5023.

Ebeling, P. and Thole, K. A. (2004) "Measurements and Predictions of the Heat Transfer at the Tube-Fin Junction for Louvered Fin Heat Exchangers," *International Journal of Compact Heat Exchangers*, Vol. 5, pp. 265-286.

Gentry, M. C. and Jacobi, A. M. (2002) "Heat Transfer Enhancement by Delta-Wing-Generated Tip Vortices in Flat Plate and Developing Channel Flows," *Journal of Heat Transfer*, Vol. 124, pp. 1158-1168.

Incropera, F. P, and DeWitt, D. P, *Introduction to Heat Transfer*, 4th ed., John Wiley & Sons, New York, 2002.

Joardar, A. and Jacobi, A. M. (2005) "Impact of leading edge delta-wing vortex generators on the thermal performance of a flat tube, louvered-fin compact heat exchanger," *International Journal of Heat and Mass Transfer*, Vol. 48, pp. 1480-1493.

Kakaç, S., Shah, R. K., Aung, W., *Handbook of Single-Phase Convective Heat Transfer*, John Wiley & Sons, New York, 1987.

Kays, W. M., and London, A. L., *Compact Heat Exchangers*, 2nd ed., McGraw-Hill, New York, 1984.

Lyman, A. C., Stephan, R. A., Thole, K. A., Zhang, L., Memory, S. (2002) "Scaling of Heat Transfer Coefficients Along Louvered Fins," *Experimental Thermal Fluid Science*, Vol. 26, pp. 547-563.

Lyman, A. (2000) "Spatially Resolved Heat Transfer Studies in Louvered Fins for Compact Heat Exchangers," *MSME Thesis*. Virginia Tech, USA.

Modest, M. F., *Radiative Heat Transfer*, 2nd ed., Academic Press, New York, 2003.

Roy, R. K., *Design of Experiments Using the Taguchi Approach: 16 Steps to Product and Process Improvement*, John Wiley & Sons, New York, 2001.

Springer, M. E. and Thole, K. A. (1998) "Experimental Design for Flowfield Studies of Louvered Fins," *Experimental Thermal and Fluid Science*, Vol. 18, pp. 258-269.

Stephan, R. A. and Thole, K. A. (2005) "Optimization Study Relevant to Louvered Fin Heat Exchangers," *International Journal of Heat Exchangers*, Vol. 6, pp. 73-92.

Tafti, D. K. and Cui, J. (2003) "Fin-tube junction effects on flow and heat transfer in flat tube multilouvered heat exchangers," *International Journal of Heat and Mass Transfer*, Vol. 46, 2027-2038.

Tiwari, S., Maurya, D., Biswas, G., and Eswaran, V. (2003) "Heat transfer enhancement in cross-flow heat exchangers using oval tubes and multiple delta winglets," *International Journal of Heat and Mass Transfer*, Vol. 46, pp. 2841-2856.

Webb, R. L. and Trauger, P. (1991) "Flow Structures in Louvered Fin Heat Exchanger Geometry," *Experimental Thermal and Fluid Science*, Vol. 4, pp.205-214.

White, F. M., *Fluid Mechanics*, 4th ed., McGraw-Hill, New York, 1999.